Modeling and Design of Betavoltaic Batteries

Tariq Rizvi Alam

Dissertation submitted to the faculty of the Virginia Polytechnic Institute and State University in partial fulfillment of the requirements for the degree of

Doctor of Philosophy
In
Mechanical Engineering

Mark A. Pierson, Co-Chair
Mark A. Prelas, Co-Chair
Michael G. Spencer
Louis J. Guido
Alireza Haghighat
Scott T. Huxtable

September 18, 2017
Blacksburg, VA

Keywords: Betavoltaic battery, nuclear battery, radioisotope battery, Betavoltaic battery model, beta particle transport, beta particle angular distribution, penetration depth, energy deposition, self-absorption, beta flux, source optimization, design principles of betavoltaic batteries

MODELING AND DESIGN OF BETAVOLTAIC BATTERIES

Tariq R. Alam

ACADEMIC ABSTRACT

The betavoltaic battery is a type of micro nuclear battery that harvests beta emitting radioactive decay energy using semiconductors. The literature results suggest that a better model is needed to design a betavoltaic battery. This dissertation creates a comprehensive model that includes all of the important factors that impact betavoltaic battery output and efficiency.

Recent advancements in micro electro mechanical systems (MEMS) necessitate an onboard miniaturized power source. As these devices are highly functional, longevity of the power source is also preferred. Betavoltaic batteries are a very promising power source that can fulfill these requirements. They can be miniaturized to the size of a human hair. On the other hand, miniaturization of chemical batteries is restricted by low energy density. That is why betavoltaics are a viable option as a power source for sophisticated MEMS devices. They can also be used for implantable medical devices such as pacemakers; for remote applications such as spacecraft, undersea exploration, polar regions, mountains; military equipment; for sensor networks for environmental monitoring; and for sensors embedded in bridges due to their high energy density and long lifetime (up to 100 years).

A betavoltaic battery simulation model was developed using Monte Carlo particle transport codes such as MCNP and PENELOPE whereas many researchers used simple empirical equations. These particle transport codes consider the comprehensive physics theory for electron transport in materials. They are used to estimate the energy deposition and the penetration depth

of beta particles in the semiconductors. A full energy spectrum was used in the model to take into account the actual radioactive decay energy of the beta particles. These results were compared to the traditional betavoltaic battery design method of estimating energy deposition and penetration depth using monoenergetic beta average energy. Significant differences in results were observed that have a major impact on betavoltaic battery design. Furthermore, the angular distribution of the beta particles was incorporated in the model in order to take into account the effect of isotropic emission of beta decay. The backscattering of beta particles and loss of energy with angular dependence were analyzed. Then, the drift-diffusion semiconductor model was applied in order to estimate the power outputs for the battery, whereas many researchers used the simple collection probability model neglecting many design parameters. The results showed that an optimum junction depth can maximize the power output. The short circuit current and open circuit voltage of the battery varied with the semiconductor junction depth, angular distribution, and different activities. However, the analysis showed that the analytical results overpredicted the experimental results when self-absorption was not considered. Therefore, the percentage of self-absorption and the source thickness were estimated using a radioisotope source model. It was then validated with the thickness calculated from the specific activity of the radioisotope. As a result, the battery model was improved significantly. Furthermore, different tritiated metal sources were analyzed and the beta fluxes were compared. The optimum source thicknesses were designed to increase the source efficiencies. Both narrow and wide band gap semiconductors for beryllium tritide were analyzed.

MODELING AND DESIGN OF BETAVOLTAIC BATTERIES

Tariq R. Alam

GENERAL AUDIENCE ABSTRACT

A betavoltaic battery is a type of micro nuclear battery that harnesses electrical energy from radioisotopes using semiconductors. It has high specific energy density and longevity but low specific power. It can be miniaturized to a micron scale size (a size of a human hair) to power micro/nano sensors or devices. They can be used in implantable biomedical devices such as pacemakers, remote areas such as high mountains, undersea, and also in embedded sensors in structures. Chemical and other types of batteries are not suitable at this scale due to their low specific energy density. A betavoltaic battery is an attractive choice in applications where reliability and long service life (up to 100 years) are required. However, their power output is very low (on the scale of microwatts) due to their low specific power. They can aid chemical batteries to increase their lifetime by designing a hybrid battery. In a hybrid battery, a betavoltaic battery can trickle charge a chemical battery to top off the depleted charge. A theoretical analysis of a battery design is useful to improve its power output and efficiency. The literature in this area suggests that a better theoretical model is required to agree well with the experimental results as well as for better design. This model comprehensively included all the important factors that impact betavoltaic battery output and efficiency. All the necessary betavoltaic battery design factors were analyzed in detail in this work in order to maximize the desired output.

ACKNOWLEDGEMENTS

First of all, I would like to praise the Almighty God for helping me complete this work. It was a long journey to come this far. I encountered many difficulties in this long journey that I endured with patience. I received advice and encouragement from numerous people in this accomplishment. I will not be able to mention all of their names and no words will be enough to express my gratitude for them. I pray to the Almighty God for their well-being.

I would like to acknowledge the help and support of Dr. Pierson in this journey. Dr. Pierson granted me a sense of authorship of my work and allowed me to choose my research topic. The entrepreneur mindset was a good motivation for me to do this task. All the hardships I endured pushed me outside of my comfort zone and made me think outside of the box. I had to take many initiatives to solve many problems. It helped me grow my knowledge and skills that prepared me for the real world challenges. I was fortunate to work with two experts, Dr. Prelas and Dr. Spencer, in the area of nuclear batteries. Their guidance and advice were invaluable to me to complete this work. I am very grateful and proud to have mentors like them.

I would like to thank my committee members Dr. Haghighat, Dr. Guido and Dr. Huxtable for their support. I have learned a lot from Dr. Haghighat by taking his classes. He always pushed me to produce high-quality work. I received much help from Dr. Guido who guided me in the right direction. Dr. Huxtable was always helpful and supportive of my work.

Last but not the least, I would like to express my deepest gratitude to my family especially my mother, Johra Begum, my other mother, Hasina Nasir, and my wife, Sarah Nasir. This work was not possible without my family's support and encouragement. They have been always there for me whenever I needed them. I would also like to thank all my friends and well-wishers.

TABLE OF CONTENTS

LIST OF FIGURES

LIST OF TABLES

CHAPTER 1: INTRODUCTION

1.1 Nuclear Battery

A nuclear battery converts radioisotope energy into electrical energy [1, 2]. It has an advantage over other types of batteries due to its high energy density. Energy density is the total energy content per unit mass. The energy density of a nuclear battery is about 10^4 times higher than a chemical battery [3]. On the other hand, a nuclear battery has a very low power density compared to other types of batteries. Power density is the rate that it can output the power at a given size. As a result, a nuclear battery cannot compete with a fuel cell or a chemical battery for applications that require high power output. Therefore, the goal of the nuclear battery design is not

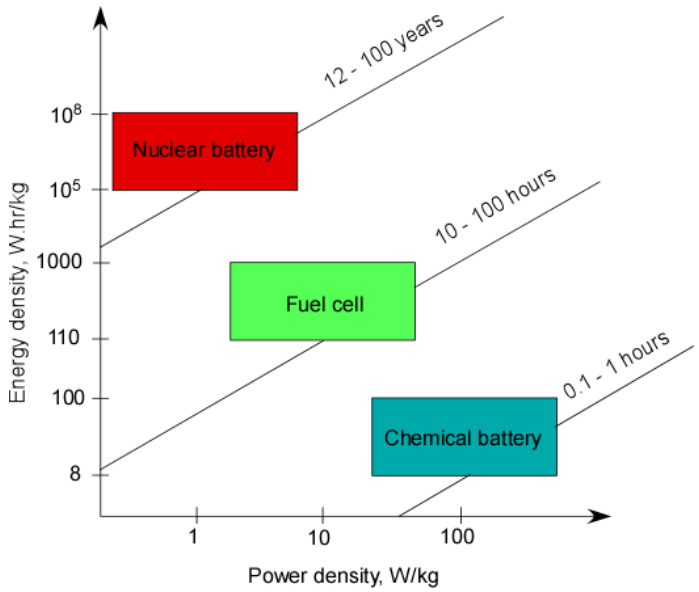

Figure 1-1: A schematic Ragone plot for nuclear batteries, fuel cells, and chemical batteries

to replace the chemical battery but to aid chemical batteries such as hybrid batteries and find applications where chemical batteries are not feasible. Thus, the targeted applications for a nuclear battery are mainly miniaturized low power output applications that cannot be fulfilled by chemical batteries. Other advantages of nuclear batteries are their reliability and longevity. A nuclear battery can output power for decades to a hundred years. A schematic Ragone plot [4] for the comparison of a nuclear battery with a fuel cell and a chemical battery is shown in Figure 1-1.

1.2 Different Types of Nuclear Batteries

The radioisotope energy can be harvested using different mechanisms. A brief discussion of some mechanisms is given below.

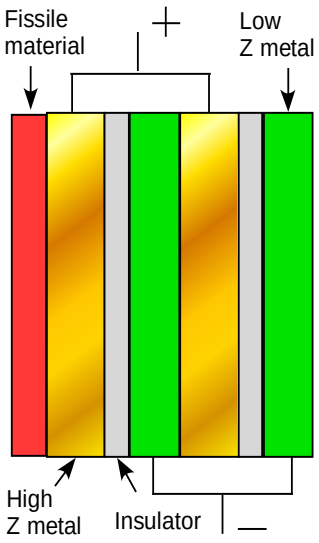

Figure 1-2: Design Concept for a fission battery

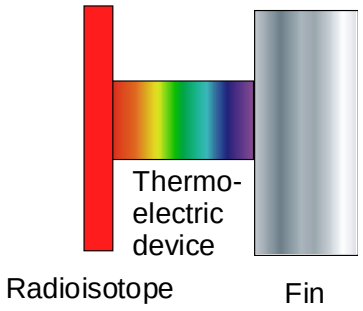

Figure 1-3: Radioisotope thermoelectric generator

A fission battery as shown in the schematic in Figure 1-2 is still a conceptual design [5]. It is a small reactor that does not require turbines and heat exchangers. Micron scale fuel is coated as a ceramic on wire meshes which reside in a liquid metal bath that transfers heat to a conventional secondary heat transfer system. The resulting fission products carry the bulk of the kinetic energy. They will deposit most of their energy in the high Z metal and create a knock-on electrons shower that will be able to pass through the thin insulator layer but will be stopped in the sufficiently thick low Z metal. The high Z metals will be positively charged and the low Z metals will be negatively charged for the battery.

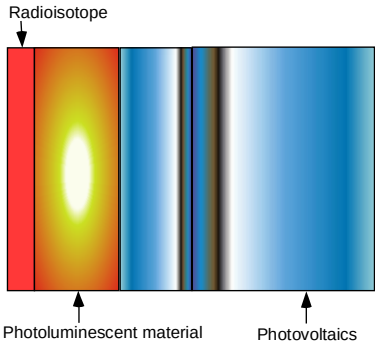

Figure 1-4: Indirect energy conversion method

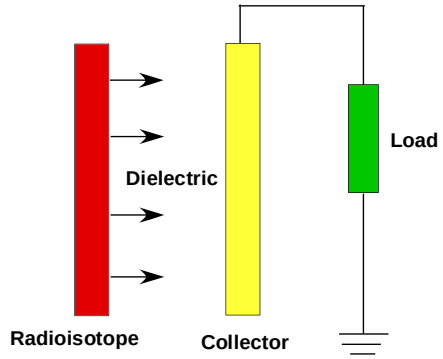

Figure 1-5: Direct Charge nuclear battery

Thermocouples, as shown in Figure 1-3, or small sterling engines are used as a thermoelectric device in a radioisotope thermoelectric generator. A large amount of radioisotopes is used to generate decay heat energy that is harvested to generate electrical energy. This type of battery has applications mainly in space. The efficiency of the battery is about 6% [6].

Figure 1-4 shows an indirect conversion method to generate electrical energy from the radioisotope energy. Production of photons is the intermediary step of energy conversion in this method. The challenge in this type of battery is the low photon intensity due to opacity of the radioluminescent materials. It mostly uses high energy alpha particles. Using 300 mCi of Pu-238 with a phosphor screen and AlGaAs photovoltiacs resulted in generating a short circuit current of 14μA and an open circuit voltage of 2.3 V using five cells with an efficiency of 0.11% [7]. It was used to power a calculator and a wrist watch. However, degradation of the output power was very rapid from damage of the radioluminescent material for this type of battery. The power output drops significantly due to the damage.

Figure 1-5 shows a direct charge battery where the radioisotope and the electrode are separated by vacuum, air or any other dielectric medium. This type of battery provides a very high open circuit voltage and the efficiency of the battery is comparatively high. For example, 2.6 Ci of Pm-147 in a vacuum generated an open circuit voltage of 60 kV and a short circuit current of 6 nA with an efficiency of 14% [4]. This type of battery has applications for electrostatic motors.

Figure 1-6 shows a cantilever method of energy conversion. The electrostatic force developed between the cantilever and the radioisotope pulls the cantilever beam to the radioisotope, after discharging it starts to oscillate. This self-reciprocating motion can be used as an electromechanical sensor. For example, 1 mCi of Ni-63 with a Cu cantilever beam (5 cm × 4 mm × 60 μm) generated 0.4 pW power with an efficiency of 0.0004% [8].

Figure 1-7 shows the direct energy conversion method using semiconductors. It can be used with alpha or beta emitting radioisotopes. However, damage of the semiconductor crystal structure is high for alpha particles. This method of energy conversion using beta particles is known as the betavoltaic battery. The betavoltaic battery design and analysis are the focus of this

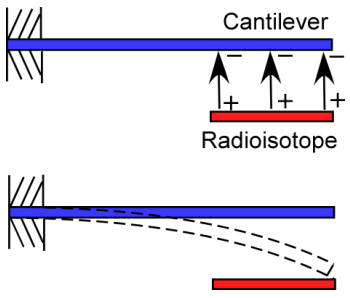

Figure 1-6: Schematic for the cantilever beam method

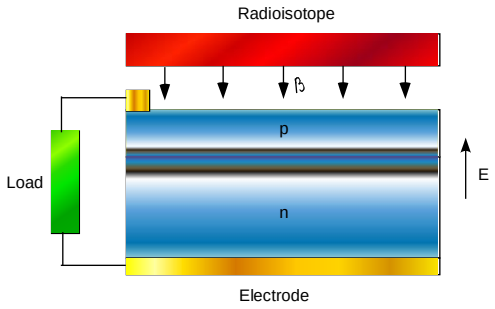

Figure 1-7: Direct conversion method

research. It appears in the literature that most betavoltaic battery models overpredict the experimental results [9-13]. Therefore, a better model and design analyses are required. The objectives of this research are to develop a better model and improve the design analyses of the betavoltaic battery.

1.3 Organization of the Dissertation

The second chapter provides a Literature Review and explains the key principles of betavoltaic battery operation. It shows that an improvement in the theoretical model is needed. The third chapter of the dissertation provides an MCNP model of Ni-63 with a silicon betavoltaic battery. Simulated modeling results are compared to some experimental results. The strengths and weaknesses of betavoltaic battery design are discussed. A source model using PENELOPE is developed in chapter four. The beta flux for titanium tritide is compared to the experimental results. Different tritiated metal sources are compared and source thicknesses were optimized. In the fifth chapter, the results from the PENELOPE model for titanium tritide with silicon carbide are

compared to experimental results. The designs and simulated results for beryllium tritide with silicon and silicon carbide are compared. Finally, the conclusions are drawn and the future work is provided in chapter six.

1.4 References

[1] Prelas, M., et al., *Nuclear Batteries and Radioisotopes*. 2016: Springer International Publishing.

[2] Bower, K.E., et al., *Polymers, Phosphors, and Voltaics for Radioisotope Microbatteries*. 2002: CRC Press.

[3] Wu, K., C. Dai, and H. Guo. *A theoretical study on silicon betavoltaics using Ni-63*. in *Nano/Micro Engineered and Molecular Systems (NEMS), 2011 IEEE International Conference on*. 2011. IEEE.

[4] Yakubova, G.N., *Nuclear Batteries with Tritium and Promethium-147 Radioactive Sources*. 2010, University of Illinois.

[5] Popa-Simil, L., *Advanced Nano-Nuclear Program Proposal*. 2010.

[6] Yang, J. and T. Caillat, *Thermoelectric materials for space and automotive power generation.* MRS bulletin, 2006. **31**(3): p. 224-229.

[7] Sychov, M., et al., *Alpha indirect conversion radioisotope power source.* Applied Radiation and Isotopes, 2008. **66**(2): p. 173-177.

[8] Li, H., et al., *Self-reciprocating radioisotope-powered cantilever.* Journal of Applied Physics, 2002. **92**(2): p. 1122-1127.

[9] Tang, X., et al., *Optimization design and analysis of Si-63Ni betavoltaic battery.* Science China Technological Sciences, 2012. **55**(4): p. 990-996.

[10] Tang, X., et al., *Optimization design of GaN betavoltaic microbattery.* Science China Technological Sciences, 2012. **55**(3): p. 659-664.

[11] Honsberg, C., et al. *GaN betavoltaic energy converters*. in *Photovoltaic Specialists Conference, 2005. Conference Record of the Thirty-first IEEE*. 2005. IEEE.

[12] Mohamadian, M., S. Feghhi, and H. Afarideh. *Conceptual design of GaN betavoltaic battery using in cardiac pacemaker*. in *Proceedings of 13th International Conf on Emerging of Nuclear Energy Systems (ICENES), Istanbul, Turkey*. 2007.

[13] San, H., et al., *Design and Simulation of GaN based Schottky Betavoltaic Nuclear Micro-battery.* Applied Radiation and Isotopes, 2013.

CHAPTER 2: PRINCIPLES OF BETAVOLTAIC BATTERY DESIGN

[publication information: Tariq R. Alam and Mark A. Pierson, Principles of Betavoltaic Battery Design, Journal of Energy and Power Sources, Vol 2, No. 1, June 30, 2016]

2.1 Abstract

Advancements in nanotechnology and electronics require next generation power sources on the order of micron size that can provide long service life. There are also needs for miniaturized on-chip power supplies, and longevity of the power sources in difficult to access areas such as on spacecraft, or in underground, undersea, polar regions and high mountainous regions. A betavoltaic battery has the potential to fulfill these requirements. It consists of a beta emitting radioisotope and a semiconductor. The battery design requires optimization of both the radioisotope selection and the semiconductor materials. The selection of a radioisotope is contingent upon battery applications. The amount of radioactivity is also optimized to minimize self-absorption. In addition, the design of a betavoltaic battery entails optimization of semiconductor parameters such as doping concentrations, minority carrier diffusion lengths, width of the depletion region, surface geometry, thickness, resistance, and temperature to increase the efficiency and maximum power output. However, the design and optimization criteria of betavoltaic batteries are not well documented in the literature. This article provides a critical review of the literature, summarizes the key design and operational principles, and gives an original analysis on end-to-end design of betavoltaic batteries including electron transport and semiconductor charge collection. Only by better understanding the state-of-the-art of betavoltaic

battery theory and technology can significant improvement in performance be made. The literature in this area suggests that further research is needed.

Keywords: betavoltaic battery, nuclear battery, radioisotope battery

2.2 Introduction

This article discusses the state-of-the-art in the area of betavoltaic batteries including theory of operation, design parameters, and recommendations for further improvement. Following a critical analysis of the literature, key principles are developed for betavoltaic battery design.

Betavoltaic batteries fall under the classification of nuclear batteries, which is a large area as shown in Figure 2-1. Betavoltaic batteries directly convert the radioactive decay energy of

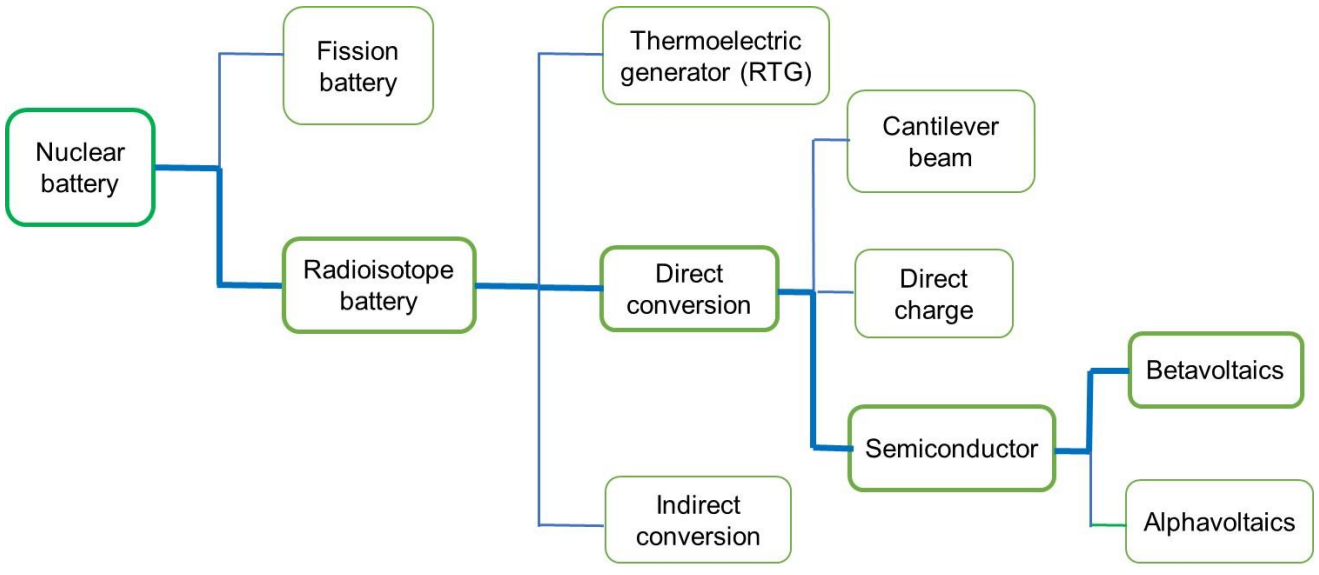

Figure 2-1: Nuclear battery classifications

a beta emitting radioisotope into electrical energy employing a semiconductor method of charge collection. Betavoltaic batteries have the advantage that they can be made into very small, reliable, and durable power sources for micro scale applications. Betavoltaic batteries can be further divided into different categories based whether they are a solid or liquid. Solid betavoltaic batteries can have either crystalline or amorphous structures.

Betavoltaic batteries are not new. The concept of radioisotope batteries was first suggested by Mosely in 1913 [1]. A betavoltaic battery design was first investigated by Rappaport at Radio Corporation of America (RCA) in 1954 [2] and later a radioactive battery using an intrinsic semiconductor was patented in 1956 [3-8]. Alphavoltaic and betavoltaic batteries were described by Pfann and Olsen [6] in 1954, where Pfann observed the lattice damage of semiconductors due to irradiation of high energy alpha and beta particles [1]. As a result, low energy betavoltaic batteries became a popular research topic in this area. In the 1970s, betavoltaics made of p-n junctions of Si at Donald Douglas Lab were used in clinical trials for pacemakers [9, 10]. In early 1970, Olsen [11] suggested that betavoltaic batteries using wide and indirect band gap semiconductors would have higher efficiency. Since 1989, many researchers [8] have worked on different semiconductor materials such as Si, AlGaAs, amorphous Si (a-Si), porous Si, SiC, and GaN. Many of these semiconductors materials were initially developed for solar photovoltaic applications. They found that wide band gap semiconductors have advantages of higher open circuit voltage, higher conversion efficiency, and greater radiation resistance.

Development of betavoltaic batteries has drawn additional researchers in recent years due to advancements in nanotechnology. Small size, reliability, and long lasting durable power sources are required for future generations of electronics. Betavoltaic batteries are very promising

sources of power that can fulfill these requirements. They can be miniaturized to the size of a human hair [12]. On the other hand, miniaturization of chemical batteries is restricted by their low energy density [13]. As an alternative, some researchers are working on scaling down power sources from fossil fuels and fuel cells. However, this is difficult because one must replenish the liquid fuel supply while eliminating byproducts inside the electronics. It also results in a low energy density even though it is 5 to 10 times better [13] than lithium ion batteries. A betavoltaic battery has an energy density that is 10^2 to 10^4 times [14] higher than that of chemical or fossil fuels. It has a long lifetime potential of several tens of years to several hundreds of years. Betavoltaic batteries are light, tiny, and integrated with the semiconductors to supply on-chip power [14, 15] without any performance compromise to the surrounding environment.

Betavoltaic batteries have applications in micro electro mechanical systems (MEMS), remote sensors, and implantable medical devices [16] such as pacemakers [10]. Due to their high energy density, long lifetime, and anti-jamming capabilities, they can also be used for remote applications including powering scientific apparatus in spacecraft, in undersea exploration, in the oil and mining industries, underground, in polar regions, in high mountainous regions, in military equipment, in sensor networks for environmental monitoring, and in bridges with embedded sensors [7, 15, 17]. Betavoltaic batteries are particularly useful for applications where solar photovoltaics are not a viable power option. They mainly work in low power electronics that require nano power sources [18]. Some researchers [10, 19] have proposed the idea of hybrid batteries for trickle charging of rechargeable chemical batteries. In other words, a betavoltaic battery can be used in combination with rechargeable chemical batteries and supercapacitors for trickle charging. Trickle charging is effective for electronics that only require intermittent power;

such an application is that of radiofrequency identification (RFID) sensors. Betavoltaic batteries can also provide an on-chip-battery to power next generation sensors and low power processors without the need for an external power source.

The topic of betavoltaic batteries is an interdisciplinary field that interfaces with energy harvesting, semiconductor theory in electrical engineering, and radiation transport in materials in nuclear engineering. They have many similarities with diode radiation detectors, which will be discussed later. Since this article is focused toward nuclear engineers and scientists, some additional discussion on semiconductor theory regarding betavoltaic battery design are provided. This article includes the theory of operation for betavoltaic batteries, a discussion on radiation damage threshold for betavoltaic batteries, the design and analysis of beta emitting radioisotope sources, radiation transport in semiconductors, semiconductor theory, a critical review of betavoltaic battery results, and a highlight of principles of betavoltaic battery design.

2.3 Basic Operation of Betavoltaic Batteries

An analysis of betavoltaic batteries is useful to identify design parameters and their optimization in order to understand the limitations and opportunities for further improvement. Betavoltaic batteries convert the kinetic energy of beta particles into electrical energy (Figure 2-2). However, not all the kinetic energy of the beta particles contributes toward generating electron-hole pairs (EHPs) and a large percentage of the energy is lost to the lattice structure of the semiconductors by phonon interaction and through x-ray generation [8] [20].

It is important to study the behavior of beta particles in semiconductor materials to optimize the battery design. In order to do so, it is also important to understand how a semiconductor behaves differently from other materials.

The conductivity of a semiconductor changes with temperature as a semiconductor behaves like an insulator at absolute zero temperature. However, as the temperature increases, it conducts more and more electrons. Thus, it behaves like a metal at higher temperatures. When thermal energy is absorbed by the semiconductor lattice structure, electrons are released by breaking the bonds with neighboring atoms allowing them to move freely in the crystal. In the absence of an electric field, the free electrons may take part in re-bonding again with neighboring atoms after giving off their energy to other electrons and lattice vibration. This unique dynamic process takes place in semiconductors at temperatures higher than absolute zero.

An intrinsic semiconductor refers to a pure semiconductor material with no impurities in the crystal lattice. The process of adding impurity atoms by diffusion is called doping. Doping

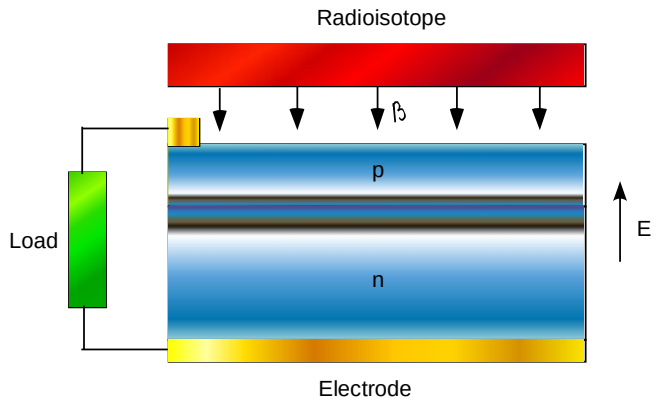

Figure 2-2: A betavoltaic battery design

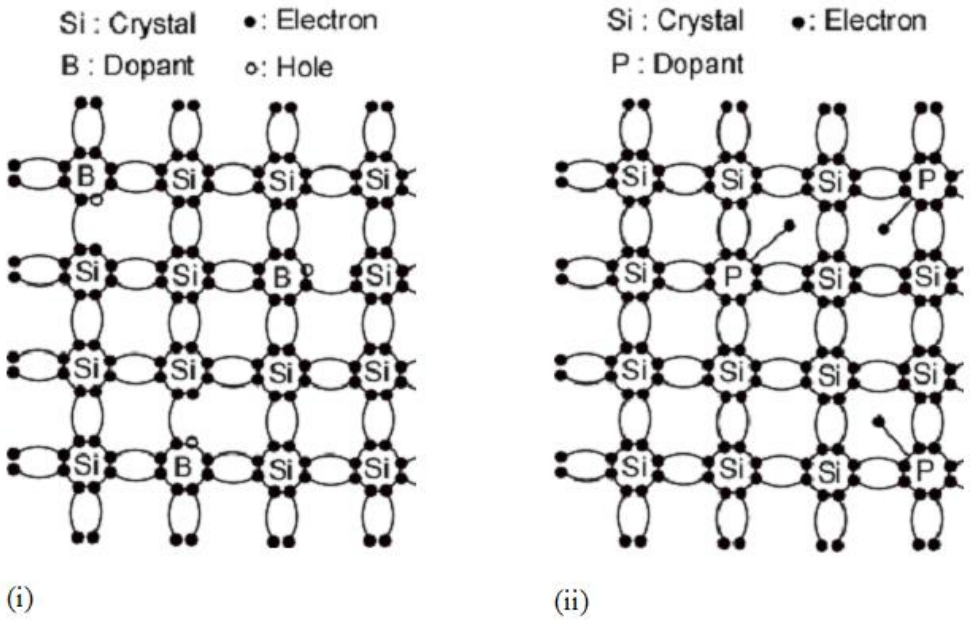

Figure 2-3: Holes or electrons in (i) p-type and (ii) n-type silicon semiconductor lattice

is a controlled method to create excessive holes and electrons in the semiconductors. When the semiconductor is doped with trivalent atoms such as boron, it creates a hole in the process of bonding with the four surrounding silicon atoms. A hole, or vacancy, is the name given to the absence of an electron in the bond. However, holes along with electrons contribute to the total current. Those semiconductors which have excessive holes are called p-type semiconductors because holes are similar to a positive charge in that they attract an electron to the vacant bond. However, a p-type semiconductor is not really positively charged, and all the atoms are neutral. Similarly, if it is doped with a pentavalent atom such as phosphorous, it will generate excessive electrons in the semiconductor. This type of semiconductor is called an n-type semiconductor due to the negative charge of the electrons, which are easily freed from the lattice. An n-type semiconductor is also neutrally charged similar to a p-type semiconductor.

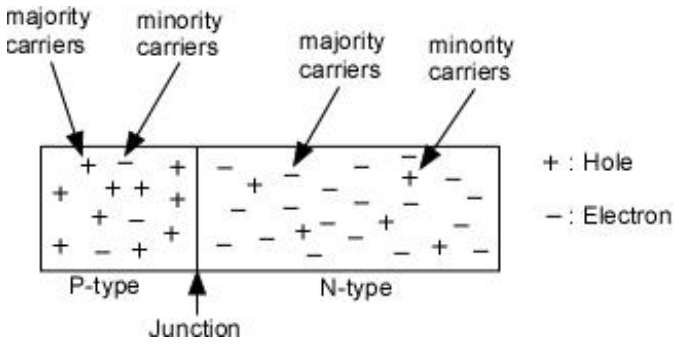

Figure 2-4: Majority and minority carriers for a p-type and an n-type semiconductor prior to diffusion

Figure 2-3 shows the majority carriers, which are the holes and electrons for a p-type and an n-type silicon semiconductor respectively. Both the majority and the minority carriers for a p-type and an n-type semiconductor are shown in Figure 2-4. Holes and electrons always move in the opposite direction. When an electron jumps to a vacant bond, it leaves a vacancy behind. This is how holes in the semiconductor appear to move. When p-type and n-type semiconductor materials are placed together to form a p-n junction, the holes and electrons diffuse from regions of higher concentration to lower concentration.

This movement upsets the charge equilibrium of the atoms on either side of the junction and creates a space charge region and resulting electric field. When excess electrons of the donor atoms from the n-type region diffuse to the p-type region, they are attracted to the vacancies of the acceptor dopant atoms on the p-type region. As a result, the donor dopant atoms release electrons that are accepted by the acceptor atoms. By doing so, the mobile charge carriers around the junction become depleted. As a result, a space charge region forms around the junction, which is also called the depletion region. A depletion region of about 1 μm thickness (depending on the dopant

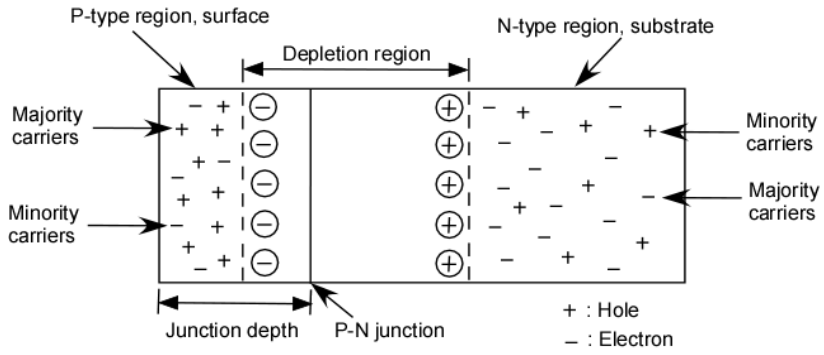

Figure 2-5: Formation of a depletion region for a p-n junction semiconductor after diffusion of the carriers

concentration and semiconductor material) occurs around the p-n junction. The dopant atoms on the p-side and the n-side of the depletion region become negatively and positively charged ions, respectively. This effect generates a potential, known as the built-in-potential, in the depletion region. It acts as a barrier for further diffusion of holes and electrons. Thus, an equilibrium condition is reached by the repulsion forces of the ionized atoms at the edges of the depletion region. Figure 2-5 shows the formation of the depletion region for a p-n junction after the diffusion of holes and electrons. It deliberately shows that the depletion region is asymmetric around the junction. This varies based on the difference in dopant concentrations inside the p-type and n-type regions. In betavoltaics, typically the p-type region is heavily doped. Therefore, the higher concentration of holes from the p-type region diffuses further into the n-type region due to the large diffusion gradient. As a result, the depletion region extends more into the n-type region in

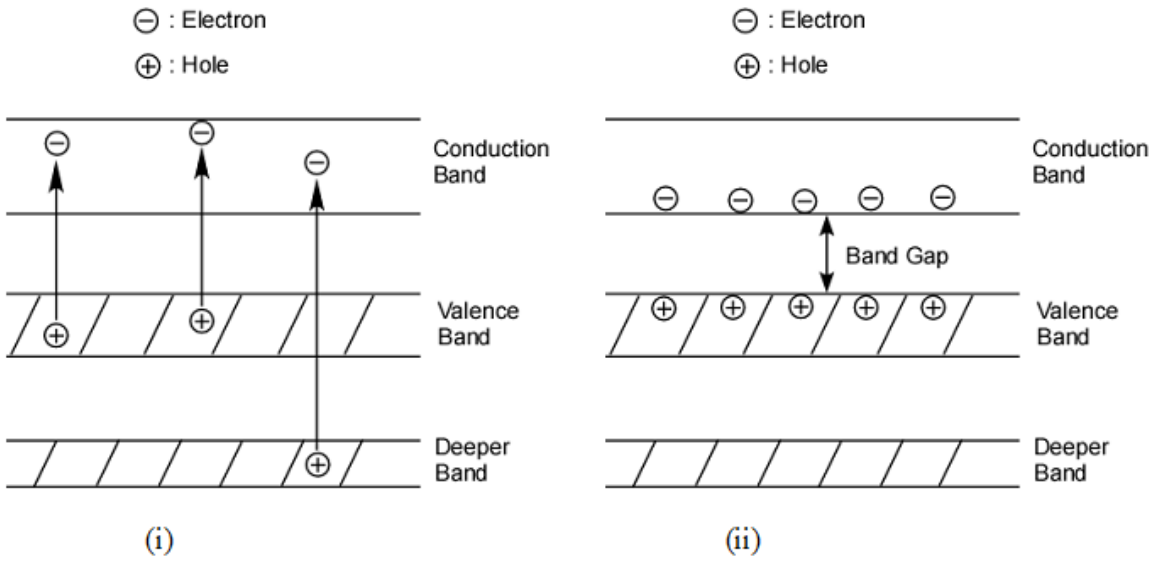

Figure 2-6: Generation of Electron Hole Pairs by (i) excitation and (ii) de-excitation process

this case. The resulting width of the depletion region is very important for betavoltaic battery design.

A key aspect of betavoltaic battery design is to understand how electron hole pairs (EHPs) are generated in the semiconductor. A band diagram explains the generation of EHPs in a simple multi-step method [21] as shown in Figure 2-6. The first step is called the excitation step. In this step, when the electrons in the valence band receive sufficient energy from collisions with the beta particles, they jump to the conduction band. Some electrons may even jump from the deeper bands below the valence band. This process leaves holes in the valence and deeper bands as well as increases the number of electrons in the conduction band. This process takes about 10 ps.

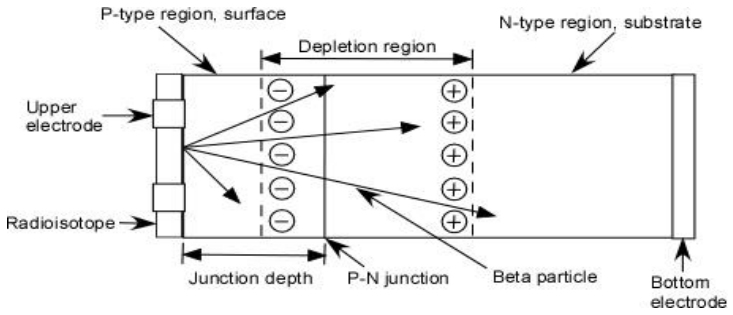

Figure 2-7: Solid p-n junction betavoltaic battery design

The next step is called the de-excitation step. In this step, electrons move to the bottom of the conduction band and holes move to the top of the valence band. Additional EHPs are generated during the de-excitation process. There is also some energy imparted to the crystal lattice structure due to the conservation of momentum that generates phonons during this process. There are many modes of crystal vibrations available at lower energies than the band gap energy. This multi-step band diagram method explains why the required energy to generate one EHP is higher than the band gap energy of the semiconductor. On average, the energy to generate one EHP is approximately three times the band gap energy. For example, the average energy required to generate one EHP in silicon is 3.64 eV, which has a band gap of 1.12 eV. It takes into account the thermalization and phonon losses in the process of EHP generation [22, 23].

There are also different types of junctions available for solid betavoltaic batteries such as a Schottky junction or a p-n junction. A beta emitting radioisotope can be placed on either the p-type region surface or n-type region surface of the semiconductor. A typical solid p-n junction betavoltaic battery design is shown in Figure 2-7 where the radioisotope is placed on the p-type region surface. This is because many semiconductors are built up with a thick n-type layer on a

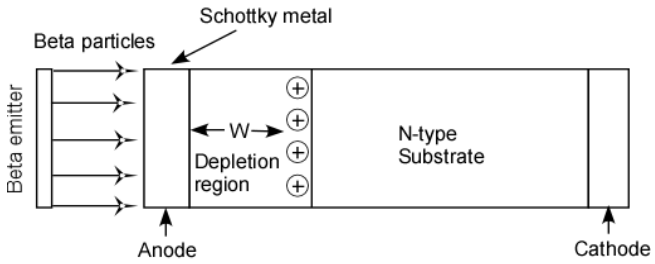

Figure 2-8: Schottky betavoltaic battery design

substrate using chemical vapor deposition. The p-type region is then created using diffusion of the dopant atoms, which is typically much thinner than the n-type region. Placing the radioisotope on the thinner p-type side allows the beta particles to reach the depletion region.

A Schottky diode is built with a Schottky metal and either a p-type or n-type substrate. The depletion region is formed in-between the metal contact and the p-type or n-type region. This type of contact is known as a Schottky contact and the metal used to create this contact is known as a Schottky metal. Examples of Schottky metals are nickel (Ni) and nickel silicide (Ni_2Si). A typical Schottky junction betavoltaic battery is shown in Figure 2-8.

The potential barrier developed in the Schottky contact is called a Schottky barrier. Schottky junction betavoltaics are low cost and easier to fabricate. They are typically useful for semiconductors that are difficult to grow a p-type layer on the substrate such as GaN. However, the power output of a Schottky junction betavoltaic battery is low because most of the beta particles are absorbed in the Schottky metal before reaching the depletion region.

Betavoltaics have a similar operating principle to that of photovoltaics where a photon is converted into electricity. One of the major differences between betavoltaics and photovoltaics

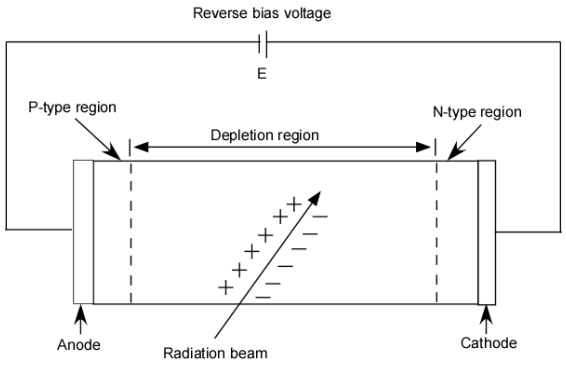

Figure 2-9: A typical radiation detector made of p-n junction semiconductor

are that each high energy beta particle can create thousands of electron-hole pairs (EHPs) whereas photons from sunlight are of much lower energy and generate only one EHP per photon absorption. The other major differences between betavoltaics and photovoltaics are that high energy beta particles can penetrate deeply into a silicon wafer [19] whereas the low energy photon penetration depth depends on the absorption coefficient of the materials. On the other hand, the principle of operation for both betavoltaic batteries and radiation detectors is similar. However, a radiation detector as shown in Figure 2-9 requires an application of an external high reverse bias voltage on the order of kilo-volts. This increases the internal electric field and creates a wide depletion region. Like betavoltaic batteries, a large depletion width is necessary to collect all the EHPs generated by the incident radiation beam. In radiation detectors, it is also useful to avoid any false positive signals. The collected charges in a radiation detector are registered in an external circuitry as a pulse signal for analysis, whereas a betavoltaic battery supplies a much higher number of charges to an external electrical load.

The design of a typical betavoltaic battery consists of an upper electrode, a p-type region (doped surface region), a depletion region, an n-type region (doped substrate), and a bottom electrode [24] as shown in Figure 2-10(a). The basic principle of this battery is to generate electron-hole pairs (EHPs) in the semiconductor materials by the beta particles and collect them at the electrodes. The energetic beta particles emitted from the radioisotope enter the semiconductor, which in turn creates EHPs through collisions, excitations, and ionization. The number of EHPs generated depends on the incident energy of the individual beta particles. Each beta particle generates several tens of thousands of EHPs [25]. Betavoltaic batteries convert a low number of high energy beta particles into a high number of low energy EHPs. To achieve maximum power from a betavoltaic battery, it is important to maximize the separation of the EHPs being generated while minimizing recombination. Recombination of the EHPs threatens energy loss in the betavoltaics. However, electron energy may also be lost due to collisions with other electrons or due to lattice vibrations resulting in a temperature increase. The separation mechanism of EHPs needs to be analyzed for maximum collection efficiency of the EHPs. If the radioisotope is placed on the p-type region of the semiconductor, electrons with higher energies from the p-type region will cross the depletion region to enter the n-type region. The EHPs generated on either the p-type or n-type region need to reach the depletion region through diffusion to be collected. Therefore, the goal is to form as many EHPs in the depletion region as possible, as opposed to outside the depletion region. Hence, a thin p-type layer is typically used in the design. The EHPs generated in the depletion region are swept across to each side due to the built-in potential of the space charge as shown in Figure 2-10(b) and Figure 2-10(c) for a p-n junction and Schottky junction, respectively. The electric field in the depletion region sends the electrons and holes to the n-type and p-type regions, respectively. The electrode on the p-type region that collects holes is called the

anode [16, 18, 26, 27]. Similarly, the electrode on the n-type region that collects electrons is called the cathode. However, this contradicts the common notation used for batteries, where the negative and positive terminals of a battery are called the anode and the cathode, respectively [28]. On the other hand, if the radioisotope is placed on the n-type side of the semiconductor, it works using similar principles as placing the radioisotope on the p-type side. However, very few researchers [14, 19, 29] have placed the radioisotope on the n-type side of the semiconductor where p-type substrates were used.

One of the first steps is to calculate the EHP generation profile inside the semiconductor material. However, this will be discussed in more detail in section IV of radioisotopes. Once it is known where and how many EHPs are formed from the beta particles, the collection process of EHPs are then important to understand for optimization of betavoltaic battery design. Not many researchers provided a good model for the charge transport within the semiconductor to the electrodes but the few that did are discussed below.

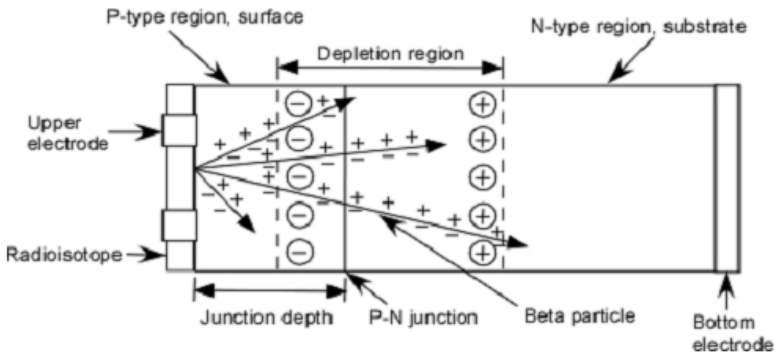

(a)

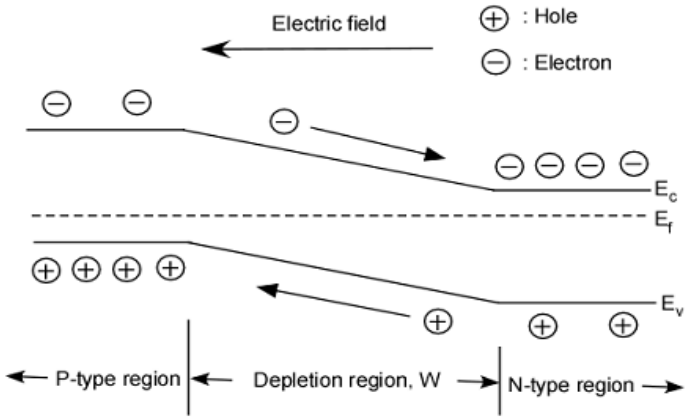

(b)

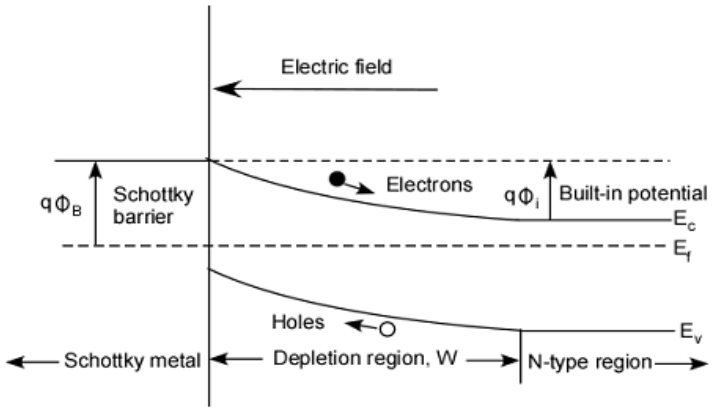

(c)

Figure 2-10: (a) EHP generation in a solid betavoltaic p-n junction battery design (b) Electron and hole movement inside the depletion region of a p-n junction and (c) a Schottky junction

One of the design requirements of betavoltaic batteries is to increase the depletion width in order to increase the charge collection efficiency. Charge collection efficiency also depends on the particular charge carrier's drift length, which is related to carrier mobility, electric field intensity, and carrier lifetime [7]. The improvement of semiconductor films by minimizing the dislocation density will also increase the charge collection efficiency. However, it is difficult to create thick high quality crystal layers for wide band gap semiconductors due to fabrication limitations. Creating a wider depletion region in GaN, which is a wide band gap semiconductor, is limited by difficulties with p-type doping. GaN typically has an n-type conductivity due to residual impurities. It is hard to create intrinsic and p-type layers for GaN. For example, Cheng et al [5] gradually developed p-i-n GaN from p-n GaN and p-u-n GaN. The unintentionally doped (u-type) layer is the layer grown with nominal doping that has an electron concentration over 5×10^{16} cm^{-3} due to residual impurities. To create an intrinsic layer, the electron concentration of the u-type material needs to be reduced. This was achieved by doping the u-region with Fe as a compensator. An intrinsic region thickness of 0.9 μm is achieved in this process with a Mg-doped p-type layer thickness of 0.05 μm and Si-doped n-type layer thickness of 1 μm to form p-i-n GaN. The collection efficiency of the EHPs generated within the depletion region is almost 100%. It was assumed in a simplified model based on collection efficiency of EHPs [19] that all the EHPs generated in the depletion region and within one minority carrier diffusion length from the depletion region mostly contribute to create a current. The EHP collection probability for the carriers generated outside the depletion region is then approximated by [24, 30, 31] equation (1)

$$CE = 1 - tanh\frac{d}{L}, \qquad (1)$$

where *CE* is the collection probability of an EHP, *d* is the distance from the depletion region boundary and *L* is the minority carrier diffusion length for either the n-type or p-type material as appropriate. This indicates that the junction depth and the width of the depletion region need to be adjusted according to the penetration depth of the beta particles. The energy of the beta particles should be deposited in the depletion region as much as possible for maximum EHP collection [32]. The collection efficiency of the EHPs generated outside the depletion region depends on the distance from the depletion region. Therefore, the wider the depletion region is, the greater the number of EHPs that would be collected. Besides the simplified model, the collection EHPs can also be calculated by the drift-diffusion model [14]. The collection of EHPs generated outside the depletion region is solved by diffusion to the depletion region.

The width of the depletion region is an important parameter for betavoltaic battery design. The width of the depletion region for a p-n junction can be calculated by (2) and (3) [24].

$$W = \sqrt{V_{bi}\,(\frac{2\varepsilon_r\varepsilon_0}{q})(\frac{N_a+N_d}{N_aN_d})}\,, \qquad (2)$$

$$V_{bi} = \frac{kT}{q}(ln\frac{N_aN_d}{n_i^2}), \qquad (3)$$

where V_{bi} is the built-in potential barrier, ε_r and ε_o are the dielectric constants in the region and in vacuum, respectively, N_a and N_d are the doping concentrations of the p-type (acceptor) and n-type (donor) regions and n_i is the intrinsic carrier concentration for a pure, undoped semiconductor.

From basic semiconductor physics, the width of the depletion region for a Schottky junction can be expressed by (4) [25]

$$W = \sqrt{\frac{2\varepsilon_s V_{bi}}{qN_D}} = \sqrt{\frac{2\varepsilon_s(\phi_B - \frac{kT}{q} ln(\frac{N_C}{N_D}))}{qN_D}}, \quad (4)$$

where ε_s is the relative dielectric constant of the semiconductor, V_{bi} is the built-in potential barrier, q is the electron charge, N_D is the dopant concentration of the semiconductor material, ϕ_B is the Schottky barrier height, k is the Boltzmann constant, T is the temperature in Kelvin, and N_C is the effective density of states in the conduction band of the semiconductor.

From these equations, it can be seen that the dopant concentration is one of the vital parameters for battery design. The dopant concentration affects depletion width, short circuit current, and open circuit voltage [24, 31]. A lower dopant concentration increases the depletion width and minority carrier diffusion length, which in turn increases the charge collection efficiency. A lower concentration is favorable for increasing the short circuit current of a betavoltaic battery. However, it is not a favorable condition for increasing the open circuit voltage. A lower dopant concentration also increases the leakage current [14], which in turn decreases the open circuit voltage. Leakage current results from all types of recombinations including the random motion of the carriers that can overcome the built-in potential barrier and recombine. The built-in potential barrier decreases with lower dopant concertation. Therefore, the dopant concentration needs to be optimized in order to achieve the best battery performance. In an analysis by Tang et al [24], heavy doping on the order of magnitude of 10^{18} cm^{-3} to 10^{19} cm^{-3} in the p-type region and light doping on the order of magnitude of 10^{16} cm^{-3} to 10^{17} cm^{-3} in the n-type region were found optimal for Si with Ni-63 at a shallow junction depth of about 0.3 μm for maximum power output. A larger difference in the doping concentration on each side of the junction increases the width of the depletion region. However, a significant difference in doping concentration can

lead to reduced power output due to increased leakage current [33], which results from increased recombination due to the lattice mismatch and defects. A small change in leakage current, which is usually several nA, has a large impact on the performance of betavoltaic batteries. The reason is the current generated due to irradiation in the battery is in the range of nA to μA, whereas the current range for a solar cell is 1 mA to 100 mA. Thus, an increase in leakage current can rapidly decrease the power output by a larger percentage in the case of a betavoltaic cell. This effect can be minimized by introducing interlayers in the semiconductor resulting in a higher conversion efficiency. The leakage current in a semiconductor such as GaAs consists of perimeter surface recombination and bulk junction recombination [34]. The leakage current can be reduced by forming perimeter depletion layers (PDLs) that create an isolation effect. It was found that a larger PDL is formed using a p^+-p-n^+ junction compared with three other investigated junctions such as n^+-p-p^+, p^+-n-n^+, n^+-n-p^+, where p^+ and n^+ regions refer to more heavily doped regions. The minimum leakage current of approximately 10^{-11} A was found for the p^+-p-n^+ junction.

Aside from the leakage current, the charge collection can be hampered from a wide depletion region. If the minority carrier diffusion lengths are smaller than the width of the depletion region, charge collection will be reduced. For example, a comparison [34] of ideal and experimental short circuit current showed that only half of the EHPs were collected due to the minority carrier diffusion lengths being half of the depletion width. It was concluded that a multi-junction structure would be a better design instead of a wider depletion region with a single junction. The suggested multi-junctions are six to ten for GaAs when the radioisotope is Ni-63. Another approach to resolve problems associated with a wider depletion region is to increase the concentration of energy deposition in a narrow region. An analysis compared both the ratio of

energy deposition on the top layer and the range of beta particles in homojunction and heterojunction semiconductors. A heterojunction of Si/SiC showed the best energy concentration in the depletion region in a study of homojunctions of Si, GaN, GaAs, SiC, InGaP and heterojunctions of these semiconductors with Si [6]. The results for a Si/SiC junction indicated 24.6% of total energy deposition in the top layer thickness of 0.3 μm with a penetration depth of 2.1 μm for beta particles from Ni-63. It reduced the depletion region thickness to 1.8 μm with a maximum energy deposition in the depletion region instead of in the top layer of the device. The radiation tolerance of the device was improved by introducing SiC, as it has better radiation tolerance than that of Si. Radiation tolerance will be discussed further in the next section.

The maximum power output and conversion efficiency of betavoltaics can be improved by two different methods: using a high energy radioisotope source and improving or developing a new type of p-n junction [35]. The performance of a betavoltaic is also dependent on the operating temperature [15]. Diffusion length, intrinsic carrier concentration, and carrier mobility in semiconductors are all a function of temperature. Diffusion length and leakage current are directly related to the short circuit current and open circuit voltage of the device. The leakage current is further dependent on the intrinsic carrier concentration. An increase in temperature decreases device performance by reduced open circuit voltage with a low fill factor. The short circuit current is negligibly affected by change in temperature. The power output and efficiency of betavoltaics decrease almost linearly with an increase in temperature.

An equivalent circuit model of a betavoltaic cell as shown in Figure 2-11(a) consists of a current source, diode, shunt resistance, series resistance, and a load resistance that represent respectively a radioisotope, a semiconductor, resistance due to leakage and carrier-recombination,

internal resistance of the diode including electrode contact, and a load to receive power. The generated current can be expressed by (5) and (6) [36].

$$I = I_{\beta} - I_{bk} - I_{sh}, \qquad (5)$$

$$I = I_{\beta} - I_0 \left[exp\left(\frac{q(V+IR_s)}{nkT}\right) - 1 \right] - \frac{V+IR_s}{R_{sh}}, \qquad (6)$$

where I_{β} is the radioisotope generated current, I_0 is the leakage current, R_s is the series resistance, R_{sh} is the shunt resistance, q is the electron charge, n is the ideality factor that defines

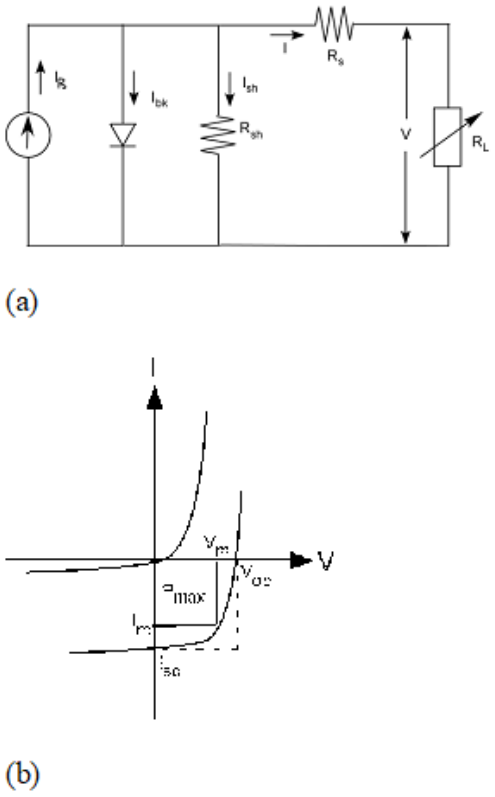

Figure 2-11: (a) Equivalent circuit model of a P-N junction betavoltaic battery and (b) current-voltage characteristics of a betavoltaic battery

how closely it follows ideal diode current-voltage characteristics (n=1 for an ideal diode), *k* is the Boltzmann constant, and *T* is the absolute temperature. Open circuit voltage and short circuit current are found from the equation by setting $I = 0$ and $V = 0$ respectively. From the equivalent circuit model, it can be seen that open circuit voltage depends on the shunt resistance and has a proportional relationship with it. Similarly, the short circuit current has a reciprocal relationship with the series resistance. In an ideal case, the series and shunt resistance are zero and infinite respectively for betavoltaic cells. Figure 2-11(b) shows the current voltage relationship of a betavoltaic battery in comparison with an ideal diode. Current is negative for betavoltaic batteries as it supplies the power. The fill factor is an important parameter that determines the proximity of the battery output at full operational load to the theoretical maximum power output. Fill factor is defined by (7)

$$FF = \frac{P_{max}}{P_{th.\,max}} = \frac{I_m V_m}{I_{sc} V_{oc}}, \qquad (7)$$

where I_m, V_m are the maximum current and voltage and I_{sc}, V_{oc} are the short circuit current and open circuit voltage.

The design of electrodes also affects the performance of a betavoltaic battery. The presence of an electrode in-between the radioisotope and the p-type region works as a dead layer to the betavoltaic batteries. It causes some beta particles to be absorbed in it and most to be reflected back. As a result, the effective energy deposited in the semiconductor is much less than the incident energy [37]. To overcome this loss, the cross-sectional area of a high-Z metal such as Au [20] can be reduced or replaced by a low-Z metal such as Al. A well designed interdigit device,

such as a comb-shaped electrode [33] with optimum interspacing instead of continuous metal, increases the short circuit current by reducing the backscattering yield of the radioisotope [10].

In summary, the semiconductor material in a betavoltaic battery design needs optimization in order to maximize power output and efficiency. This includes doping concentrations, junction depth, width of the depletion region, minority carrier diffusion lengths, leakage current, internal defects, junction type, interlayer structure, temperature effect, and electrodes. Besides the design parameters of semiconductors, the radiation tolerance of semiconductors also needs to be considered in order to maintain consistent battery performance. This topic is taken up in the next section.

2.4 Radiation Hardness

Betavoltaic battery performance can suffer from degradation of the semiconductor materials due to irradiation over time. When this occurs, the power output deteriorates and the battery may fail prematurely. Different measurements and calculations have been used to determine radiation damage. These include deterioration of the power output, normalized power output decay, capacitance voltage (CV), deep level transient spectroscopy (DLTS), minority carrier diffusion length, charge carrier concentration, open circuit voltage, and radiation damage factor. However, a decay in the power output may not be an indication of radiation degradation as the radioactive source also decays based on its half-life. Therefore, the source decay also needs to be considered when measuring radiation damage by means of power output.

The radiation damage by beta particles to the semiconductor material depends on both the particle energy emitted by the radioisotope and the radiation hardness of the semiconductor material. The probability of radiation damage in materials can be minimized by reducing the energy of incident beta particle radiation and increasing the strength of the atomic bonds in the materials [30]. In the process of the creation of radiation-induced defects, atomic bonds in the material are broken after absorbing enough radiation energy and then the released atom diffuses inside the material. Wide band gap materials have a higher bond strength with minimal diffusion. The lower diffusivity then increases the self-annealing effect of the materials. However, due to the low diffusivity of the wide band gap semiconductors, it is also difficult to dope them sufficiently to form a p-n junction.

GaN is a wide band gap semiconductor, which is one of the popular radiation tolerant materials used in betavoltaic batteries. It can also be used in space applications due to its radiation hardness. Ionascut-Nedelcescu et al. [38] determined the radiation hardness properties of GaN in an experiment where it was irradiated by electrons with an energy range of 300 keV to 1400 keV at room temperature to determine the threshold energy for damage. The electron threshold energy of GaN was found to be 440 keV with a measured atomic displacement energy of 19 ± 2 eV for Ga. The atomic displacement energy is a measure of the minimum kinetic energy required to displace an individual atom from its regular crystal lattice site to a defect position. There is no displacement energy found for the Nitrogen atoms, which indicates self-annealing is occurring. Self-annealing is a recombination of vacancy-interstitial pairs. If the distance between a vacancy-interstitial pair is small, the recombination takes place by diffusion and it is temperature dependent. Other radiation hard semiconductor materials are SiC, GaAs, $Al_{0.7}Ga_{0.3}N$, a-Si:H, AlGaAs, InP,

InGaP, and diamond. However, GaN is chosen over SiC by Mohamadian et al. [31] in their battery design for its slightly better radiation hardness and its larger heat capacity. The radiation hardness of GaN is also much higher than that of GaAs. It requires two orders of magnitude higher radiation fluence at the same energy to degrade GaN compared to GaAs. The reason why GaN has better radiation tolerant properties over many other semiconductor materials can be explained by its high bond strength over its minimal atomic displacement. Furthermore, it can be attributed to the presence of a high density of nitride materials, which have a low atomic number. Low atomic number materials reduce the interaction of core electrons in the lattice with the high energy radiation electrons. As a result, fewer defects occur due to radiation. For example, $Al_{0.7}Ga_{0.3}N$ with a wide band gap of 5.8 eV has a radiation resistance six times higher than Si, since Al and N have lower atomic numbers [30]. In addition to higher radiation tolerance, the use of wide band gap semiconductors will increase the power conversion efficiency [30] since their leakage current is very low. However, an arbitrary increase of the band gap will also reduce the conductivity of the semiconductors, which will hamper the charge collection in the semiconductor. Among all other radiation tolerant semiconductors, SiC and GaN are the most popular wide band gap semiconductors used in betavoltaic batteries.

There are some experimental results reported to investigate the radiation damage of semiconductors. They showed that there was no radiation damage for semiconductors irradiated by beta particle energies lower than the radiation threshold energy of the semiconductors. For example, some researchers reported no evidence of radiation damage for a Si p-n junction with Ni-63 (66.9 keV; max beta energy) [39], a p-i-n junction of SiC irradiated with P-33 (248.5 keV) [8], and a 4H-SiC p-n junction with Ni-63 (66.9 keV) [20] observed for six months, three months, and

ten days, respectively. However, radiation damage was observed in SiC, InP, GaN, and Si by some researchers [30, 40] when the semiconductors were irradiated by high energy electrons. In an experiment by Rybicki [40], both SiC and InP were irradiated by 1 MeV electrons. The result was that the radiation resistance of SiC was not much better than that of InP. In another experiment [30], a set of Si solar cells and n-type GaN were irradiated by Co-60 (317 keV) beta particles and gamma rays with a dose of 10 Mrad and 100 Mrad. The open circuit voltage and photoluminescence peak were then measured for the Si and GaN to analyze the radiation damage. The open circuit voltage is related to the minority carrier life-time in terms of diffusion length. A maximum reduction factor of five for the minority carrier life-time with a degradation voltage of 1.6% was observed for GaN whereas a reduction factor of 52 for the minority carrier lifetime with a degradation voltage of 25% was measured for Si solar cells. Therefore, GaN was found to be a better radiation tolerant material compared to Si, and it showed very little degradation even with a very high radiation dose from Co-60. On the other hand, a-Si:H is claimed to have superior radiation hardness, and is used in space applications for solar cells. Maturation of a-Si:H solar cells made it possible to have increased radiation hardness over crystalline semiconductors especially when operated at a low annealing temperature of 70°C. However, it was reported in an experiment by Deus [41] that a-Si:H had higher degradation than that of AlGaAs under a tritium (18.59 keV) gas atmosphere when the batteries were observed for 46 days. The efficiency decreased by 94% and 69% for a-Si:H and AlGaAs respectively. The radiation damage was high due to the high diffusion of H-3, which was about one H-3 atom per three Si atoms for thin film a-Si:H. The type and structural form (or phase state) of the radioisotope is believed to be the reason for the degradation. It was suggested that the radiation damage could be minimized by using tritiated titanium thin film instead of a free gas for the radioisotope form.

There were some techniques that can be employed to increase the radiation tolerance of semiconductors. For example, introduction of an intrinsic region in the junction [42] and a low doping concentration such as 2×10^{12} cm^{-3} in the intrinsic region [6] has been shown to improve the radiation degradation of the semiconductor materials in betavoltaic batteries. Non-crystalline structures like a liquid semiconductor may also limit the radiation damage [43].

In betavoltaic batteries, the radiation damage to the semiconductor depends on the beta particle energy, the atomic bond strength, and the migration barriers of vacancy and interstitial of the semiconductor, and the size of the atoms in the crystal lattice structure that are interacting with the impinging high energy beta particles. Wide band gap materials such as GaN and SiC showed much better radiation tolerance due to their above mentioned qualities. However, there is a trade-off for using wide band gap semiconductors, which must be considered. The charge (electron hole pairs) collection is difficult in wide band gap semiconductors due to their low diffusivities.

2.5 Radioisotopes

Not all the beta particles from the radioisotope reach the semiconductor due to self-shielding (or self-absorption). The energy deposited in the semiconductor depends on the volume of the radioisotope. The radioisotope thickness needs to be optimized to minimize self-shielding effects. The radioactivity available for use by the battery can be represented by the actual activity and the apparent activity. Actual activity is the inherent activity of the radioisotope depending on its specific activity and mass. Apparent activity is the effective activity that is emitted by the source and would be measured by a radiation detector. Apparent activity differs from actual activity due

to the self-absorption of the beta particles inside the source before they can exit [16], and it is always less than the actual activity. The apparent activity is given by (8) and (9) [18, 21],

$$\Phi = \frac{C}{\mu_m}(1 - e^{-\mu_m t_m}), \quad (8)$$

$$\mu_m = 0.017/E_{max}^{1.43}, \quad (9)$$

where C is the specific activity (mCi/mg), μ_m is the mass attenuation coefficient (cm^2/mg) of the radioactive source material, t_m is the mass thickness (mg/cm^2) of the radioactive source, and E_{max} is the maximum beta particle energy of the radioisotope in MeV. The variation in actual and apparent activity with mass thickness of Ni-63 is shown in Figure 2-12 for a surface area of 0.05×0.05 cm^2.

The radioisotope mass thickness (g/cm^2) is an important parameter for battery design because the surface activity (mCi/cm^2) of a radioisotope increases initially with an increase in mass

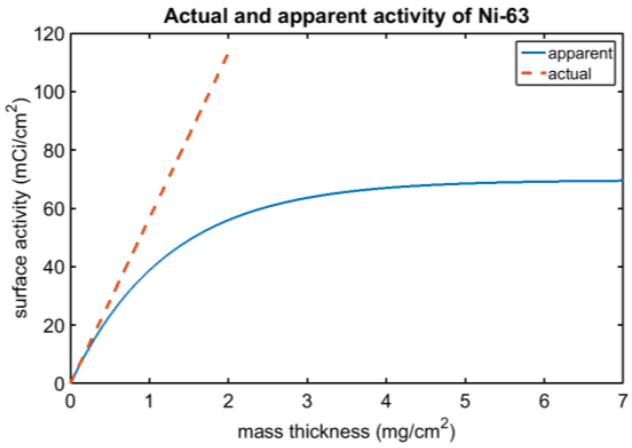

Figure 2-12: Plot of actual and apparent activity of Ni-63 versus its mass thickness

thickness (g/cm^2) but then saturates due to the self-absorption effect as shown in Figure 2-12. For Ni-63, the difference in actual and apparent activity becomes 32% at a mass thickness of 1 mg/cm^2 in this case. However, a mass thickness of 1 mg/cm^2 results in an activity that is 56% of the saturation value with a mass reduction of 86%. This analysis is useful for designing a radioisotope source with maximum utilization and reduced cost when the surface area of a betavoltaic battery is limited in size. Designing a betavoltaic battery with multiple betavoltaic cells stacked in series

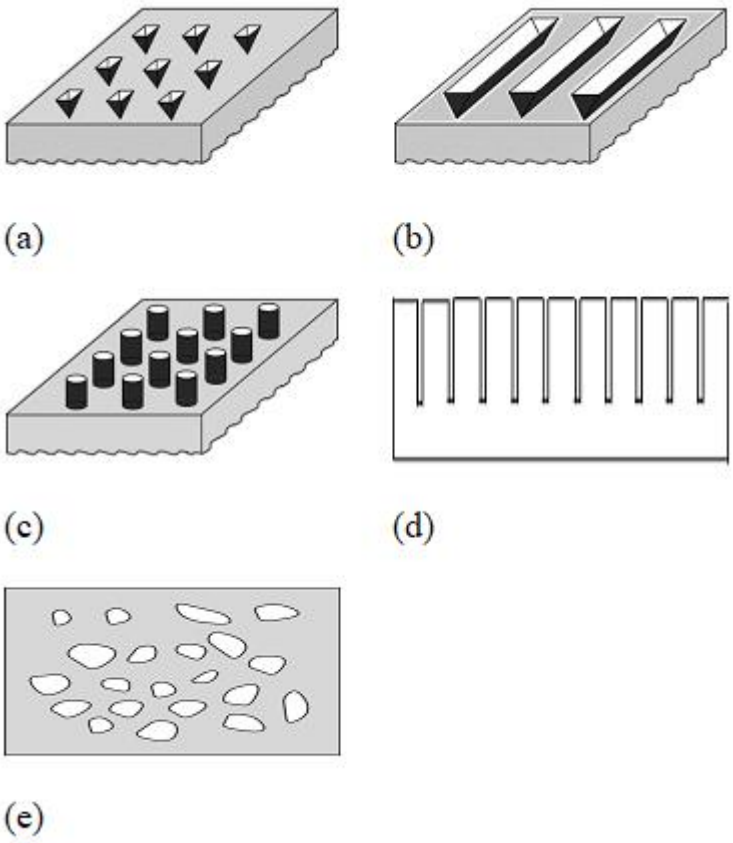

Figure 2-13: : Different surface geometries, (a) inverted pyramid (b) V-channel (c) cylindrical holes (d) porous (e) amorphous

or parallel, depending on the application can be an effective way to reduce the self-shielding effect. However, increasing the surface area of the radioisotope source and semiconductor can be another effective method of betavoltaic battery design to reduce the self-shielding effect. One way to increase the surface area is to modify the surface geometry of the semiconductor.

Aside from a planar surface, there are different surface geometries that can be used with semiconductors to increase the effective surface area, such as using inverted pyramids, a porous surface, or a hydrogenated amorphous material, as shown in Figure 2-13. They offer a larger surface area for the beta particles to enter the material resulting in greater energy deposition. A larger surface area will therefore generate higher power in betavoltaics [30].

To take full advantage of the modified semiconductors with an increased surface area, the recesses need to be filled with the radioisotope. However, the use of a solid planar radioisotope without filling the recesses in the semiconductor can still increase the energy conversion efficiency somewhat due to better trapping of the beta particles inside the recesses resulting in less backscattering off of the semiconductor surface. Using a liquid state for the radioisotope makes it much easier to fill the recesses of the modified surface geometry semiconductor. An experiment [39] was conducted using a radioisotope source of ^{63}NiCl/HCl solution with a bulk micromachined inverted pyramid Si p-n diode, which is similar to the technique used in solar cells. The surface area with the inverted pyramid geometry is increased by a factor of 1.85 compared to a planar surface. In comparison with the planar Si p-n diode for the same amount of radioactivity, the short circuit current, open circuit voltage and power output for the inverted pyramid array p-n Si diode increased by 18.67%, 11.3%, and 33.33% respectively.

Table 2.1: Stopping Range of Beta Particles in Semiconductors

Radioisotope	Semiconductor	Energy deposition (keV)	Penetration depth (μm)	Method	Author
Ni-63	Si	80% of total deposition, 99.9% of total deposition	5 20	MCNP	[24]
Ni-63	Si	17.4	2.2	Katz-Penfold maximum range equation	[19]
Ni-63	Si	17.1 66.7	3 43	Continuous slowing down approximation (CSDA)	[39]
Ni-63	Si	17.1 66.7	2.68 27	MATLAB/SIMULINK for ionization and radiation loss theory	[45]
Ni-63	Si	17.4	3.76	Theoretical analysis	[14]
Ni-63	GaN	17.4 100 % of full spectrum, 95% of full spectrum	1.3 13 8	MCNP	[25]
Ni-63	GaN	17.1	1.52	MCNP	[46]
Ni-63	GaN	17 67	1.136 16.2	MCNP	[17]
Ni-63	GaN	17.4	1.5	SRIM	[37]
Ni-63	GaN (Schottky)	8.3	1.7	SRIM	[7]
Pm-147	GaN	62 224.7 62 224.7	11.8 100 9.5 81.9	MCNP Katz and Penfold	[32]
Ni-63	SiC	17	3	Empirical equation	[10]
Ni-63	4H-SiC		3		[20]
Ni-63	4H-SiC (Schottky)	17.1	2	Katz and Penfold	[27]
Ni-63	GaAs	80% of energy deposition, 100% of energy deposition	5 15	Kanaya-Okayama (K-O) model	[33]
Ni-63	Air Ni Cr Au	17.1	6000 0.73 2.52 0.58	Calculated by ionization and radiation loss theory	[18]
Ni-63	Most solids	17.3	< 10		[47]
H-3	Si	5.7	0.2		[4, 48]
H-3	a-Si:H		0.5		[41]
S-35	Se (liquid)	49	50		[43]

Pores that are on the scale of a nanometer act like one dimensional wells for electrons. This mechanism increases the existing band gap of the semiconductor by $E_g + \Delta E$ ($\Delta E = \Delta E_c + \Delta E_v$). For example, the introduction of pores in Si increases its band gap energy to 2 eV from 1.12 eV [44]. By trapping electrons in the well, it will reduce the backscattering effect resulting in a higher power output with a higher conversion efficiency. As an example, the maximum power output was increased by 42 % using porous Si in comparison to using non-porous Si, where the nano-pores protruded into the depletion region [35]. A mathematical model developed by Zhao et al. [45] for the energy conversion of a solid radioisotope by a three-dimensional p-n Si diode showed that the short circuit current increased with an increase in the cylindrical hole-radius. However, the open circuit voltage decreased with an increase in cylindrical hole-radius, and the net power decreased compared with the two-dimensional model with no holes. The cylindrical holes on the surface of the p-n diode did not improve the power due to an increase in the dark current. However, a simulated semiconductor [6], that had 10^6 cylindrical holes with a depth-to-diameter ratio of 10:1 on the surface with Ni-63 embedded in the holes, showed an 18.15 times increase in energy deposition for only a 5 times magnification of the effective surface area. A decrease in the cylindrical hole diameter further increased the energy deposition. A cylindrical surface area was found to be more efficient than the inverted pyramid and planar surface area configurations. The power density for a cylindrical p-n junction also increases with the height-to-diameter ratio (HDR) of the holes. However, the height of a cylinder is limited by the thickness of any MEMS components, such as less than 1 mm. A maximum HDR of about 1150 was obtained [17] within this limitation for Ni-63 with a p-n junction of GaN using MCNP analysis with a cylinder height and diameter of 970 μm and 0.8342 μm respectively. Besides different shapes of a crystalline semiconductor, a non-crystalline semiconductor like amorphous silicon (a-Si), which

is a low cost thin film semiconductor, can increase the conversion efficiency by 1.2%, as shown in an experimental work by Deus [41]. Amorphous silicon is expected to have a higher conversion efficiency due to a low thickness and high intrinsic shunt resistance.

The penetration depth of the beta particles in a semiconductor determines the effective thickness and junction depth needed for the semiconductor material in a battery design. Different methods have been used to calculate the penetration depth of the beta particles in semiconductors, such as MCNP, the Katz-Penfold maximum range equation, the continuous slowing down approximation (CSDA), the Kanaya-Okayama (K-O) model, collision and radiative stopping power equations, and empirical equations.

Results, as shown in Table 2.1, vary widely for combinations of radioisotopes and semiconductor materials. The combination of a high density semiconductor with a low energy radioisotope will result in a shorter penetration distance for generating all the EHPs [30]. A thin thickness for a semiconductor can meet the design requirement if the density of the material is high [31].

The MCNP code for transport of beta particles can be used to calculate beta particle deposition energy and penetration depth in the semiconductor very accurately due to its high precision [24].The deposition energy is required to estimate the number of EHPs generated in the semiconductor. The generation rate of EHPs for unit thickness of the semiconductor can be calculated using MCNP by [24] equation (10)

$$G(x) = \frac{AE(x)}{E_{EHP}}, \qquad (10)$$

where *A* is the activity of the radioisotope, *E(x)* is the energy deposition estimated by MCNP as a function of the distance into the semicondcutor, and E_{EHP} is the average energy required to generate one EHP, which is a property of the material. However, the generation rate of EHPs can be approximated without MCNP by [30] equation (11)

$$G = \frac{A(1-f)E_{beta}}{E_{EHP}}, \qquad (11)$$

where E_{beta} is the single beta particle energy, and *f* is the backscatter coefficient. Not all beta particles are transmitted into the semiconductor due to backscattering, which is taken into account by the backscatter coefficient *f*. Aside from backscattering, the generation of EHPs can be affected by the directionality of the radioactive beta particles. Beta particles from the radioisotope travel randomly in all directions. They may escape instead of reaching the semiconductor because of this random directionality. For example, if the radioisotope is placed on one side of the

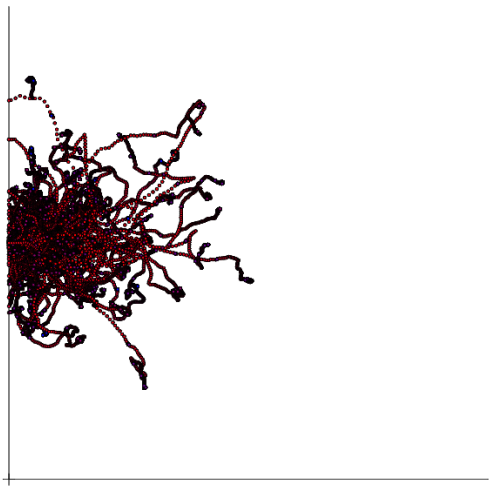

Figure 2-14: Stopping range vs penetration depth for beta particles

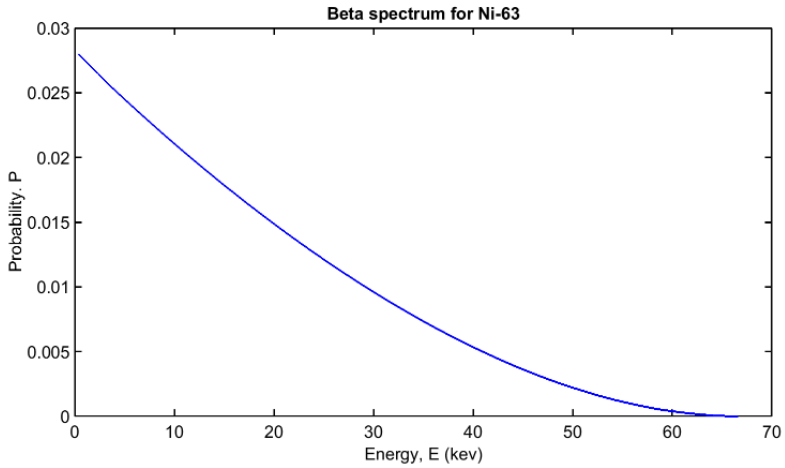

Figure 2-15: Full beta energy spectrum of Ni-63

semiconductor, then almost 50% of the beta particles may not contribute in generating EHPs because they are heading in the opposite direction toward the backside of the radioisotope source. This would be another reason to use stacked betavoltaic cells where one can capture the beta particles going in both directions. If the cells are not stacked, some improvement in radioisotope source efficiency can be made by placing a scattering plate on the backside of the source to redirect some of the beta particles towards the semiconductor.

Beta particle energy deposition in the thickness direction of a semiconductor becomes almost insignificant beyond half of the beta particle stopping range in the material. This is because the trajectory of a beta particle is randomly scattered as shown in Figure 2-14. Therefore, very few beta particles penetrate along the thickness direction in a semiconductor material. As a result, the average penetration depth for energetic beta particles is less than the stopping range. In fact, the rule of thumb is that the penetration depth is about half of the stopping range [49]. In addition, the majority of the beta particle energy for low energy radioisotopes such as Ni-63 is accumulated near the surface of a semiconductor material, and it becomes negligible beyond the penetration

depth [32]. An MCNP calculation is a more precise method to calculate the penetration depth. Penetration depth changes with different beta particle energies. It is to be noted that the beta particles are emitted in a continuous energy spectrum during radioactive beta decay as shown in Figure 2-15. Using MCNP a full beta particle energy spectrum can be considered instead of only monoenergetic beta particles. Therefore, a full spectrum analysis of beta particle energy using MCNP is important to get a better estimate of the penetration depth.

The radioisotope is the power source that drives the radioisotope battery. Betavoltaics use beta emitting radioisotopes to create the battery mechanism. It is a generic practice to select a radioisotope for betavoltaics that has a maximum beta particle energy less than 250 keV. This energy value is lower than most of the electron radiation damage threshold values of the semiconductors. For example, the threshold beta particle energy for radiation damage to a silicon crystalline structure is about 250 keV [24, 50]. However, beta emitters with higher energy can be used for wide band gap semiconductors. For example, beta emitters with a maximum energy of 440 keV can be used with GaN due to its high threshold energy for radiation damage[38].

Safe handling of the radioisotope would be required when making the batteries to avoid skin penetration from high energy beta particles. Usually, the threshold energy of beta particles for skin penetration is about 70 keV to 150 keV [51, 52]. Nevertheless, eyes are very sensitive to beta particles even at much lower energies. Wearing safety glasses and protective shielding clothes should be considered as a safety precaution for handling radioisotopes even at lower energies.

Some of the beta emitters that were identified in the literature for betavoltaic applications [32] [35] [8] are listed in Table 2.2 in order of low to high average beta particle energy.

When two isotopes are listed in the same row, the first isotope is the parent and the second one is the radioactive daughter isotope. Otherwise, the daughter decay products are non-radioactive.

Table 2.2: Radioisotopes Listed in the Literature

β-emitter	Half-life	Average energy (keV)	Maximum energy (keV)	Average specific power (mW/g)
ǂH-3	12.32 y	5.69	18.59	324.914
ǂRu-106	1.02 y	10.03	39.4	196.948
ǂNi-63	100.2 y	17.42	66.94	5.796
ǂS-35	87.37 d	48.76	167.33	12339.148
Pm-147	2.62 y	61.93	224.6	340.367
ǂP-33	25.35 d	76.43	248.5	70701.623
Ca-45	162.61 d	76.86	255.8	8129.21
Cs-137	30.08 y	187.1	1175.63	96.241
ǂSr-90	28.79 y	195.8	546	160.238
Y-90	64 h	933.6	2280.1	3.011E+06
Tl-204	3.783 y	244.05	763.76	669.977
Kr-85	10.76 y	250.7	687.4	581.465

ǂ : pure beta emitters, no x-rays or gamma-rays are emitted
Data source: National Nuclear Data Center, Brookhaven National Laboratory

In order to increase the betavoltaic power output, a radioisotope with high specific power should be selected. The average specific power is directly proportional to the average energy of the beta particles emitted but inversely proportional to the half-life of the radioisotope. Selection of half-life depends on the service life requirement of the battery application. Service life can be longer than the half-life. For example, the service life can be three times the half-life if the application load requires only 12.5% of the battery's initial power output. It is ideal in betavoltaic battery design to choose a radioisotope with medium or high half-life and high beta energy. However, very high beta energy can cause radiation damage in semiconductors. The maximum

beta energy needs to be below the threshold energy of radiation damage for the particular semiconductor. Not all of the radioisotopes in Table 2.2 are an ideal choice for betavoltaic battery design. Only H-3, Ni-63, S-35, Pm-147, P-33 and Sr-90 have been used in the manufacture of betavoltaic battery devices. Ni-63 is the most widely used radioisotope for betavoltaic batteries and is a pure beta emitter. However, it has a very low specific power of 5.8 mW/g compared to the other beta emitters. The specific power of Ni-63 is very low because of its long half-life and low average beta energy. Both S-35 and P-33 have very short half-lives. S-35 was only used with liquid semiconductors because of its compatibility. H-3 has a good specific power of about 325 mW/g with a half-life of 12.3 years. However, it is a gas and hard to handle as well as difficult to obtain in high concentrations, which gives it a low effective specific activity. In general, it is used in the form of a tritiated metal in order to avoid low gas density and radiation hazards from a gas leak. Sr-90 is a pure beta emitter that decays to Y-90, which is also a beta emitter. However, Y-90 has a very short half-life of 64 hours with a very high average beta energy of 933.6 keV. This high energy for its beta particles may cause significant radiation damage to the semiconductors. Pm-147 has a reasonable half-life of 2.6 years with a specific power of 347 mW/g. It seems like a very good radioisotope candidate for betavoltaic batteries, and its maximum beta energy (224.6 keV) is low enough to minimize radiation damage. Pm-147 does give off some low energy gamma-rays with low probability which do not impact the battery design. Thus, use of Pm-147 will primarily be based on if it meets the required service life of the battery application.

Table 2.3: Other Potential Radioisotopes for Betavoltaic Batteries

β-emitter	Half-life	Average energy (keV)	Maximum energy (keV)	Average specific power (mW/g)
Os-194	6 y	16	96.6	29.123
Ir-194	19.28 h	800	2233.8	3.97E+06
Sm-151	90 y	19.63	76.6	3.061
Tm-171	1.92 y	24.77	96.4	159.876
Eu-155	4.753 y	47	252.7	135.209
Th-234	24.1 d	47.9	273	6566.085
ǂC-14	5700 y	49.47	156.475	1.313
Hg-203	46.594 d	57.87	492.1	4731.189
Ru-103	39.247 d	63.8	763.4	12213.974
ǂSi-32	153 y	69.55	227.2	30.116
ǂP-32	14.27 d	695.03	1710.66	11.78E+05
Ce-144	284.91 d	82.1	318.7	1548.169
Pr-144	17.28 m	1208	2997.5	5.408E+08
Sb-125	2.76 y	86.7	766.7	533.025
W-188	69.78 d	99	349	5836.159
Re-188	17.004 h	763	2120.4	4.43E+06
Zr-95	64.032 d	117	1123.6	14885.746
Nb-95	34.991 d	43.43	925.6	10111.622
Fe-59	44.495 d	118	1565.2	34792.309
Hf-181	42.39 d	121	1029.8	12196.924
W-185	75.1 d	126.9	432.5	7063.894
Ce-141	32.508 d	145.3	580.7	24525.828
Tb-160	72.3 d	210	1835.1	14042.472
ǂAr-39	269 y	218.8	565	44.22
ǂAr-42	32.9 y	233	599	357.507
K-42	12.36 h	1430.5	3525.45	5.118E+07
Tm-170	128.6 d	317	968	11215.49
Sn-123	129.2 d	523.1	1403.6	25470.351
Sr-89	50.563 d	587.1	1500.9	100977.803
Y-91	58.51 d	603	1544.3	87654.311

Some beta emitters like Sr-90 and Si-32 decay into a daughter, which also emits beta particles. In most cases, the daughter radioisotope has a much shorter half-life and a much higher

average beta particle energy than that of its parent. In this particular case, the activity of the daughter will already be in secular equilibrium with the parent. In secular equilibrium, the average specific power of a mixture becomes higher than that of the parent radioisotope alone. The average specific power also increases due to the high average energy and short half-life of the daughter radioisotope with a similar mass to the parent radioisotope. This could be an advantage for increasing the power output of a betavoltaic battery. However, the resulting high energy of the daughter radioisotope beta particles can cause significant damage to the semiconductor materials. Along with a high average energy beta particle, some daughter radioisotopes also emit high energy x-rays and gamma rays. This type of radioisotope either needs to be avoided or requires special shielding. The following list of radioisotopes from the National Nuclear Data Center (NNDC) was generated to investigate other possible beta emitters not considered in the literature with a maximum energy of less than 2000 keV. Table 2.3 lists these other possible radioisotopes that might potentially be used in betavoltaic batteries. This table does not take into account the feasibility of producing these isotopes or their availability. The radioisotopes are listed in order of increasing average beta particle energy of the parent isotope.

Many of the beta emitters in Table 2.3 have half-lives less than a year. Ar-42 has a half-life twelve times higher than that of Pm-147 and is a pure beta emitter. It has also a high specific power of 357 mW/g, which is more than that of Pm-147. However, it is a noble gas and cannot be used in a solid state. In addition, it is in secular equilibrium with its daughter K-42. However, K-42 emits very high energy beta particles. Thus, this will rule out using Ar-42. Ce-144 also looks like a good choice with a high specific power of 1565 mW/g if the application only needs a service life of nine to thirty months. But it also has a daughter in secular equilibrium that emits a very high

energy beta particle. Other radioisotopes that have stable daughters that may be possible candidates for betavoltaic batteries are Tm-171, Eu-155, and Sb-125.

In conclusion, the self-shielding effect of the radioisotope needs to be considered in betavoltaic battery design. The self-shielding effect can be reduced by increasing the surface area of the radioisotope, which will increase the power output of the battery for the same amount of radioactivity. A modified surface geometry of the semiconductor such as inverted pyramid and cylindrical holes is useful to increase the power output. In addition, the analysis of penetration depth of beta particles in the semiconductor is very important for betavoltaic battery design. An MCNP analysis using the full beta energy spectrum of the radioisotope will provide a better estimate of the penetration depth. Furthermore, selection of a radioisotope for betavoltaic batteries is an important choice to make [30]. The most important factor for selection of a radioisotope is the power output requirement [31]. For example, an average energy deposition of 3.3 eV will generate one EHP in Si. When Ni-63 is used as a radioisotope source with Si, it generates almost 5000 EHPs per average beta particle energy of 16.7 keV. Similarly, Pm-147 generates 19,000 EHP per average beta particle energy of 62 keV. From this, it is predicted that the maximum power output using Pm-147 is more than three times higher than that of using Ni-63 with the same amount of radioactivity [35]. Other factors for the selection of the radioisotope involving more tradeoffs are the application service life, radiation damage, cost, availability, and shielding. Factors like the beta particle energy spectrum, the penetration depth of the particles in the semiconductor, the specific activity, and the radioisotope half-life determine the performance of the betavoltaics. Instead of using a real radioisotope in experiments, some researchers have used monoenergetic electrons produced by a scanning electron microscope (SEM) [20, 47, 53]. This technique is useful

for testing battery design, such as optimizing the junction depth and the depletion region width of a battery by checking the output [19]. However, an actual radioisotope is needed to characterize actual conversion efficiencies and power outputs.

2.6 Results and Analysis

A summary of betavoltaic battery results will be useful to understand the state-of-the art technology. The performance of a betavoltaic battery is measured by its open circuit voltage, short circuit current, maximum power output, efficiency, and fill factor. The performance metrics for both simulated and experimental results of betavoltaic batteries are summarized in Table 2.4 by type of semiconductor material. A range of minimum to maximum values is then provided for each performance metric. Although the short circuit current and the maximum power output in Table 2.4 are shown in terms of nA/cm^2 and nW/cm^2 respectively, most of the batteries have sizes on the scale of few mm^2 or few μm^2. Some researchers reported short circuit current and maximum power output on the scale of nA/cm^2 and nW/cm^2 respectively, whereas others reported the net short circuit current and maximum power output in terms of nA or μA and nW or μW respectively. The net short circuit current and maximum power output were then converted to units of nA/cm^2 and nW/cm^2, respectively, using the reported sizes of the batteries for the sake of comparison. Some researchers provided the net short circuit current and maximum power output without reporting the size of the battery. For these results, it was difficult to do a comparison and they were not included in Table 2.4. However, they will be included in the results discussion. The betavoltaic battery results for net short circuit current (nA) and maximum power output (nW) are much lower than that of their short circuit current density (nA/cm^2) and maximum power output (nW/cm^2) due

to their size often being much less than a square centimeter. In addition, the net results are low as they are reported for single cells only in order to do the comparison. However, the open circuit voltage, short circuit current, and maximum power output will increase when multiple cells are used in series or parallel for specific applications. The efficiency and fill factor will not be changed for multiple cells.

Table 2.4: Summary of Results

Semiconductor Material	**Open circuit voltage (V)**	**Short circuit current (nA/cm^2)**	**Maximum power output (nW/cm^2)**	**Overall Efficiency (%)**	**Fill factor**
Si	0.25 to 0.54	3.92 to 3200	1.04 to 500	4.94 to 13.7	0.79 to 0.81
ǂ Si	0.0008 to 0.46; mostly 0.12	4.44 to 1490; mostly below 55	0.12 to 4.6	0.01 to 1.75 mostly below 1	0.27 to 0.83
GaN	0.46 to 3.16; mostly above 2	7.5 to 5000; mostly below 1600	2.3 to 4927	4.1 to 25.4	0.57 to 0.94
ǂ GaN	0.025 to 1.65	1.2 to 89.2; mostly below 20	1.75 to 14.26	0.21 to 1.13	0.14 to 0.55
4H-SiC	0.72 to 2.1	16.8 to 24.31	6.17	14.5	0.51
ǂ 4H-SiC	0.26 to 0.49	3.46 to 29.44	0.513 to 4.85	<0.5 to 1.2	0.34 to 0.59
ǂ SiC	0.95 to 2.06	5.25 to 2300; mostly below 31	3.5 to 2400; mostly below 10	0.52 to 1.99	0.47 to 0.75
ǂ a-Si:H	0.02 to 0.46	5.3 to 637	0.26 to 136	0.1	0.59
ǂ GaAs	0.28 to 0.32	0.3 to 28	0.05 to 0.07		0.58 to 0.61
ǂ Se (liquid)	0.34	102.4	15.58	1.19	
ǂ AlGaAs	0.47	937	259		

ǂ: Experimental results

Only overall conversion efficiencies are considered for comparison among different types of efficiencies. The overall conversion efficiency of a betavoltaic battery is calculated by equation (12)

$$\eta = \frac{P_{max}}{P_{theory}} = \frac{FFI_{sc}V_{oc}}{1.6\times10^{-19}\times3.7\times10^{7}AE_{avg}} \qquad (12)$$

where P_{max} is the maximum power output of a betavoltaic battery and P_{theory} is the theoretical maximum thermal power of the radioisotope used in the battery, the activity A is in mCi, and the average beta particle energy E_{avg} is in eV. The overall conversion efficiency can also be defined by equation (13)

$$\eta = \eta_s \times \eta_c \quad (13)$$

where η_s and η_c are the source efficiency, and semiconductor conversion efficiency, respectively. Source efficiency is defined by the ratio of the energy deposited in the semiconductor to the actual energy of the radioisotope. It takes into account the self-shielding effect of the radioisotope, all the geometry factors and losses including the fraction of beta particles that are not directed towards the semiconductor. The semiconductor efficiency is determined by the maximum power output of the battery divided by the rate of the energy deposited in the semiconductor. It takes into account recombination and heat losses within the semiconductor. Table 2.4 shows the overall conversion efficiency values for betavoltaic batteries. It is noted that the semiconductors were placed only one side of the radioisotopes for making betavoltaic batteries, therefore, almost 50% of the beta particles did not reach the semiconductors. It is noted that the reported efficiencies could be doubled if the radioisotopes were sandwiched by the semiconductors. Thus, a proper overall conversion efficiency calculation for a single cell should only use half the radioisotope activity.

Results for different semiconductor materials are listed in Table 2.4. Note that 4H-SiC and SiC are shown as different categories since that is how they were reported in the literature. However, 4H-SiC is a polytype of SiC and n-type 4H-SiC substrates were used to fabricate

different junctions of SiC. To summarize all the experimental results from Table 2.4, it can be seen that the ranges of open circuit voltage, short circuit current, maximum power output, efficiency, and fill factor from experimental results are 0.01 to 2.06 V, 0.3 to 2300 nA/cm^2, 0.05 to 2400 nW/cm^2, 0.01 to 1.99%, and 0.14 to 0.83, respectively.

The betavoltaic battery performance results listed in Table 2.4 cannot be directly compared to each other. It shows the range of results obtained for different semiconductors, different radioisotopes, and different activities used in betavoltaic battery design. The battery performance does not depend only on the semiconductor material but depends also on the type of junction, the radioisotope and the amount of radioactivity, which were not incorporated in Table 2.4 in order to keep it readable. However, some key results can still be highlighted from Table 2.4. It shows that the theoretical models (those rows without the ǂ symbol) tend to overpredict the experimental results. For example, the higher ranges of open circuit voltage and short circuit current for Si are 0.54 V and 3200 nA/cm^2, respectively, whereas the open circuit voltage and short circuit current from experiments are mostly below 0.12 V and 55 nA/cm^2 respectively. It also shows that wide band gap semiconductors such as GaN and SiC provide higher open circuit voltage and efficiency compared to narrow band gap semiconductors such as Si. However, the short circuit currents from narrow band gap semiconductors are higher than that of wide band gap semiconductors. Despite the lower short circuit current, the power output is still generally higher for the wide band gap semiconductors. A comparison of band gaps for different semiconductor materials used in betavoltaic batteries is shown in Table 2.5.

Table 2.5 shows that Si is a narrow band gap semiconductor with a band gap of 1.12 eV, whereas GaN is a wide band gap semiconductor with a band gap energy of 3.4 eV. A brief

summary and comparison of results are given below based on the semiconductor material in the betavoltaic batteries.

Table 2.5: Band Gap of Different Semiconductor Materials

Semiconductor materials	**Si**	**GaN**	**4H-SiC**	**a-Si:H**	**GaAs**	**Se**	**AlGaAs**
Band gap (eV)*	1.12 [32]	3.4 [32]	3.3 [20]	1.75 [41]	1.42 [54]	1.77 [43]	1.55-1.97 [54]

* at room temperature

2.6.1 Si Betavoltaic Battery

The open circuit voltage, short circuit current density, power output density, and efficiency from one MCNP simulation for a Si semiconductor were about 0.25 V, 600 nA/cm^2, 100 nW/cm^2, and 5%, respectively [24]. However, the experimental results for a Si semiconductor were much less than the simulation results. For experimental results, the reported power output range was from 0.0025 nW [19] to 44 nW [35]. Some power output results were reported in the form of power density, which is good for a comparative analysis. The power density ranged from 0.25 nW/cm^2 [39] to 4.6 nW/cm^2 [4]. Similarly, short circuit current ranged from 1.31 nA [6] to 550 nA [35], and some reported current densities ranged from 4.44 nA/cm^2 [39] to 1.49 µA/cm^2 [4]. A wide range of open circuit voltages was reported from 0.0008 V [19] to 0.46 V [15]. The conversion efficiency ranged from 0.01% [15] to 1.75% [35]. The fill factor was reported only for a temperature analysis. In that case, the fill factor varied from 0.27 to 0.83 [15] with changes in temperature. Overall, the open circuit voltage, short circuit current density, and efficiency of silicon betavoltaic batteries from the experimental results were about 0.1 V, less than 60 nA/cm^2

which was mostly around 4 nA/cm^2 to 30 nA/cm^2, and mostly below 1%, respectively. The maximum power density for a Si semiconductor betavoltaic obtained from experimental results was 4.6 nW/cm^2.

Most of the betavoltaic battery research was carried out on Si semiconductors, as Si is readily available and well-studied. It is widely used in the IC industry and in MEMS with developed micromachining technology [19]. Si is also easy to manufacture with relatively lower cost than other semiconductors. Different types of radioisotopes such as Ni-63, Pm-147, and H-3 were used with the Si semiconductors. Most of the reported Si betavoltaic batteries were planar p-n junctions. Different surface geometries such as porous, cylindrical holes, and inverted pyramid were investigated for Si semiconductors in order to increase the power output. Porous and inverted pyramid surfaces were analyzed experimentally [4, 35, 39] whereas a surface with cylindrical holes was analyzed analytically [45]. Using a porous surface instead of a planar surface magnified the surface area, which increased the entrapment of beta particles due to a decrease in the backscattering effect. As a result, the power output of the betavoltaic battery with a porous surface with a p-n junction improved significantly [35] due to an improvement in open circuit voltage and short circuit current for the same type of solid radioisotope. An improvement in the power output was also observed for an inverted pyramid array surface with a liquid radioisotope [39] that had the potential to take full advantage of the surface magnification. An inverted pyramid array Si p-n junction semiconductor with liquid Ni-63 was reported [6] to increase the efficiency compared to a planar Si p-i-n junction semiconductor from 0.042% to 1%. Using a porous surface or inverted pyramids with an increased surface area makes it possible to put the radioisotope into the pores. This tends to improve the efficiency and power output of the betavoltaic battery due to the

increased surface area of the source as discussed in the Radioisotopes section. In addition, higher energy and source activity for the beta particles tend to give more power. However, this does not take into account possible radiation damage effects. Porous Si p-n junctions were used with Pm-147 [35] and H-3 [4]. Compared to a non-porous Si p-n junction in an experiment using Pm-147, the porous Si p-n junction increased the power output by 13 nW (42%) with an increase in open circuit voltage and short circuit current of 0.01 V (9%) and 0.14 μA (34%), respectively [35]. The battery performance for porous Si p-n junction improved due to the increase in band gap energy with the introduction of nano-pores and better absorption of beta particles with reduced backscattering. The beta particle energy of Pm-147 is higher than that of H-3. A 1.53% greater efficiency was reported [35, 55]for a porous Si p-n junction with Pm-147 than that of a H-3 betavoltaic battery as the pores do not have better retention of the H-3 gas. However, in another experiment [4], tritium was used in three different forms: gas, surface occluded and solid ScT. Among the three different forms of tritium sources, gaseous tritium at 0.8 atm pressure with a porous Si p-n junction provided the highest power output density of 4.6 nW/cm^2. The efficiency for the gaseous tritium source was 0.09%, which is 0.04% greater than the next best ScT source.

Betavoltaic battery performance is also affected by temperature. A temperature analysis showed [15] that the open circuit voltage, the short circuit current, the maximum power output, the efficiency, and the fill factor for betavoltaic batteries made of Ni-63 with a p-n junction of Si improved by a significant margin at a very low temperature due to the reduction in leakage current. This analysis shows that the battery performance degrades at higher temperatures, which may result from the decay heat and conversion losses. Hence, multiple cell batteries, passive cooling

mechanisms may need to be incorporated in the design to minimize degradation in performance due to temperature effects.

A very wide range of betavoltaic battery performance for crystalline Si semiconductors resulted from different types and quality of semiconductor junctions, various radioisotope sources with different amounts of radioactivity, and different design parameters for batteries. However, an increased surface area such as nano-pores or inverted pyramid array of Si would be a better design due to their better performance in betavoltaic batteries.

2.6.2 GaN Betavoltaic Battery

Gallium nitride is a wide band gap semiconductor with a band gap of 3.4 eV that attracted the second most attention after that of silicon semiconductors by the researchers. Overall, gallium nitride betavoltaic batteries showed a much higher open circuit voltage and a better efficiency than that of the planar silicon betavoltaic batteries. The open circuit voltage, short circuit current density, and efficiency for non-Schottky junction GaN betavoltaic batteries using MCNP simulation were about 2 V [30] to 3 V [32], 1 μA/cm^2 [31] to 1.6 μA/cm^2 [32], and 13% [32], respectively, where a non-Schottky junction refers to other types of junctions such as p-n, p-u-n, and p-i-n. One analytical result reported [30] very high efficiency of about 25% for GaN. From MCNP simulations, the reported short circuit currents were on the scale of a micro-ampere except for a Schottky junction, which was on the scale of a nano-ampere. Besides Ni-63, some other radioisotopes such as Pm-147 and H-3 were used in the simulations. However, Ni-63 was the only radioisotope used in the experiments for GaN with a radioactivity density of 3 mCi/cm^2 to 20

mCi/cm^2. Unlike in the simulation, the actual experimental results using GaN suffered from poor output and efficiency. In fact, most of the experimental results were not optimized. Several experimental results for GaN betavoltaic batteries are listed in Table 2.6.

Table 2.6: Some GaN Experimental Results

Semiconductor (junction type)	Radioactivity (mCi/cm^2)	Open circuit voltage (V)	Short Circuit current (nA/cm^2)	Maximum power output (nW/cm^2)	Overall Efficiency (%)	Fill factor
GaN (Schottky) [7]	Ni-63 (3)	0.1	1.2		< 0.32	
GaN (p-n) [56]	Ni-63 (11)	0.025	2		< 1	
GaN (p-i-n) [46]	Ni-63 (12.5)	0.47	17	2.72	0.21	0.34
GaN (p-i-n) [57]	Ni-63 (12.5)	1.65	12	10.69	0.82	0.54

Some researchers [7, 25] focused on using a Schottky junction for GaN betavoltaic batteries due to the fabrication limitation of a thick high quality junction in GaN semiconductors. A Schottky junction for a GaN betavoltaic battery is easy to fabricate with an n-type GaN material and a metal electrode. However, it generates much lower output than that of a non-Schottky junction GaN semiconductor. The open circuit voltage, short circuit current density, and efficiency for a Schottky junction GaN betavoltaic battery using MCNP and semiconductor simulation were about 0.5 V, 7.5 nA/cm^2, and 2.25%, respectively [25]. However, the open circuit voltage, short circuit current density, and efficiency obtained from experimental results for Schottky junction GaN betavoltaic batteries were about 0.1 V, 1.2 nA/cm^2, and less than 0.32%, respectively as shown in Table 2.6. The actual device results were much lower than that predicted from simulation. Most of the beta particles were absorbed and reflected in the dead layer, which is the Schottky electrode. The experimental results also suffered from a very small depletion layer width of 0.07 μm [7]. Nevertheless the Schottky junction GaN betavoltaic battery results for open circuit voltage and efficiency were comparable to that of planar silicon betavoltaic batteries. However, the short

circuit current density from the Schottky junction GaN betavoltaic battery was lower than that for a silicon betavoltaic battery.

Some researchers were able to manufacture p-n and p-i-n junctions of GaN semiconductors for betavoltaic batteries as shown in Table 2.6. The open circuit voltage, short circuit current density, and efficiency for non-Schottky junction GaN betavoltaic batteries from experimental results were about 1.6 V, less than 20 nA/cm^2, and below 1.2%, respectively. Cheng et al [56] reported a low open circuit voltage of 0.025 V and a short circuit current of 2 nA/cm^2 for a betavoltaic battery made of a GaN p-n junction with Ni-63 and compared experimental results with simulation results. They showed discrepancies between the two results of about 95% for both open circuit voltage and short circuit current. The experimental results were much worse than the optimized simulation results for several reasons. First, an actual junction depth of only 0.4 μm was achieved during GaN fabrication, but was 1.3 μm in the simulation. Second, the fabricated GaN semiconductor had a cross-sectional area of 1 cm^2, which was large enough to generate crystalline defects in the fabrication process and contributed to a large recombination current. Finally, the poor crystalline quality of the p-type region of the GaN semiconductor increased the leakage current. The open circuit voltage was then improved to 0.47 V [46] for a GaN p-i-n junction as shown in Table 2.6. Although it was called a p-i-n junction, it was actually a p-u-n junction. A u-type region in GaN is an unintentionally doped region with a high background electron carrier concentration (like an n-type region) due to impurities. However, the introduction of a u-type region of 0.3 μm increased the depletion width, which in turn improved the battery output. It was further improved to 1.65 V [57] by introducing an intrinsic region of 0.6 μm and creating a p-i-n junction. The p-type, i-type, and n-type regions of a GaN were created by doping with Mg, Fe, and

Si respectively. It is still challenging to grow a thick p-type region using GaN. A non-Schottky junction GaN betavoltaic battery [57] showed much higher open circuit voltage than a silicon betavoltaic battery [6] but the short circuit current density was lower, for Ni-63 with equivalent activity. However, the power density of a non-Schottky junction GaN battery was almost two times higher than the maximum power density for a silicon betavoltaic battery.

The p-i-n junction for GaN betavoltaic batteries showed better battery performance when compared with other types of junctions for GaN. The maximum efficiency of a GaN betavoltaic battery was 1.13% [36], which is much lower than its theoretical efficiency due to fabrication limitations.

2.6.3 SiC Betavoltaic Battery

4H-SiC is a hexagonal polytype of SiC that has a band gap of 3.3 eV. The availability of high quality substrate and the advancement in epitaxial growth technology has made 4H-SiC a better candidate for betavoltaics. 4H-SiC is a semiconductor material that has one of the best qualities for electronic device fabrication [10]. It has some good properties such as high thermal conductivity, temperature stability, radiation hardness, and good electronic mobility that are useful in betavoltaics [20]. A Schottky barrier of 4H-SiC can be a promising design option for betavoltaics [27]. It is less expensive with easier fabrication. It has already been used for detecting solar-blind ultraviolet (UV) with a response only to the UV and not to visible light [10].

Simulation, analytical, and experimental work has been done for both Schottky and p-n junctions of 4H-SiC betavoltaic batteries. All of them used Ni-63 as the radioisotope source. A

Schottky junction using 4H-SiC [27] showed better performance than that of a Schottky junction GaN betavoltaic battery [7] for the same radioisotope of Ni-63 with almost similar activity. Maximum open circuit voltages of about 1 V [10] and 0.5 V [18] were achieved for Schottky junction 4H-SiC betavoltaic batteries from an SEM beam of electrons and from a Ni-63 radioisotope experimental analysis, respectively. In experimental analysis, it generated a maximum short circuit current density of about 30 nA/cm^2 [18] with an efficiency of about 1% [18, 27]. The Schottky junction for 4H-SiC showed an almost similar power density [18] compared to the maximum power density of a Si semiconductor [4]. A p-n junction using 4H-SiC [20] showed a slightly higher power density than the maximum power density obtained from a Si semiconductor [4]. The experimental results of 4H-SiC p-n junction [20] showed almost 160% greater open circuit voltage than that of a 4H-SiC Schottky junction [27] with about 30% reduction in short circuit current for Ni-63 with almost similar activity. However, a net increase in power density of 50% was found for a 4H-SiC p-n junction over that of a Schottky junction.

Table 2.7: Some SiC Experimental Results

Semiconductor (junction type)	**Radioiactivity (mCi/cm^2)**	**Open circuit voltage (V)**	**Short Circuit current (nA/cm^2)**	**Maximum power output (nW/cm^2)**	**Efficiency (%)**	**Fill factor**
SiC (p-i-n) [8]	P-33 (820)	2.04	2000	2100	0.56	0.51
SiC (p-n) [47]	Ni-63 (1.5)	1.9	30			
SiC (p-i-n) [58]	Ni-63 (4) (2.4)	0.98 0.95	12.75 5.25	8 3.5	1.99 1.5	0.64 0.75

In addition to 4H-SiC betavoltaic batteries, some SiC betavoltaic batteries were reported as shown in Table 2.7. However, p-type epilayer growth on a 4H-SiC substrate is expensive.

A much larger open circuit voltage of about 2 V was achieved for both p-i-n and p-n junctions in SiC compared to other semiconductor materials as shown in Table 2.7. Short circuit

current densities of 2000 nA/cm^2 [8] and 30 nA/cm^2 [47] were reported corresponding to SiC p-i-n and p-n junctions. The reported short circuit current density and power density for a SiC p-i-n junction [8] on the scale of ~1 μA/cm^2 and ~1 μW/cm^2 respectively are very attractive for betavoltaic battery applications. However, this high short circuit current density was achieved using the P-33 radioisotope that has a very short half-life of about 25 days, whereas the other one was achieved using Ni-63 that has a long half-life of about 100 years. On the other hand, a SiC p-i-n junction [8] showed about a 20% increase in open circuit voltage compared to a GaN p-i-n junction semiconductor [57]. However, it showed an efficiency of 0.56% [8], which was lower than that of a GaN p-i-n junction semiconductor [57]. The battery results for SiC with Ni-63 were not as high as it was when used with P-33 as shown in Table 2.7. In SiC betavoltaic batteries, a wafer substrate with thickness of usually 300-500 um is used [59] that has too many defects. The battery results improved significantly for a 4H-SiC p-n junction semiconductor with Ni-63 [47] as compared to a 4H-SiC p-i-n junction semiconductor with Ni-63 [58], as shown in Table 2.7, due to substrate thickness down to 50 μm using a wafer thinning technology.

Comparison of the SiC betavoltaic battery results in Table 2.7 shows that the use of substrate thinning technology improved the results significantly. The SiC betavoltaic battery results as shown in Table 2.7 are found to be better than the GaN betavoltaic battery results as shown in Table 2.6. It is difficult to compare the results when radioisotopes, activity, and semiconductor junctions are not the same. Further investigation is required to do a better comparison.

2.6.4 GaAs Betavoltaic Battery

GaAs has a band gap of 1.42 eV, which is slightly higher than Si. Different types of junctions such as p-i-n, p^+pn^+, and p^+pinn^+ were investigated for GaAs betavoltaic batteries [33, 34]. They generated an open circuit voltage of about 0.3 V [33, 34], which is slightly higher than that of a Si betavoltaic battery [35, 39]. However, it showed a very wide range of short circuit current density ranging from 0.3 nA/cm^2 to 28 nA/cm^2 as shown in Table 2.4 that makes it difficult to compare with other betavoltaics. A betavoltaic battery made of a p-n junction of AlGaAs with H-3 in the gaseous state [41] showed much better initial results than that of a GaAs betavoltaic battery [33, 34]. The AlGaAs battery generated almost one and a half times higher open circuit voltage (0.5 V) than that of the GaAs betavoltaic batteries. The short circuit current density obtained from the AlGaAs battery was almost on the scale of 1 μA/cm^2, and the power density was about sixty times higher than the maximum power density from a silicon betavoltaic battery using H-3 in gaseous state[4]. However, the battery performance degraded rapidly due to high diffusion of tritium into the semiconductor that created defects.

2.6.5 a-Si:H and Other Betavoltaic Batteries

Besides crystalline betavoltaic batteries, some non-crystalline betavoltaic batteries such as liquid selenium and hydrogenated amorphous silicon (a-Si:H) were used by the researchers. Tritium, or a tritiated metal was used as a radioisotope for the non-crystalline semiconductors except for the liquid semiconductor, where a radioactive sulphur (S-35) was used as the radioisotope.

Like crystalline semiconductors, a-Si:H is a semiconductor material with low cost and good optoelectronic properties [48]. The presence of hydrogen in it reduces the dangling bond defects, which in turn reduces the localized states. The experimental work on a-Si:H by Kosteski et al [48] showed very low open circuit voltage of about 0.02 V and short circuit current less than 1 nA using a tritiated layer of intrinsic semiconductor material. The results were not consistent with the experimental work on a-Si:H by Deus [41]. Although both works were done on a p-i-n junction of a-Si:H with the radioisotope H-3, Deus [41] achieved a higher open circuit voltage of 0.46 V and a higher current density of 637 nA/cm^2 with a power density of 136 nW/cm^2. However, the use of the radioisotope H-3 in gaseous form degrades the battery output rapidly. A wide range of open circuit voltage from 0.02 V to 0.46 V and a short circuit current density from 5.3 nA/cm^2 to 637 nA/cm^2 make it difficult to compare hydrogenated amorphous silicon semiconductors with other semiconductor materials.

In an experimental analysis [43], a selenium (Se) semiconductor was used with S-35 as a radioisotope source that is compatible with liquid semiconductors. Selenium (Se) is a liquid semiconductor created by a eutectic mixture of $Se_{65}S_{35}$, which has a reduced melting point of 105°C from 221°C. The selenium betavoltaic battery then was operated at 140°C. Liquid betavoltaics produced the open circuit voltage of 0.34 V similar to GaAs [33] but almost 79% and 83% less than that of the experimental p-i-n junction of GaN (1.65 V) with Ni-63 and the p-i-n junction of SiC (2.04 V) with P-33 betavoltaics respectively. The open circuit voltage of the liquid betavoltaic using a Schottky junction was much lower than that of a p-i-n junction of GaN and SiC. However, it generated a short circuit current and power densities of 104.4 nA/cm^2 and 15.58 nW/cm^2, which were much higher than that of GaAs [33, 34] and about nine times higher in current

density and slightly higher in power density than that of the p-i-n junction GaN with Ni-63 betavoltaic battery [57]. Although it produced better results, S-35 has a short half-life of about 87 days, which is one reason for its high short circuit current and power. Ni-63 and H-3 with a better half-life were used for GaAs and a-Si:H, respectively. On the other hand, liquid betavoltaics have the advantage of embedding the radioisotope with the semiconductor material, which will increase the beta particle absorption. However, the device may require external energy to maintain its high operating temperature of 140°C. A leak-tight package of the device is also required to avoid a hazardous condition.

$Al_{0.7}Ga_{0.3}N$ is a wide band gap semiconductor with a band gap of 5.8 eV [30], which is even much higher than the wide band gap semiconductor GaN. In a theoretical analysis, an $Al_{0.7}Ga_{0.3}N$ semiconductor showed very high output with the highest efficiency of 27.4%. However, no $Al_{0.7}Ga_{0.3}N$ betavoltaic battery has been built experimentally.

2.6.6 Results Conclusion

Analytical and simulation results usually predicted a better output than that obtained in experimental results. Part of that may be that the experimental batteries were not optimized and part of that may be from fabrication limitations or poor crystal structure due to lattice defects. A betavoltaic battery output depends on the semiconductor material, the type of junction, the radioisotope, the amount of radioactivity, the type of electrodes, and the overall design parameters. A Schottky junction 4H-SiC betavoltaic battery with Ni-63 showed better output than a Schottky junction GaN betavoltaic battery with Ni-63. It also showed higher open circuit voltage than a

silicon betavoltaic battery. Similarly, a p-i-n junction SiC betavoltaic battery with P-33 showed much higher output compared to other betavoltaic batteries. However, that result is partly due to the short half-life of P-33. From the actual built device, the best open circuit voltage of 2.06 V, the best short circuit current density of 2300 nA/cm^2 and the best maximum power density of 2400 nW/cm^2 were reported for the betavoltaic battery made of a p-i-n junction of SiC using P-33 with an activity of about 230 mCi [8]. On the other hand, the best efficiency of 1.99% was reported for the betavoltaic battery made of a p-i-n junction of SiC using Ni-63 with an activity of 0.16 mCi [58]. However, more analysis is required to validate the aforementioned comparisons and to draw any conclusions.

In conclusion, use of a wide band gap semiconductor in a betavoltaic battery increases the open circuit voltage, power output, and efficiency. Higher energy beta particles and larger activity increase the short circuit current. The summary of results in Table 2.4 is not a very direct comparison but it does give an indication of about the wide range in performance of actually built betavoltaic batteries and a comparison with the theoretical models. It suggests that a better theoretical model and better betavoltaic battery performance optimization are needed.

2.7 Principles of Betavoltaic Battery Design

Based on all of the discussions in the previous sections, it has been determined that the following principles should be followed in designing a betavoltaic battery.

1. The selection of a radioisotope source for a betavoltaic battery depends on the specific application. It is driven by the service life and specific power requirements of the application.
2. The choice of radioisotope is limited by its availability, its half-life, the average and maximum energy of its beta particles, whether significant gamma-rays are emitted during decay, and by its physical form or phase.
3. The maximum beta particle energy of a radioisotope needs to be below the threshold energy for the radiation damage of the chosen semiconductor material.
4. The self-shielding effect of the radioisotope and the geometry of its interface with the semiconductor need to be considered to maximize the energy deposition in the semiconductor materials. Electrode design needs to be optimized with an interdigit structure and low-Z metal so that backscattering and energy absorption of the beta particles from the radioisotope source in the dead layer (electrode) can be minimized, especially for Schottky junctions.
5. The efficiency of a betavoltaic battery can be increased (almost doubled) by placing the semiconductors on each side of the radioisotope to form a double cell sandwich.
6. A wide band gap semiconductor material has higher radiation tolerance. Therefore, a radioisotope with higher beta particle energy can be chosen for a wide band gap semiconductor in betavoltaic battery design. However, the minority carrier diffusion lengths of EHPs in wide band gap semiconductor materials are lower, which makes it difficult to collect them.
7. The penetration depth of the beta particles is important in order to design the junction depth and the depletion region.

8. Use of full beta energy spectrum is important in order to determine the penetration depth. An MCNP analysis provides a better estimate of the penetration depth and energy deposition due to its high accuracy and precision.
9. The width of the depletion region for a betavoltaic battery design needs to be optimized so that the majority of the beta particles deposit their energy in the depletion region. A wide depletion region is a favorable condition for a betavoltaic battery design. The width of the depletion region depends on the doping concentrations of the semiconductor.
10. A depletion region cannot be made too wide to introduce crystal mismatch, which in turn will increase the leakage current. Furthermore, if the width of the depletion region is much larger than the minority carrier diffusion length, most of the EHPs will not be collected.
11. A lower doping concentration increases the minority carrier diffusion length, which in turn increases charge collection efficiency.
12. Leakage current is dependent on the doping concentration. The leakage current increases with a decrease in doping concentration.
13. The open circuit voltage depends on the leakage current, which in turn depends on the intrinsic carrier concentration. Open circuit voltage decreases with an increase in leakage current and intrinsic carrier concentration.
14. Intrinsic carrier concentration depends on temperature. It increases with an increase in temperature. Open Circuit voltage, fill factor, efficiency, and power output decrease with the increase in temperature. However, the temperature effect on short circuit current is negligible. Some type of cooling or low temperature operation will increase the battery performance. Thus, cell packaging becomes important.

15. A wide band gap semiconductor increases the efficiency, the open circuit voltage, and the power output but reduces the short circuit current.
16. A higher activity for the radioisotope increases the short circuit current.
17. A high quality crystalline structure for the semiconductor material and surface passivation are important in order to reduce recombination losses.
18. It is important that the electrodes have a good ohmic contact with low contact resistance.
19. A better theoretical model on EHP transport in the semiconductor will improve the design of actual betavoltaic batteries.

Overall, many of these principles conflict with each other. Therefore, specific optimization of parameters is required for each application.

2.8 Conclusions

High energy density, long service life, and miniaturization to fit on a chip give betavoltaic batteries some advantages over chemical batteries. The working principle of a betavoltaic battery has both similarities and differences with photovoltaic cells and radiation detectors. It converts the kinetic energy of beta particles from a beta emitting radioisotope into electrical energy using semiconductors. The design of a betavoltaic battery involves optimization of both the radioisotope and the semiconductor material. The radioisotope for a betavoltaic battery is selected based on its maximum beta particle energy and the type of application. The energy deposition in semiconductors is maximized by minimizing self-absorption in the radioisotope source and by increasing the surface geometry of the semiconductor interface.

The primary focus of betavoltaic battery design is to increase the beta particle energy deposition in the depletion region of the semicondcutor. An MCNP analysis is useful in order to determine the penetration depth and energy deposition in semiconductors. The junction depth and the width of the depletion region are then based on the MCNP analysis. EHPs generated in the depletion region have a higher collection probability at the electrodes. A wide depletion region can accommodate most of the energy deposition in it and increase the charge collection. A low doping concentration increases the depletion region, which in turn increases the short circuit current by increasing the charge collection. However, a low doping concentration also increases the leakage current, which in turn reduces the open circuit voltage. Therefore, an optimization of the doping concentration is necessary in order to obtain maximum power output. In addition, increasing the effective shunt resistance and lowering the series resistance of the semiconductor improves the power output. Good crystal quality is required in order to increase the shunt resistance. The thickness of a semiconductor needs to be based on the minority carrier diffusion lengths and the width of the depletion region in order to decrease the series resistance. Increasing the width of the depletion region may introduce some crystal lattice mismatch that decreases the shunt resistance, which in turn increases the leakage current. It is difficult to obtain a wider depletion region for wide band gap semiconductors due to the limitation of semiconductor fabrication techniques. However, wide band gap semiconductors provide higher open circuit voltage, power, and efficiency. In addition, they have high radiation resistance, which can be further increased by modifying the junction such as introducing an intrinsic region.

Different types of junctions such as p-n, p-i-n, and Schottky junctions were investigated for betavoltaic batteries. Schottky junctions were mainly used for wide band gap semiconductors

GaN and SiC, as they are easier to manufacture compared to a p-n junction. The power output obtained from a Schottky junction of 4H-SiC was similar to the p-n junction of Si, and better than that of a Schottky junction of GaN. However, non-Schottky junction betavoltaic batteries showed better results. A maximum short circuit current of 937 nA/cm^2 and a maximum power output of 259 nW/cm^2 were obtained for AlGaAs in an experimental device, which were the best results out of all the experimental betavoltaic batteries. However, the result was obtained from only one experiment with AlGaAs where H-3 gas was used and the power output degraded rapidly due to high diffusion of H-3 into the semiconductor. Similarly, a maximum open circuit voltage of 2.06 V and an efficiency of 1.99% were obtained experimentally for SiC. Among other wide band gap semiconductors, GaN is difficult to fabricate. Therefore, SiC may be a better choice when a wide band gap semiconductor is considered in betavoltaic battery design. The wide range of performance of betavoltaic batteries suggests that most of the experimental research devices were not optimized. In addition, the choice of radioisotope and the semiconductor design parameters need to be similar for better comparison.

In summary, while much research has been conducted in the area of betavoltaic battery design, there is still more significant progress that can be made. Just like the significant breakthroughs that have been made in improved overall efficiency for photovoltaic cells through better modeling and optimization in design, the field of betavoltaic batteries is now ready for its own revolutionary progress.

2.9 References

[1] W. Pfann and W. Van Roosbroeck, "Radioactive and Photoelectric p-n Junction Power Sources," *Journal of Applied Physics,* vol. 25, pp. 1422-1434, 1954.

[2] P. Rappaport, "The electron-voltaic effect in p-n junctions induced by beta-particle bombardment," *Physical Review,* vol. 93, p. 246, 1954.

[3] P. Rappaport, "Radioactive battery employing intrinsic semiconductor," ed: Google Patents, 1956.

[4] B. Liu, K. P. Chen, N. P. Kherani, and S. Zukotynski, "Power-scaling performance of a three-dimensional tritium betavoltaic diode," *Applied Physics Letters,* vol. 95, pp. 233112-233112-3, 2009.

[5] Z. Cheng, X. Chen, H. San, Z. Feng, and B. Liu, "A high open-circuit voltage gallium nitride betavoltaic microbattery," *Journal of Micromechanics and Microengineering,* vol. 22, p. 074011, 2012.

[6] H. Gao, S. Luo, H. Zhang, H. Wang, and Z. Fu, "Demonstration, radiation tolerance and design on a betavoltaic micropower," *Energy*, 2013.

[7] M. Lu, G.-g. Zhang, K. Fu, G.-h. Yu, D. Su, and J.-f. Hu, "Gallium Nitride Schottky betavoltaic nuclear batteries," *Energy Conversion and Management,* vol. 52, pp. 1955-1958, 2011.

[8] C. Eiting, V. Krishnamoorthy, S. Rodgers, T. George, J. D. Robertson, and J. Brockman, "Demonstration of a radiation resistant, high efficiency SiC betavoltaic," *Applied physics letters,* vol. 88, pp. 064101-064101-3, 2006.

[9] M. Lewis and S. Seeman, "Performance Experience with Prototype Betacel Nuclear Batteries," *Nuclear Technology,* vol. 17, pp. 160-167, 1973.

[10] A. Sciuto, G. D'Arrigo, F. Roccaforte, M. Mazzillo, R. Spinella, and V. Raineri, "Interdigit 4H-SiC vertical Schottky diode for betavoltaic applications," *Electron Devices, IEEE Transactions on,* vol. 58, pp. 593-599, 2011.

[11] L. Olsen, "Betavoltaic energy conversion," *Energy Conversion,* vol. 13, pp. 117-127, 1973.

[12] J. Kwon and J. D. ROBERTSON. (2009, World's smallest nucleat battery. *American Ceramic Society Bulletin 88(10),* 13-14.

[13] A. Lal and J. Blanchard, "Daintiest dynamos [nuclear microbatteries]," *Spectrum, IEEE,* vol. 41, pp. 36-41, 2004.

[14] K. Wu, C. Dai, and H. Guo, "A theoretical study on silicon betavoltaics using Ni-63," in *Nano/Micro Engineered and Molecular Systems (NEMS), 2011 IEEE International Conference on*, 2011, pp. 724-727.

[15] G. Wang, R. Hu, H. Wei, H. Zhang, Y. Yang, X. Xiong, *et al.*, "The effect of temperature changes on electrical performance of the betavoltaic cell," *Applied Radiation and Isotopes,* vol. 68, pp. 2214-2217, 2010.

[16] D.-Y. Qiao, X.-J. Chen, Y. Ren, and W.-Z. Yuan, "A Micro Nuclear Battery Based on SiC Schottky Barrier Diode," *Microelectromechanical Systems, Journal of,* vol. 20, pp. 685-690, 2011.

[17] M. Mohamadian, S. Feghhi, and H. Afariadeh, "Geometrical optimization of GaN betavoltaic microbattery," in *Proceedings of the 7th WSEAS International Conference on Power Systems, Beijing, China*, 2009, pp. 247-250.

[18] D.-Y. Qiao, Y. Wei-Zheng, G. Peng, Y. Xian-Wang, Z. Bo, Z. Lin, *et al.*, "Demonstration of a 4H SiC betavoltaic nuclear battery based on Schottky barrier diode," *Chinese Physics Letters,* vol. 25, p. 3798, 2008.

[19] B. Ulmen, P. Desai, S. Moghaddam, G. Miley, and R. Masel, "Development of diode junction nuclear battery using 63 Ni," *Journal of radioanalytical and nuclear chemistry,* vol. 282, pp. 601-604, 2009.

[20] M. Chandrashekhar, C. I. Thomas, H. Li, M. G. Spencer, and A. Lal, "Demonstration of a 4H SiC betavoltaic cell," *Applied physics letters,* vol. 88, pp. 033506-033506-3, 2006.

[21] N. Tsoulfanidis, *Measurement and detection of radiaiton*, 3rd ed. Boca Raton, FL 33487: CRC, 2010.

[22] C. A. Klein, "Bandgap dependence and related features of radiation ionization energies in semiconductors," *Journal of Applied Physics,* vol. 39, pp. 2029-2038, 1968.

[23] M. Chandrashekhar, C. I. Thomas, and M. G. Spencer, "Measurement of the mean electron-hole pair ionization energy in 4H SiC," *Applied physics letters,* vol. 89, 2006.

[24] X. Tang, D. Ding, Y. Liu, and D. Chen, "Optimization design and analysis of Si-63Ni betavoltaic battery," *Science China Technological Sciences*, vol. 55, pp. 990-996, 2012.

[25] H. San, S. Yao, X. Wang, Z. Cheng, and X. Chen, "Design and Simulation of GaN based Schottky Betavoltaic Nuclear Micro-battery," *Applied Radiation and Isotopes*, 2013.

[26] C. D. Cress, B. J. Landi, and R. P. Raffaelle, "Modeling laterally-contacted nipi-diode radioisotope batteries," *Nuclear Science, IEEE Transactions on*, vol. 55, pp. 1736-1743, 2008.

[27] X.-Y. Li, Y. Ren, X.-J. Chen, D.-Y. Qiao, and W.-Z. Yuan, "63Ni schottky barrier nuclear battery of 4H-SiC," *Journal of Radioanalytical and Nuclear Chemistry*, vol. 287, pp. 173-176, 2011.

[28] G. Pistoia, *Batteries for portable devices*. San Diego, CA 92101: Elsevier, 2005.

[29] J. Chu, X. Piao, L. Jian, and H. Lin, "Research of radioisotope microbattery based on β-radio-voltaic effect," *Journal of Micro/Nanolithography, MEMS, and MOEMS*, vol. 8, pp. 021180-021180-6, 2009.

[30] C. Honsberg, W. A. Doolittle, M. Allen, and C. Wang, "GaN betavoltaic energy converters," in *Photovoltaic Specialists Conference, 2005. Conference Record of the Thirty-first IEEE*, 2005, pp. 102-105.

[31] M. Mohamadian, S. Feghhi, and H. Afarideh, "Conceptual design of GaN betavoltaic battery using in cardiac pacemaker," in *Proceedings of 13th International Conf on Emerging of Nuclear Energy Systems (ICENES), Istanbul, Turkey*, 2007.

[32] X. Tang, Y. Liu, D. Ding, and D. Chen, "Optimization design of GaN betavoltaic microbattery," *Science China Technological Sciences*, vol. 55, pp. 659-664, 2012.

[33] L. Da-Rang, J. Lan, Y. Jian-Hua, T. Yuan-Yuan, and L. Nai, "Betavoltaic Battery Conversion Efficiency Improvement Based on Interlayer Structures," *Chinese Physics Letters*, vol. 29, p. 078102, 2012.

[34] H. Chen, L. Jiang, and X. Chen, "Design optimization of GaAs betavoltaic batteries," *Journal of Physics D: Applied Physics*, vol. 44, p. 215303, 2011.

[35] H. Guo, H. Yang, and Y. Zhang, "Betavoltaic microbatteries using porous silicon," in *Micro Electro Mechanical Systems, 2007. MEMS. IEEE 20th International Conference on*, 2007, pp. 867-870.

[36] Z. Cheng, S. Hai-Sheng, C. Xu-Yuan, L. Bo, and F. Zhi-Hong, "Demonstration of a high open-circuit voltage GaN betavoltaic microbattery," *Chinese Physics Letters*, vol. 28, p. 078401, 2011.

[37] M. Lu, G. Wang, and C. S. Yao, "Gallium nitride for nuclear batteries," *Advanced Materials Research*, vol. 343, pp. 56-61, 2012.

[38] A. Ionascut-Nedelcescu, C. Carlone, A. Houdayer, H. Von Bardeleben, J.-L. Cantin, and S. Raymond, "Radiation hardness of gallium nitride," *Nuclear Science, IEEE Transactions on*, vol. 49, pp. 2733-2738, 2002.

[39] H. Guo and A. Lal, "Nanopower betavoltaic microbatteries," in *TRANSDUCERS, Solid-State Sensors, Actuators and Microsystems, 12th International Conference on, 2003,* 2003, pp. 36-39.

[40] G. Rybicki, C. Vargas-Aburto, and R. Uribe, "Silicon carbide alphavoltaic battery," in *Photovoltaic Specialists Conference, 1996., Conference Record of the Twenty Fifth IEEE*, 1996, pp. 93-96.

[41] S. Deus, "Tritium-powered betavoltaic cells based on amorphous silicon," in *Photovoltaic Specialists Conference, 2000. Conference Record of the Twenty-Eighth IEEE*, 2000, pp. 1246-1249.

[42] C. D. Cress, B. J. Landi, R. P. Raffaelle, and D. M. Wilt, "InGaP alpha voltaic batteries: synthesis, modeling, and radiation tolerance," *Journal of applied physics,* vol. 100, pp. 114519-114519-5, 2006.

[43] T. Wacharasindhu, J. Kwon, D. Meier, and J. Robertson, "Radioisotope microbattery based on liquid semiconductor," *Applied physics letters,* vol. 95, pp. 014103-014103-3, 2009.

[44] L. T. Canham, "Silicon quantum wire array fabrication by electrochemical and chemical dissolution of wafers," *Applied Physics Letters,* vol. 57, pp. 1046-1048, 1990.

[45] Z. Zhao, Z. Cheng, S. Yao, Z. Deng, Y. Li, and H. San, "Effect of three-dimensional cylindrical hole array on energy conversion efficiency of radioisotope battery," in *Nano/Micro Engineered and Molecular Systems (NEMS), 2011 IEEE International Conference on*, 2011, pp. 992-995.

[46] Z. Cheng, Z. Zhao, H. San, and X. Chen, "Demonstration of a GaN betavoltaic microbattery," in *Nano/Micro Engineered and Molecular Systems (NEMS), 2011 IEEE International Conference on*, 2011, pp. 1036-1039.

[47] S. Tin and A. Lal, "ULTRA-HIGH EFFICIENCY HIGH POWER DENSITY THINNED-DOWN SILICON CARBIDE BETAVOLTAICS."

[48] T. Kosteski, N. Kherani, P. Stradins, F. Gaspari, W. Shmayda, L. Sidhu, *et al.*, "Tritiated amorphous silicon betavoltaic devices," in *Circuits, Devices and Systems, IEE Proceedings-*, 2003, pp. 274-81.

[49] J. E. Turner, *Atoms, radiation, and radiation protection*: John Wiley & Sons, 2008.

[50] L. Romano, V. Privitera, and C. Jagadish, *Defects in Semiconductors*: Elsevier Science, 2015.

[51] I. Gusev, A. Guskova, and F. A. Mettler, *Medical management of radiation accidents*: CRC Press, 2001.

[52] J. Shapiro, *Radiation protection: a guide for scientists, regulators, and physicians*: La Editorial, UPR, 2002.

[53] S.-K. Lee, S.-H. Son, K. Kim, J.-W. Park, H. Lim, J.-M. Lee, *et al.*, "Development of nuclear micro-battery with solid tritium source," *Applied Radiation and Isotopes*, vol. 67, pp. 1234-1238, 2009.

[54] S. Adachi, "GaAs, AlAs, and AlxGa1− xAs: Material parameters for use in research and device applications," *Journal of Applied Physics,* vol. 58, pp. R1-R29, 1985.

[55] W. Sun, N. Kherani, K. Hirschman, L. Gadeken, and P. Fauchet, "A three-diomensional porous silicon p-n diode for betavoltaics and photovoltaics," *Advance Materials,* vol. 17, pp. 1230-1233, 2005.

[56] Z. Cheng, H. San, Y. Li, and X. Chen, "The design optimization for GaN-based betavoltaic microbattery," in *Nano/Micro Engineered and Molecular Systems (NEMS), 2010 5th IEEE International Conference on*, 2010, pp. 582-586.

[57] Z. Cheng, H. San, Z. Feng, B. Liu, and X. Chen, "High open-circuit voltage betavoltaic cell based on GaN pin homojunction," *Electronics letters,* vol. 47, pp. 720-722, 2011.

[58] H. Guo, Y. Shi, Y. Zhang, Y. Zhang, and J. Han, "Fabrication of SiC pin betavoltaic cell with< sup> 63</sup> Ni irradiation source," in *Electron Devices and Solid-State Circuits (EDSSC), 2011 International Conference of*, 2011, pp. 1-2.

[59] S. Tin and A. Lal, "A radioisotope-powered surface acoustic wave transponder," *Journal of Micromechanics and Microengineering,* vol. 19, p. 094014, 2009.

CHAPTER 3: BETA PARTICLE TRANSPORT AND ITS IMPACT ON BETAVOLTAIC BATTERY MODELING

[Publication information: Tariq R. Alam, Mark A. Pierson, and Mark A. Prelas, Beta Particle Transport and Its impact on Betavoltaic Battery Modeling, Applied Radiation and Isotopes, Vol. 130 (2017)]

3.1 Abstract

Simulation of beta particle transport from a Ni-63 radioisotope in silicon using the Monte Carlo N-Particle (MCNP) transport code for monoenergetic beta particle average energy, monoenergetic beta particle maximum energy, and the more precise full beta energy spectrum of Ni-63 were demonstrated. The beta particle penetration depth and the shape of the energy deposition varied significantly for different transport approaches. A penetration depth of 2.25±0.25 μm with a peak in energy deposition was found when using a monoenergetic beta particle average energy and a depth of 14.25±0.25 μm with an exponential decrease in energy deposition was found when using a full beta energy spectrum and a 0 degree angular variation. For a 90 degree angular variation, i.e. an isotropic source, the penetration depth was decreased to 12.75±0.25 μm and the backscattering coefficient increased to 0.46 with 30.55% of the beta energy escaping when using a full beta energy spectrum. Similarly, for a 0 degree angular variation and an isotropic source, an overprediction in the short circuit current and open circuit voltage solved by a simplified drift-diffusion model was observed when compared to experimental results from the literature. A good agreement in the results was found when self-absorption and isotope dilution in the source was

considered. The self-absorption effect was 15% for a Ni-63 source with an activity of 0.25 mCi. This effect increased to about 28.5% for a higher source activity of 1 mCi due to an increase in thickness of the Ni-63 source. Source thicknesses of approximately 0.1 μm and 0.4 μm for these Ni-63 activities predicted about 15% and 28.5% self-absorption in the source, respectively, using MCNP simulations with an isotropic source. The modeling assumptions with different beta particle energy inputs, junction depth of the semiconductor, backscattering of beta particles, an isotropic beta source, and self-absorption of the radioisotope have significant impacts in betavoltaic battery design.

Keywords: Betavoltaic battery model, beta particle transport, beta particle angular distribution, penetration depth, energy deposition, self-absorption

3.2 Introduction

Betavoltaic batteries harvest energy from beta emitting radioisotope sources using semiconductors. The kinetic energy of the beta particles from the radioisotope is converted into electrical energy in the semiconductor. Betavoltaic batteries have some unique features such as a long service life (several years to several decades) and small size [1, 2]. They can be miniaturized to micron sizes due to their high energy density. These advantages of betavoltaic batteries over other types of batteries make them an attractive power source for fulfilling the requirements of future generation electronic devices [3, 4].

This work examines and contrasts the strengths and weaknesses of the main modeling philosophies applied to betavoltaic batteries. The analysis of the energy deposition of beta particles

in semiconductors, the estimation of their penetration depth, and the profile of electron-hole pair (EHP) generation in semiconductors are of utmost importance in betavoltaic battery design. These analyses are important in order to get a better estimate of EHP production, which determines the semiconductor design parameters such as top layer thickness or junction depth, doping concentrations, and thickness. The design of the battery varies depending on how the beta particle energy is chosen such as average beta particle energy or the full beta energy spectrum, beta particles angular emission such as isotropic or non-isotropic emission, and the consideration of self-absorption effects [5]. Many researchers have used different methods such as the Katz-Penfold range equation, the Everhart and Hoff range equation, the Kanaya-Okayama model, and Monte Carlo methods such as Monte Carlo N-Particle (MCNP) transport code for determining energy deposition and penetration depth [6-9]. Most of the available betavoltaic designs have only considered the average beta particle energy. The Monte Carlo method using MCNP software [10] was used in this work because of its comprehensive atomic physics model which obtains better estimates of energy deposition and penetration depth. Monoenergetic beta particle average energy, monoenergetic beta particle maximum energy, and a full beta energy spectrum of Ni-63 were considered as different types of source inputs in the MCNP model to analyze the energy deposition and penetration depth in silicon (Si). Some recent works showed the qualitative difference in energy deposition for different beta input energies and discussed the importance of modeling full beta energy spectrum [11-15]. In this work, it will be shown that different input energy profiles could have a significant impact on betavoltaic battery design based on the junction depth analysis. The penetration depths obtained from the MCNP model and the Katz-Penfold range equation for monoenergetic beta particle average energy and monoenergetic beta particle maximum energy of Ni-63 in Si were compared. The MCNP model was further analyzed for different angular

distributions of the beta particle's initial direction for a full beta energy spectrum. In reality, beta particles are emitted isotropically from a radioisotope source. It will be shown that the variation in angular distribution of the beta particles is an important factor for betavoltaic battery design. The analysis of a backscattering effect due to various angular emissions of beta particles has significant impact in the design. A simplified drift-diffusion semiconductor model was then used to calculate the short circuit current, the open circuit voltage, and the leakage current for the betavoltaic batteries. It was shown that the junction depth is a very important design parameter in determining the short circuit current, open circuit voltage, and leakage current. However, the optimum junction depth depends on the beta particle energy input and its angular distribution. The simulated betavoltaic battery results were then compared to some results from the literature for actual betavoltaic batteries. The results were explained by the self-absorption effect of the beta particles in the radioisotope source. The self-absorption has normally been overlooked in the theoretical modeling of betavoltaic battery design. In reality, the efficiency of a betavoltaic battery is limited by the self-absorption effect of the radioactive source. Therefore, consideration of the self-absorption effect will provide a better estimate of betavoltaic battery outputs such as the short circuit current, open circuit voltage, and leakage current. It was noted that Zuo et al. [11] also modeled Ni-63 with silicon and validated their results. However, the detailed studies and analyses of beta particles angular emission, backscattering effect, penetration depths, self-absorption effect, and the importance of optimum junction depth are presented in this work. Furthermore, the self-absorption effect of the source was analyzed using MCNP and compared with the results obtained by the chord method [13].

The organization of the paper includes a brief summary of the MCNP method and a brief discussion of the beta particle energy spectrum used in this work. It also includes the statistical reliability analysis of the MCNP outputs for convergence. Finally, the important effects of the penetration depth, EHP estimates, angular variation, junction depth, and self-absorption on the short circuit current, open circuit voltage, and leakage current are presented and discussed and then conclusions are drawn.

3.3 Method

The electron-photon-positron transport feature of MCNP6 (version Beta 3) was used in this work. MCNP uses a detailed physics model of electron-photon-positron transport. The physical events for electron transport are elastic and inelastic collisions of the incoming electrons (beta particles) emitted from a radioisotope source with the atomic electrons and nuclei in the material. An electron mainly loses its energy by inelastic collisions with the atomic electrons and changes direction by elastic collisions with the electrostatic field of the atomic nuclei [16, 17]. The inelastic collisions with orbital electrons dominate at lower kinetic energies such as less than 10 MeV. In this case, the energy is lost due to atomic excitation and ionization, which in turn creates soft x-rays and knock-on electrons. When the electron energy is higher than a few MeV, the inelastic collisions with both atomic nuclei and electrons become dominant, which causes sudden speed changes in the incoming electrons. In this case, the energy is lost due to the bremsstrahlung effect, which in turn creates photons. A photon loses its energy and changes direction by physical events such as photoelectric effect, coherent and incoherent scattering, and pair production [18]. A positron is created during the pair production event. A positron experiences similar scattering

events like electrons and annihilates with electrons. MCNP considers all the physical events for each particle by employing different types of cross sections. In this work, Nickel-63 is the beta emitter which has a maximum beta particle energy of 66.7 keV. Thus, the photon energy loss compared to the atomic excitation and ionization, which is the radiation yield, is on the order of 10^{-4}. MCNP uses the continuous slowing down approximation (CSDA) method to estimate the energy loss by collisional stopping power. It also uses Goudsmit-Saunderson's theory for the multiple scattering method to estimate the angular deflections of electrons using the numerically tabulated Riley cross section for electrons under 256 keV. The Moller cross-section is used in MCNP to calculate the generation of knock-on electrons.

Electrons are tracked down to 20 eV in this work. MCNP uses two different algorithms such as the condensed history and the single event method depending on the energy of a particle [19-21]. The condensed history algorithm is applicable for the energy range of 1 keV to 100 GeV [19], where it condenses multiple electron interactions in each logarithmic energy step size. It is computationally expensive for the electron transport to track all the interactions as it goes through a large number of collisions due to long range coulomb interactions for small energy loss [22]. Thus, the net effect of energy loss and angular deflection are estimated in the condensed history algorithm within a small energy step size. On the other hand, MCNP uses the single event method for particles with energy below 1 keV to 10 eV [21]. In the single event method, MCNP calculates the path lengths for all four physical events such as elastic scattering, atomic excitation, knock-on, and bremsstrahlung, then, takes the shortest path length of the associated physical events. It estimates the energy loss and angular deflection from the cross sections of the selected physical

events. The average behavior of the physical system such as the energy deposition was inferred by MCNP from the statistics of individual particles.

3.4 Precise beta spectrum vs generalized beta spectrum for MCNP input

The amount of energy deposited and the depth of penetration of the beta particles emitted by the radioisotope source depends on their initial kinetic energy. Examples of radioisotopes that undergo radioactive decay by emitting beta particles are Ni-63, Sr-90, S-35, and P-32 [6]. Each beta particle emitted in decay has a continuous energy spectrum between zero and a maximum value. This maximum beta particle energy varies for different radioisotopes. The result is that each radioisotope will have a continuous energy probability distribution, which is known as the beta energy spectrum. The beta energy spectrum is derived from Fermi's golden rule based on the weak force interaction in the atomic nucleus [23]. The transition probability rate of beta particles, λ, is related to the final density of states by equations (1) to (3),

$$\lambda = \frac{2\pi}{\hbar}\left|V_{fi}\right|^2 \rho\left(E_f\right), \tag{1}$$

$$V_{fi} = \int \Psi_f^* V \Psi_i d\tau, \tag{2}$$

$$\rho\left(E_f\right) = \frac{dn}{dE_f}, \tag{3}$$

where, V_{fi} is the matrix element, which is the integral of all the interactions V between initial and final states, Ψ is the wave function of the initial and final atomic states, and density of the final states, $\rho(E_f)$, represents the number of accessible final states dn within the energy dE_f. The

beta energy spectrum is then derived from the allowed approximation of the electron wave function in Fermi's golden rule, where the matrix element has no influence on the shape of the beta energy spectrum, and is given by equation (4),

$$N(T_e) \propto (T_e^2 + 2T_e m_e c^2)^{1/2}(Q - T_e)^2(T_e + m_e c^2), \qquad (4)$$

where, T_e is the electron kinetic energy, m_e is the electron mass, Q is the decay energy, and c is the speed of light. This spectrum vanishes at $T_e = 0$ and $T_e = Q$, which is a generalized spectrum with similar shape for all beta emitting radioisotopes based on their maximum beta energy as shown in Figure 1. This beta energy spectrum shows a peak around the average energy, which is typically one-third of its maximum energy. However, the inclusion of the Fermi function that takes into account coulomb interaction of the beta particles with the atomic nucleus can change this typical generalized spectrum shape. In the case of Ni-63, it exhibits a different type of beta energy spectrum, where the peak of the probability distribution of the beta particle energy is observed at low beta particle energy instead of at the average beta particle energy [24, 25]. The

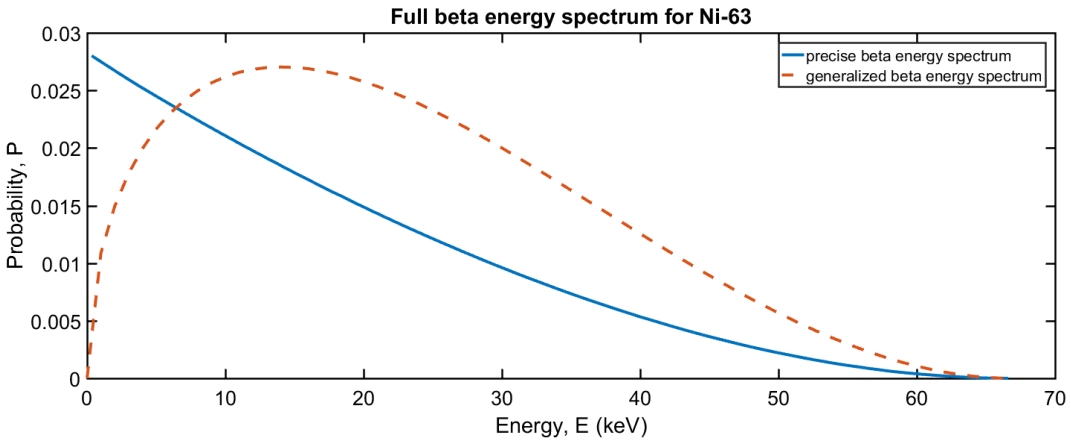

Figure 3-1: Different types of continuous beta energy distributions for Ni-63

probability distribution then decreases with increasing beta particle energy and becomes a minimum at the maximum energy as shown in Figure 3-1. This is therefore a more accurate representation of the beta energy spectrum for Ni-63 [9].

It is important to note that many previous simulations [26, 27] of betavoltaic batteries used either a single monoenergetic average beta particle energy or the maximum beta particle energy. This significantly affects the resulting energy deposition profile and penetration depth estimates. As a result, the simulated outputs of these models will not be accurate. This phenomenon is also emphasized by some recent works [11-15, 28]. More specifically, the qualitative difference in energy deposition for monoenergetic average beta energy and full beta energy spectrum was highlighted using in-house Monte Carlo simulation and scanning electron microscope [14]. Thus, an accurate continuous beta energy spectrum will be used for comparison in all of the simulations presented in this paper.

3.5 Convergence and reliability of MCNP simulation results

An MCNP simulation using a Ni-63 full beta energy spectrum with silicon was analyzed. The energy deposition F6 tally was scored for a Ni-63 point source placed on the side wall of a slab geometry of silicon with a dimension of 500×500×50 μm as shown in Figure 3-2. The simulation was run with different particle histories of 10^3, 10^4, 10^5, 10^6, 10^7, and 10^8 to study the convergence of the energy deposition tally and the reliability of the results.

For the MCNP simulation, the silicon slab was divided into 100 cells, each 0.5 μm thick for a spatial resolution of ±0.25 μm, in the thickness direction in order to achieve a fine tally

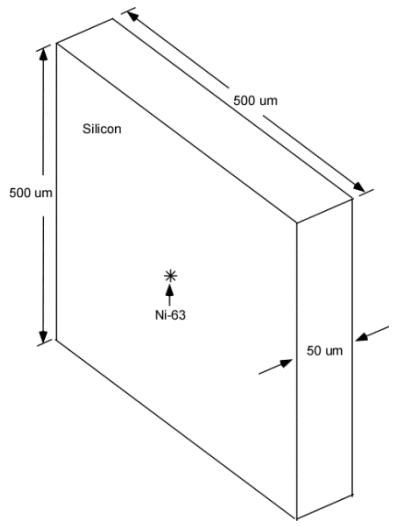

Figure 3-2: MCNP simulation setup for a Ni-63 point source with silicon slab geometry

resolution. The volumetric energy deposition of each cell was tallied along the thickness direction until the full 50 µm thickness was reached. As expected, the energy deposition was very high near the surface and dropped exponentially along the thickness direction. It is noted that as further penetration is achieved into the silicon, the energy deposition eventually becomes less than that needed for electron hole pair formation. This point is reached after about 21 µm thickness. No electron hole pair will be generated beyond this maximum penetration depth. However, the design will be optimized for a thickness where 99% of the total energy of the incoming beta particles is deposited. This depth will be less than the maximum possible penetration depth, but does not result in any loss of performance in the battery.

To study the reliability and convergence of the energy deposition tally, the relative errors were plotted against the penetration depth for different particle histories. Figure 3-3 shows the relative error of each tally score for all particle histories up to a thickness of 21 µm. The plot

indicates that the energy deposition tally is converging since the relative error decreases with an increasing number of particles. The relative error also increases along the thickness direction, since there are fewer particles remaining at greater depths which reduce the statistical accuracy. However, the relative error is still less than 0.045 (or 4.5%) even at the maximum penetration depth for 10^6, 10^7, and 10^8 particle histories. For 10^7 and 10^8 particle histories, the relative errors are 0.0145 (or 1.45%) and 0.0046 (or 0.46%), respectively, at the maximum penetration depth.

Figure 3-4 shows the variation in the Figure of Merit (FOM) with different particle histories. FOM is expressed by $1/R^2T$, where R is the relative error and T is the computation time. It is a dimensionless number, where a higher number indicates a more efficient simulation. The relative error can be reduced with the expense of higher computation time by increasing the number of particle histories. In Figure 3-4, FOM is almost constant for a large variation in particle histories. This implies that the energy deposition (F6 tally) results are stable.

Both Figure 3-3 and Figure 3-4 indicate that the energy deposition tally is converging. From this analysis of the relative error, a 10^7 particle history is chosen to provide reliable statistics for the energy deposition tally. A semi-log plot of energy deposition with uncertainties for 10^7 particle histories is shown in Figure 3-5. As the uncertainties are very low, the vertical error bars with maximum and minimum are shown as horizontal lines in Figure 3-5.

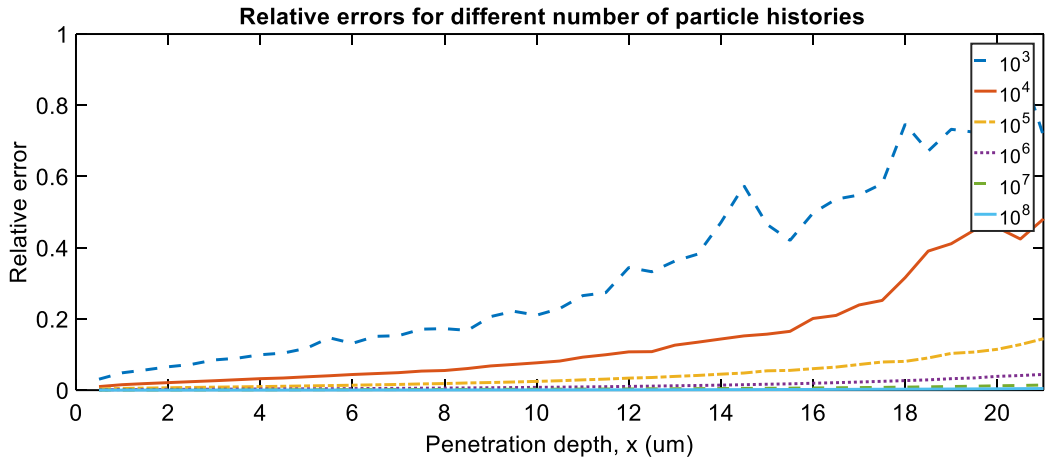

Figure 3-3: Relative error vs penetration depth for different particle histories

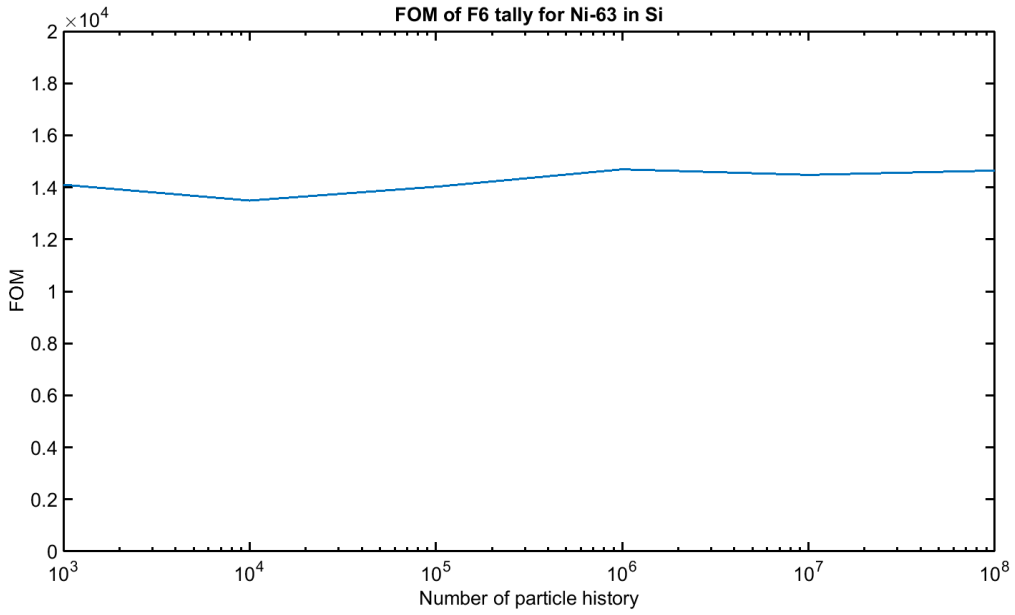

Figure 3-4: FOM vs number of particle histories

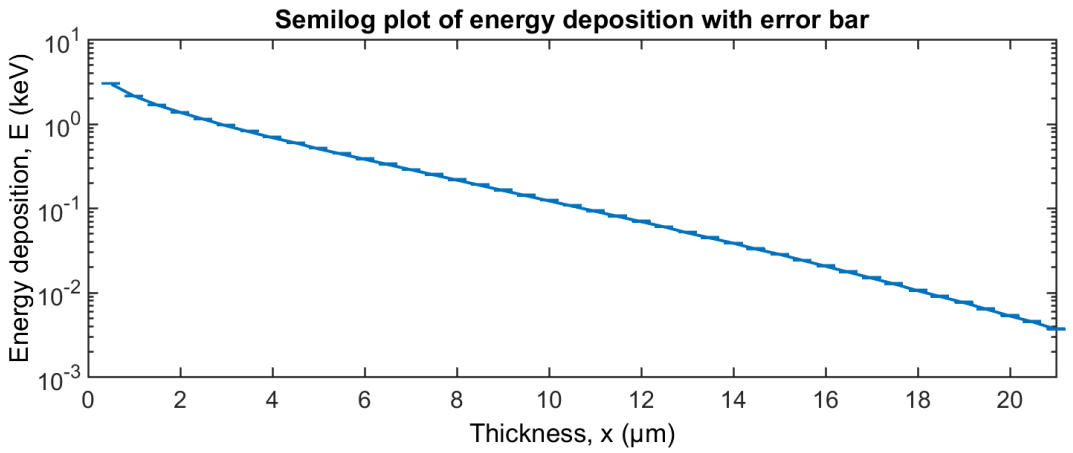

Figure 3-5: Energy deposition along the thickness direction for Ni-63 in Si

Figure 3-5 shows that the energy deposition decreases exponentially with thickness and uncertainty of the results is insignificant along the penetration depth of 21 μm. Therefore, the energy deposition using 10^7 number of particle histories is reliable for this analysis and will be used in the rest of the simulations.

3.6 Analysis of beta particle transport results using MCNP

To compare the effects of using different beta particle energies, a similar geometry and source setup like that in Figure 3-2 was used to determine the penetration depth in silicon for three different Ni-63 energy cases. These cases used (1) the monoenergetic average beta particle energy for Ni-63, (2) the monoenergetic maximum beta particle energy for Ni-63, and (3) the full beta energy spectrum (precise) for Ni-63 shown in Figure 3-1. Since 10^7 particle histories showed convergence and a low relative error for this slab configuration in the previous section, this number

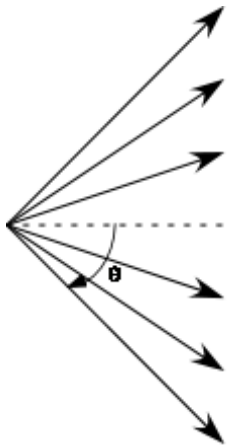

Figure 3-6: Conical distribution of beta particles in different angular directions

of particle histories was used in this analysis for the different beta particle energy cases listed above. The penetration depth of electrons in a material will vary with the different input energies. The penetration depth is the maximum thickness required for a material to stop the majority of the beta particles. It can be determined by observing the depth at which the MCNP energy deposition values become negligible. From a betavoltaic battery perspective, any energy deposition amount that is less than the energy required to create one electron hole pair can be considered negligible. However, from an engineering design perspective, the energy deposition beyond 99% of the total energy deposition can be neglected. The penetration depths for Ni-63 in silicon are determined based on these two criteria. The penetration depths from the MCNP energy deposition simulation results are compared in Table 3.1 for the three different input energy cases described above. For the case where the Ni-63 full beta energy spectrum is used, Table 3.1 also provides results based on the angular dependency of the initial direction of the emitted beta particles. The beta particles conical distribution or angular direction, θ, emitted from a radioisotope source is shown in Figure 3-6. An actual radioisotope source emits the beta particles in an isotropic direction. In other words,

the beta particles are not emitted only in the straight-line x-axis direction as the first three rows of results imply. To simulate the effect of isotropic emission of beta particles from the Ni-63 source, the third case for the full energy spectrum was modified to show three different isotropic spreading cones: 30 degrees, 60 degrees, and 90 degrees. The 90 degree cone should provide a more realistic estimate of how the beta particles are emitted toward the semiconductor material used in betavoltaic batteries. For each of these cones, the total source strength, in this case the same number of particle histories, was emitted over the spherical angle indicated. As expected, this angular emission reduced the penetration depth somewhat. For the two cases involving monoenergetic beta particle energies, a comparison was made by estimating the penetration depth using the empirical Katz-Penfold equation for low Z materials [29, 30], which is given in equation (5),

$$R = 0.412T^{1.27-0.0954lnT}, (0.01 \leq T \leq 2.5\ MeV) \qquad (5)$$

where R is the range density in g/cm^2 and T is the electron kinetic energy in MeV. R is then divided by the density of silicon to get the penetration depth. Note that this equation assumes the beta particles are emitted in the straight-line x-axis direction. The Katz-Penfold predictions are shown in the far right column of Table 3.1. These values are close to those predicted by MCNP for the case where 99% of the total beta particle energy has been deposited. However, as expected, the Katz-Penfold estimated values are quite different than those predicted by MCNP when the full beta energy spectrum is used.

Table 3.1: Variation of penetration depth for different energy inputs

Input type	Penetration depth up to 1 EHP energy (µm)	Penetration depth up to 99% energy deposited (µm)	Penetration depth by Katz-Penfold (µm)
Monoenergetic beta average energy (17.4 keV) 0 degree	3.75±0.25	2.25±0.25	2.16
Monoenergetic beta maximum energy (66.9 keV) 0 degree	37.25±0.25	29.25±0.25	28.49
Full beta energy spectrum (0-66.9 keV) 0 degree	20.75±0.25	14.25±0.25	
Beta energy spectrum 30 degree cone	20.25±0.25	14.25±0.25	
Beta energy spectrum 60 degree cone	19.25±0.25	13.25±0.25	
Beta energy spectrum 90 degree cone	17.75±0.25	12.75±0.25	

The determination of penetration depth using two different criteria indicates that a considerable amount of additional thickness, which is about 6 µm for the full beta energy spectrum, is required to absorb a negligible amount of energy. The results show a slight dependency of penetration depth based on angular variation of the initial direction of flight of the beta particles. The penetration depth decreases with higher initial angular direction of flight of the beta particles. In reality, since beta particles emit a continuous beta energy spectrum in a random direction from a radioisotope, the predicted penetration depth of 12.75±0.25 µm for Ni-63 beta particles in silicon provides a better estimate.

In addition, the backscattering coefficient, which is the percentage of beta particles scattered back from the surface, depends on the angular variation of the initial direction of impinging beta particles. A point source and a silicon surface that had a much larger cross-sectional area of 500×500 μm^2 compared to the MCNP penetration depth was used to calculate the backscattering coefficient in terms of the particles weight lost from the impinging surface.

Figure 3-7 shows that the backscattering coefficient increases with increasing angle of the initial direction of flight of a single beta particle. It also shows the percentage of the beta particle energy lost due to the backscattering effect of the surface. For 0 degree to 90 degrees, the backscattering coefficient varies from 0.16 ± 0.001 to 0.426 ± 0.002 and the percentage of energy lost varies from $8.92 \pm 0.06\%$ to $30.42 \pm 0.1\%$ respectively. It indicates that more beta particles with lower energies are lost due to the backscattering effect. It means that even though beta particles that are emitted at a large angle contribute most to the efficiency by generating more EHPs in the depletion region [31], they will also have a large electron backscattering effect which reduces efficiency. Furthermore, it was noted that the theoretical beta energy spectrum changes with the source thickness [13, 32]. Figure 3-7 also shows the backscattering coefficient and energy lost for the modified spectrum of a 0.1 μm thick Ni-63 source. The backscattering coefficient was almost the same for the modified spectrum. However, the energy escape increased due to higher source thickness. Thus, the angular distribution of beta particles needs to be considered in the model in order to take into account the energy lost due to the backscattering effect for a better estimate of energy deposition. This will be discussed further in the next section.

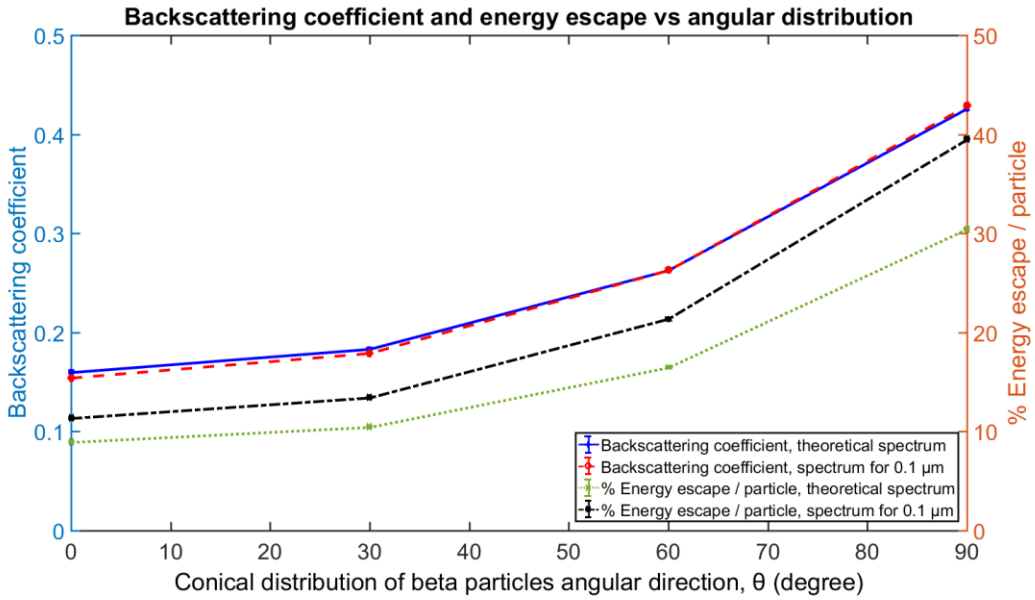

Figure 3-7: Backscattering effect with different initial beta particle direction of flight

The plots of energy deposition in silicon vary significantly for the monoenergetic average beta particle energy, the monoenergetic maximum beta particle energy, and the full beta particle energy spectrum cases for Ni-63 as seen in Figure 3-8.

A peak in the energy deposition plot occurs in Figure 3-8 for both the monoenergetic average and maximum beta particle energies. On the other hand, the energy deposition plot along the thickness direction is almost exponential for the full beta particle energy spectrum [11]. Therefore, in this latter case, most of the energy is deposited near the surface. Furthermore, the energy deposition near the surface increases with a higher angular beta particle direction and their

penetration depth decreases. Increased angular direction makes the exponential curve for the energy deposition plot steeper.

Thus, an MCNP analysis of beta particle transport provides a better estimate for energy deposition in the semiconductor due to its detailed physics model. This variation in the angular distribution of beta particles with a full beta energy spectrum is incorporated to provide a more accurate betavoltaic battery model. The energy deposition estimate determines the semiconductor device design parameters for the betavoltaic battery, which will be discussed in the following section.

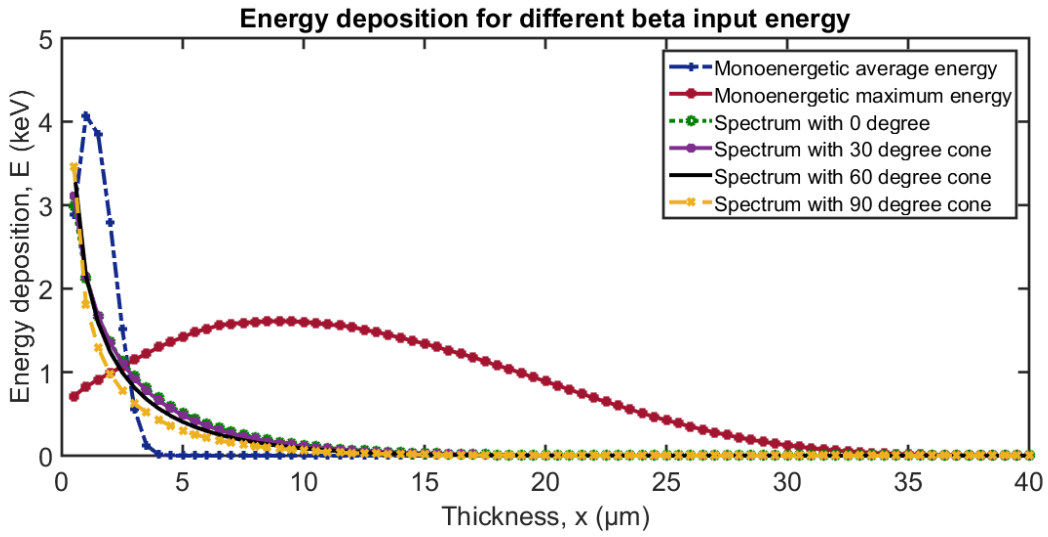

Figure 3-8: Energy deposition for monoenergetic average beta particle energy, monoenergetic maximum beta particle energy, and full beta energy spectrum with different initial beta particle direction of flight for Ni-63 in Si

3.7 Semiconductor device model for betavoltaic battery

MCNP only provides the beta particle energy deposition and does not provide an estimate of EHP generation in semiconductors. The electron hole pair ionization energy of 3.64 eV for silicon was used in a linear relationship to calculate the number of EHPs generated from the energy deposition as shown in Figure 3-9. As a result, the plot for EHP generation in a semiconductor has the same shape as the energy deposition plot from MCNP. After calculating the generation of EHPs from the MCNP energy deposition results, a semiconductor model is then required to estimate the collection of EHPs at the electrodes for the betavoltaic battery output. A closed form solution of the semiconductor drift-diffusion model with Boltzmann approximation was used to calculate the short circuit current, the open circuit voltage, and the leakage current of the betavoltaic battery. The drift current due to the electric field was considered only in the

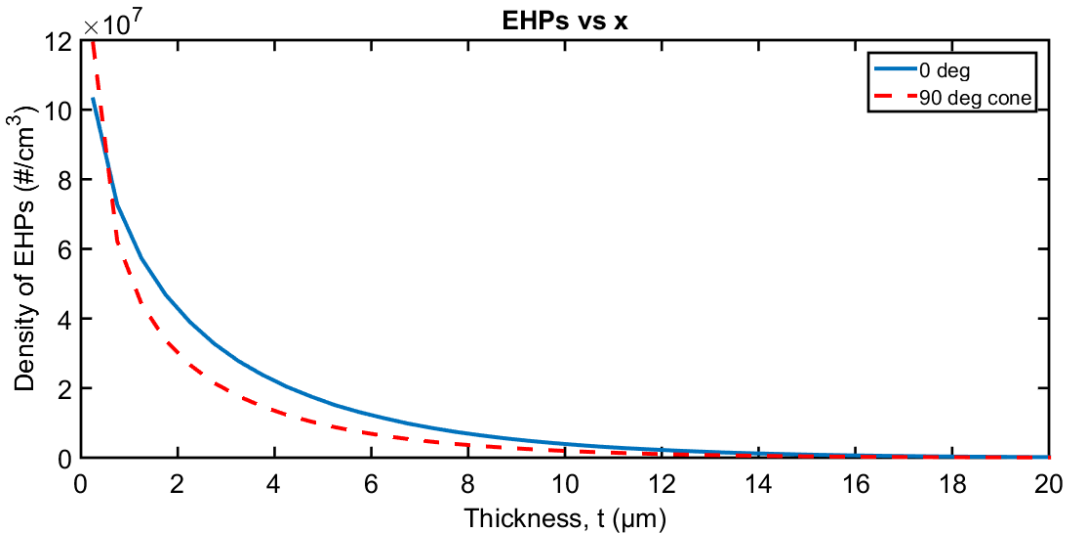

Figure 3-9: The generation of EHPs in Si for full beta energy spectrum of Ni-63 with 0 degree and 90 degree cone of initial direction

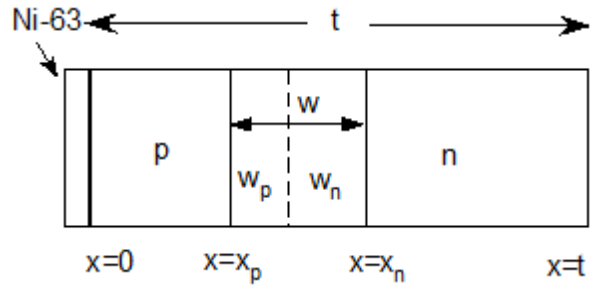

Figure 3-10: Drift-diffusion semiconductor model for betavoltaic batteries

depletion region, whereas the diffusion equations were solved in p-type and n-type regions for the minority carriers. Finally, the results were compared to experimental results with a betavoltaic battery using Ni-63 and a silicon transducer [26].

Figure 3-10 is a sketch of a p-n junction semiconductor used in this betavoltaic battery model. Similar to the experimental battery design, the Ni-63 radioisotope was placed on the outer surface of the p-side of the p-n junction silicon semiconductor. The EHPs that are generated in the semiconductor from the beta particle energy deposition are separated by the built-in electric field at the p-n junction. An exponential approximation of the above EHP generation plot was used in equations (6) and (7) represented by the term $A_0 a e^{-bx}$ or $A e^{-bx}$, where $A = A_0 a$.

$$\frac{d^2 \Delta n}{dx^2} - \frac{\Delta n}{L_n^2} = -\frac{A_0 a e^{-bx}}{D_n} \tag{6}$$

$$\frac{d^2 \Delta p}{dx^2} - \frac{\Delta p}{L_p^2} = -\frac{A_0 a e^{-bx}}{D_p} \tag{7}$$

The diffusion equations (6) and (7) for the minority carriers were solved in the p-type and n-type regions of the semiconductor with two boundary conditions.

$$D_n \frac{dn}{dx} = S_n \Delta n \quad (8)$$

$$\Delta n(x_p) = 0 \quad (9)$$

$$-D_p \frac{dp}{dx} = S_p \Delta p \quad (10)$$

$$\Delta p(x_n) = 0 \quad (11)$$

Equations (8) and (9) are the boundary conditions for the p-type region, whereas equations (10) and (11) are the boundary conditions for the n-type region. The boundary conditions given in equations (8) and (10) were applied at the surface considering the surface recombination. Similarly, equations (9) and (11) were applied at the edge of the depletion region representing no excess minority carriers at that location. After solving the minority carrier diffusion equations, the short circuit currents in the n-type and p-type regions are given in equations (12) and (13) respectively. The depletion region current in equation (14) is the integral of the EHPs in the depletion region.

$$J_n = \left\{\frac{qAL_n}{b^2L_n^2-1}\right\}\left[\frac{\left(\frac{S_nL_n}{D_n}+bL_n\right)-e^{-bx_p}\left\{\frac{S_nL_n}{D_n}cosh\left(\frac{x_p}{L_n}\right)+sinh\left(\frac{x_p}{L_n}\right)\right\}}{\frac{S_nL_n}{D_n}sinh\left(\frac{x_p}{L_n}\right)+cosh\left(\frac{x_p}{L_n}\right)} - bL_ne^{-bx_p}\right] \quad (12)$$

$$J_p = \left\{\frac{qAL_p}{b^2L_p^2-1}\right\}\left[\frac{\left(\frac{S_pL_p}{D_p}-bL_p\right)e^{-bt}-e^{-bx_n}\left\{\frac{S_pL_p}{D_p}cosh\left(\frac{t-x_n}{L_p}\right)+sinh\left(\frac{t-x_n}{L_p}\right)\right\}}{\frac{S_pL_p}{D_p}sinh\left(\frac{t-x_n}{L_p}\right)+cosh\left(\frac{t-x_n}{L_p}\right)} + bL_pe^{-bx_n}\right] \quad (13)$$

$$J_{dep} = \frac{qA}{b}e^{-bx_p}[1-e^{-bw}] \quad (14)$$

The short circuit current of the battery is the sum of the short circuit currents in the p-type, n-type, and depletion regions. The short circuit current is directly proportional to the activity

of the radioisotope. The open circuit voltage of the battery and the leakage current of the semiconductor are given in equations (15) and (16) respectively.

$$V_{oc} = \frac{kT}{q} ln\left(\frac{J_{sc}}{J_0} + 1\right) \tag{15}$$

$$J_0 = \frac{qD_n n_{p_0}}{L_n}\left\{\frac{\frac{S_n L_n}{D_n} cosh\left(\frac{x_p}{L_n}\right) + sinh\left(\frac{x_p}{L_n}\right)}{\frac{S_n L_n}{D_n} sinh\left(\frac{x_p}{L_n}\right) + cosh\left(\frac{x_p}{L_n}\right)}\right\} + \frac{qD_p p_{n_0}}{L_p}\left\{\frac{\frac{S_p L_p}{D_p} cosh\left(\frac{t-x_n}{L_p}\right) + sinh\left(\frac{t-x_n}{L_p}\right)}{\frac{S_p L_p}{D_p} sinh\left(\frac{t-x_n}{L_p}\right) + cosh\left(\frac{t-x_n}{L_p}\right)}\right\} \tag{16}$$

The open circuit voltage is dependent on the ratio of the short circuit current to the leakage current. In equations (6) to (16), *n* is the minority carrier concentration in the p-type region, *p* is the minority carrier concentration in the n-type region, *L* is the minority carrier diffusion length, *D* is the diffusion coefficient, A_0 is half of the total source activity assuming that only half of the beta particle emissions are in the direction of the semiconductor surface since the source is isotropic , *S* is the surface recombination, and *a* and *b* are the coefficients for the EHP generation plot exponential curve fitting. The values of the parameters used in this work for silicon at a temperature of 300 K are listed in Table 3.2.

Table 3.2: Parameters used in the model

Minority carrier diffusion length (μm)		**Diffusion coefficient (cm^2/s)**		**Activity (mCi)**		**Surface recombination velocity (cm/s)**		**Coefficients of the exponential curve fitting (ae^{-bx}) of EHPs**	
L_n	L_p	D_p	D_n	Case 1	Case 2	S_p	S_n	a (cm^{-3})	b (cm^{-1})
0.68	49	6.02	6.08	0.25 (0.125 mCi on each side)	1 (0.5 mCi on each side)	10^6	10^6	1.03×10^8 (0 degree); 1.284×10^8 (90 degree)	3952 (0 degree); 7123 (90 degree)

The junction depth in the silicon was varied to estimate the short circuit current densities, open circuit voltage, and the leakage current densities for the Ni-63 full beta particle energy spectrum with a 0 degree and a 90 degree cone of initial beta particle direction. The resulting variation in short circuit current density, open circuit voltage density, and the leakage current density is shown in Figure 3-11, Figure 3-12, and Figure 3-13 respectively. Furthermore, the power density and efficiency analysis with the junction depth is shown in Figure 3-14.

The silicon based betavoltaic battery usually provides the largest short circuit current density compared to wide band gap semiconductors. Figure 3-11 shows that the short circuit current density decreases with the junction depth and becomes almost zero beyond 12 µm junction depth. It is attributed to the fact that the penetration depth for Ni-63 in silicon is about 13 to 14 µm and the minority carrier diffusion length in p-type region is about 0.68 µm due to heavy doping in the p-type region. On the other hand, the minority carrier diffusion length in the n-type region is

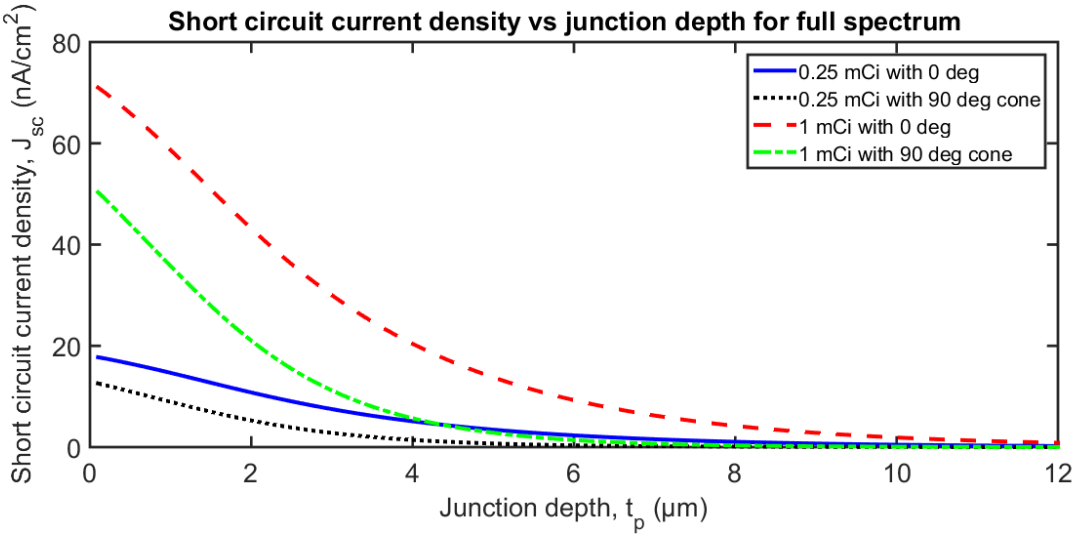

Figure 3-11: Variation in short circuit current density with junction depth

about 49 µm, which is much larger than the penetration depth. As a result, the highest short circuit current density is obtained for a junction depth near to the surface as the generations of EHPs are higher due to the maximum energy deposition near to the surface as modeled by the full beta energy spectrum. Furthermore, the short circuit current density is higher near to the surface irrespective of the beta particles angular distribution. However, the magnitude of the short circuit current density for the 90 degree angular distribution is lower than that for the 0 degree angular distribution. These differences between the two angular distributions increase with higher activity. Nevertheless, an increased activity increases the short circuit current density regardless of the angular distribution, as the short circuit current is directly proportional to the activity. A more realistic betavoltaic battery model should assume a 90 degree angular distribution and a junction depth closer to the surface may be required to optimize current output.

The open circuit voltage in Figure 3-12 increases with the junction depth, reaches a peak and then decreases. The peaks in open circuit voltage are obtained at about 1 µm and 0.8 µm

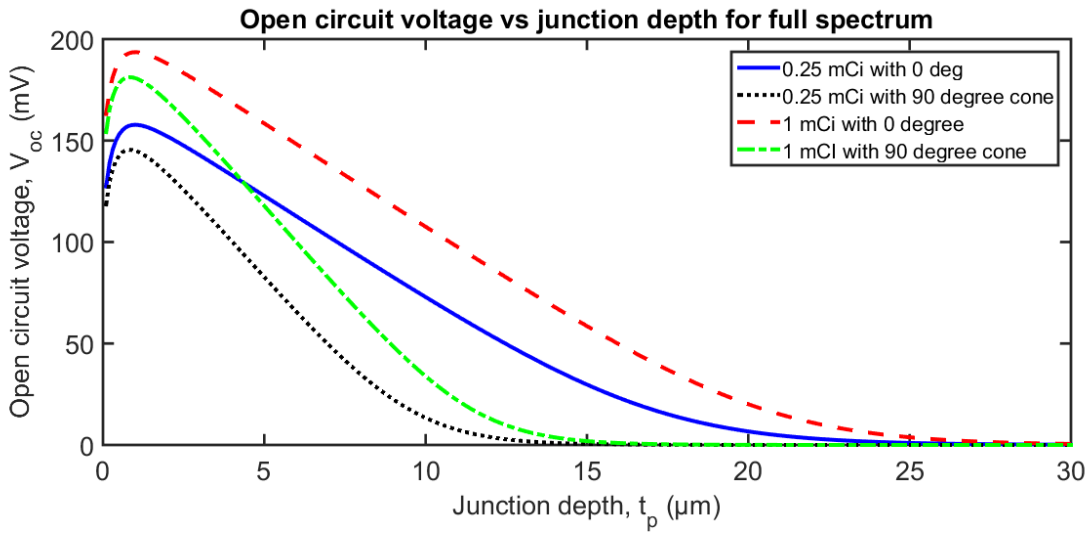

Figure 3-12: Variation in open circuit voltage density with junction depth

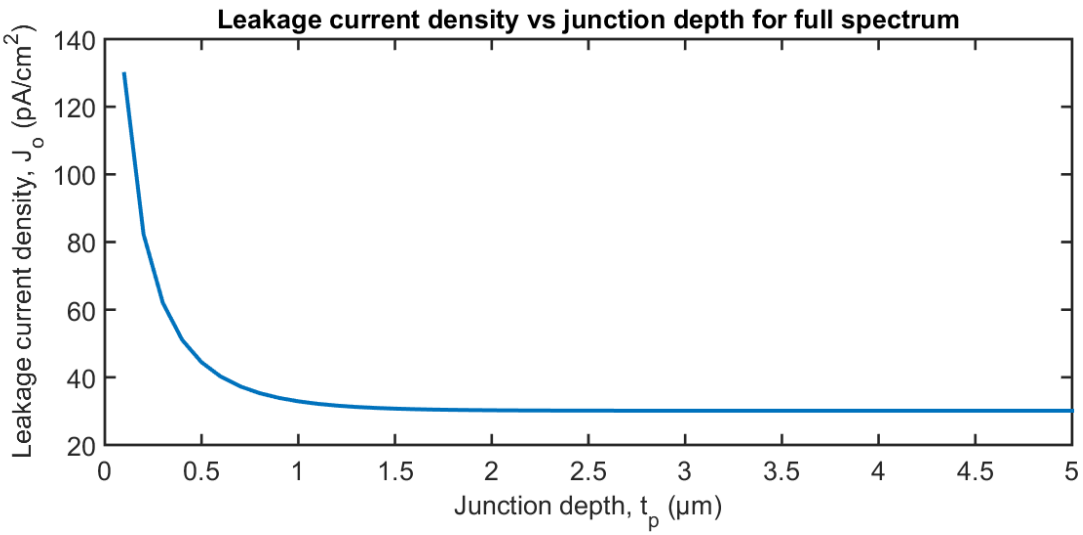

Figure 3-13: Variation in leakage current density with junction depth

junction depths for 0 degree and 90 degree distributions, respectively, regardless of the activities. After the peak, the open circuit voltage decreases almost linearly with the junction depth. The decrease in the ratio of the short circuit current to the leakage current could be the reason for low open circuit voltage with higher junction depth. For 0 degree and 90 degree angular distributions, the open circuit voltage becomes almost zero beyond about 25 μm and 15 μm respectively. With increased activity, the open circuit voltage density curve has the same shape except that the magnitude increases with higher activity.

The leakage current density is about three orders of magnitude lower than the short circuit current density. The leakage current density is very high when the junction depth is near to the surface. However, it decreases significantly once the junction depth reaches 0.5 μm from the surface. It does not decrease much further once the junction depth is greater than 2 μm. The leakage

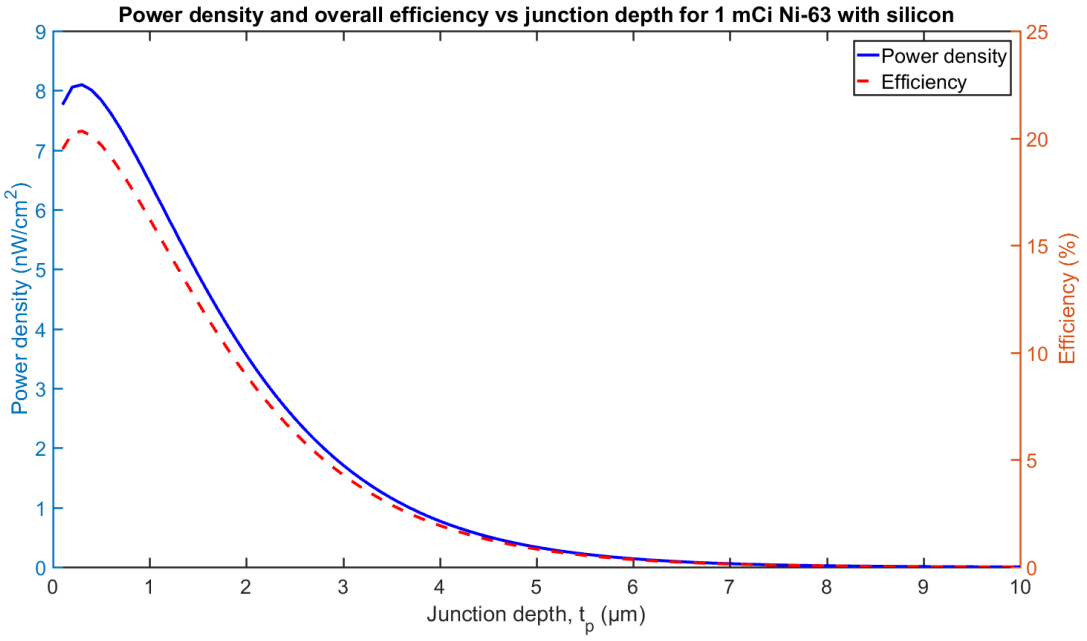

Figure 3-14: Variations in power density and efficiency with the junction depth for 90 degree distribution

current density is not dependent on the radioisotope and its activity. Therefore, the variation in the angular distribution of beta particles does not have any effect on it.

Figure 3-14 shows the power output and the device efficiency with the junction depth for the activity of 1 mCi Ni-63 without considering the self-absorption effect in the source. The device efficiency was defined in equation (17) by the ratio of the power output obtained from the device to the maximum theoretical power output.

$$Device\ efficiency = \frac{P_{out}}{P_{theor\ max}} \qquad (17)$$

Figure 3-14 indicates that there is an optimum power output and for a junction depth near to the surface at about 0.3 μm. Therefore, it shows the importance of an optimum junction

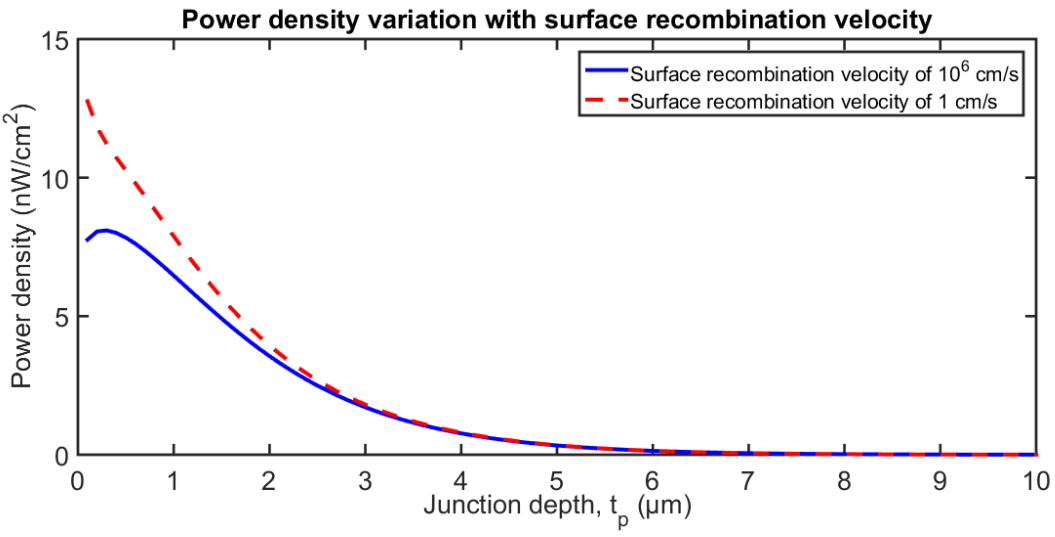

Figure 3-15: Surface passivation impact on power output analysis for 90 degree distribution

depth to maximize the power output and efficiency. However, this optimization is dependent on the surface recombination velocity as shown in Figure 3-15. For a very well passivated silicon surface, the surface recombination velocity can be reduced significantly [33]. In this case, a junction depth closer to the surface will provide the maximum power output.

For further analysis, a junction depth of 2 μm was chosen. For this junction depth, a leakage current of 4.8 pA was estimated which agrees well with the theoretical estimates provided by Guo et al [26]. However, the experimentally measured leakage current of 24 pA is much higher due to the defects created in the heavily doped p-type glass-source [26]. Guo et al. placed electroplated Ni-63 on a p-type region surface of a silicon p-n junction. They built the silicon p-n junction using doping concentrations of $10^{20}/cm^3$ and $10^{17}/cm^3$ in the p-type and n-type regions respectively. They measured the short circuit current and open circuit voltage for 0.25 mCi and 1 mCi of Ni-63. Similar to the experiment, the short circuit current and the open circuit voltage were

estimated using the model from above for two different Ni-63 source activities of 0.25 mCi and 1 mCi as shown in Table 3.3 and Table 3.4. They were also estimated for two different beta particle angular variations of 0 degrees and 90 degrees in Table 3.3 and Table 3.4 respectively. A short circuit current of 1.73 nA and an open circuit voltage of 152 mV were calculated for the case of 0.25 mCi with 0 degree angular distribution. Similarly, a short circuit current of 6.91 nA and an open circuit voltage of 187.8 mV were calculated for the case of 1 mCi with 0 degree angular distribution. The short circuit current increased about four times with the use of a factor of four higher activity, as the short circuit current is linearly proportional to the activity. For a junction depth of 2 μm, the short circuit current decreases by a factor of two for the 90 degree angular distribution. However, the open circuit voltage does not reduce as significantly as the short circuit current density with the angular distribution. Furthermore, the beta particle transport approach such as using the monoenergetic beta particle average energy or the full beta energy spectrum has a significant impact in estimating the junction depth for an optimum battery output. In these cases, the energy deposition peak appears at a different thickness in the semiconductor as shown in Figure 3-8. This creates EHPs with a similar profile i.e. the EHP peak is at the same thickness. Ideally, the junction depth is chosen at a thickness where the EHP generation is maximum. Maximum EHP collection occurs in the depletion region around the junction depth. Therefore, a better choice of junction depth that considers the full beta energy spectrum with an isotropic angular distribution will improve the battery output and provide a higher efficiency.

In Table 3.3 and Table 3.4 for all cases, it was observed that the predicted results for the short circuit current and the open circuit voltage were higher than the actually measured short

Table 3.3: Results for full beta particle energy spectrum MCNP input with 0 degree angular distribution

Activity	0.25 mCi (case 1)			1 mCi (case 2)		
Outputs	Simulation results		Experimental results	Simulation results		Experimental results
	No self-absorption	59% self-absorption		No self-absorption	65.1% self-absorption	
Short circuit current (nA)	1.73 $\pm$ 0.0073	0.71 $\pm$ 0.003	0.71	6.91 $\pm$ 0.0291	2.41 $\pm$ 0.0102	2.41
Open circuit voltage (mV)	152 $\pm$ 0.1	129.1 $\pm$ 0.1	64	187.8 $\pm$ 0.1	160.6 $\pm$ 0.1	115

Table 3.4: Results for full beta energy spectrum MCNP input with 90 degree angular distribution

Activity	0.25 mCi (case 1)			1 mCi (case 2)		
Outputs	Simulation results		Experimental results	Simulation results		Experimental results
	No self-absorption	15% self-absorption		No self-absorption	28.5% self-absorption	
Short circuit current (nA)	0.84 $\pm$ 0.0053	0.71 $\pm$ 0.0045	0.71	3.36 $\pm$ 0.0211	2.41 $\pm$ 0.0151	2.41
Open circuit voltage (mV)	133.5 $\pm$ 0.2	129.3 $\pm$ 0.2	64	169.2 $\pm$ 0.2	160.6 $\pm$ 0.2	115

circuit current and open circuit voltage in the experiment. This phenomenon of overprediction of the results [6] was also observed for other theoretical models in the literature. It is proposed in this analysis that one of the main reasons for this overprediction of results is due to the self-absorption

effect of the beta particles in the source. The self-absorption effect reduces the effective activity of a radioisotope depending on its thickness as some of the beta particle energy deposits in the source before it can exit.

A percentage reduction in the effective activity was applied to the results shown in Table 3.3 and Table 3.4 in order to predict the amount of self-absorption needed to match with the short circuit current. The discrepancies in the open circuit voltage are attributed to the p-type glass-source defects explained by Zuo et al. [11]. For 0.25 mCi, 59% and 15% self-absorption effect would explain the observed results for 0 degree and 90 degree angular distribution respectively. The self-absorption effect of the radioactive source depends on the surface area and the thickness of the radioisotope. Therefore, when the activity is increased to 1 mCi while keeping the surface

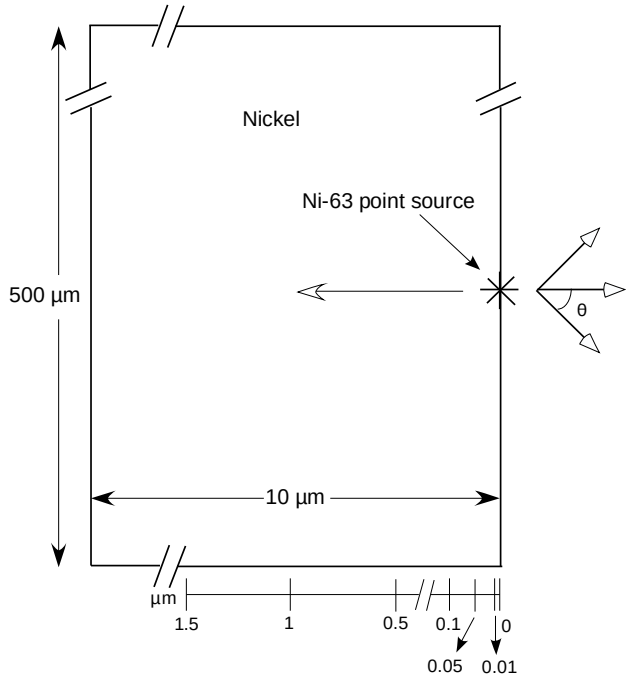

Figure 3-16: Schematic diagram of Ni-63 source in MCNP simulation

area the same, the self-absorption effect further increases as that means the thickness of the source material must increase. As a result, the self-absorption effect increased to about 65.1% and 28.5% for 0 degree and 90 degree angular distribution, respectively, for a higher activity of 1 mCi. The variation in self-absorption effect is significant with various angular distributions. It is difficult to compare the simulated self-absorption effect with the experimentally used radioisotope source because Guo et al. did not report the source dimensions. They reported an electroplated Ni-63 was used in the experiment. It was assumed in this analysis that the source has a surface area of 4×4 mm^2 similar to the p-n junction silicon semiconductor. The source thickness was estimated by MCNP simulations using the problem setup shown in Figure 3-16 to justify the self-absorption effect in this analysis. A Ni-63 point source was moved from the surface along the thickness direction at different source positions of 0.01 μm, 0.05 μm, 0.1 μm, and up to 1.5 μm with an increment of 0.1 μm. The energy absorbed in the source was estimated using full beta energy spectrum for different source positions along with different angular distributions of 0 degree and 90 degree. Figure 3-17 shows the percentage of beta energy absorbed along with uncertainty bars in the Nickel source for different source positions and angular distributions. It indicates that about 50% of the beta particle energy was absorbed within 1 to 1.5 μm thickness of Ni-63 due to the very high nickel density of 8.91 g/cm^3. The estimated thicknesses for 0.25 mCi and 1 mCi activities of Ni-63 are 0.03 μm and 0.12 μm, respectively, based on the specific activity of 56.18 Ci/g for Ni-63. Figure 3-17 shows that about 15% and 28.5% of the beta particle energy is absorbed for approximately 0.1 μm and 0.4 μm thicknesses, respectively, for 90 degree angular variation, which is more realistic. These percentages of energy absorption in the source are comparable to the percentages of reduction in battery outputs for self-absorption effect considered in Table 3.3 and Table 3.4. However, the thicknesses are higher than the theoretical thicknesses estimated from the

specific activity. The isotope dilution factor, which is very high for a Ni-63 source [13], could be the reason for this. Assuming about 30% of Ni-63 by atoms in the source would explain the estimates of higher thicknesses. The primary effect of self-absorption is to reduce the number of beta particles reaching the semiconductor surface and to let mainly higher energy particles get through. The net effect is to reduce the total energy available for deposition in the semiconductor which directly affects the betavoltaic battery output. This shows that the self-absorption of the beta particles coming from the source can have a significant impact on betavoltaic battery outputs. The effects of self-absorption and variation in beta particle angular distribution need to be further investigated and justified for betavoltaic battery model development. A self-absorption model was developed by Gui et al. [13] using the direct chord method for a Ni-63 source. The model predicted the particle escape probability and the energy escape probability with thickness for Ni-63. The particle escape probability and the energy escape probability for Ni-63 from the chord method

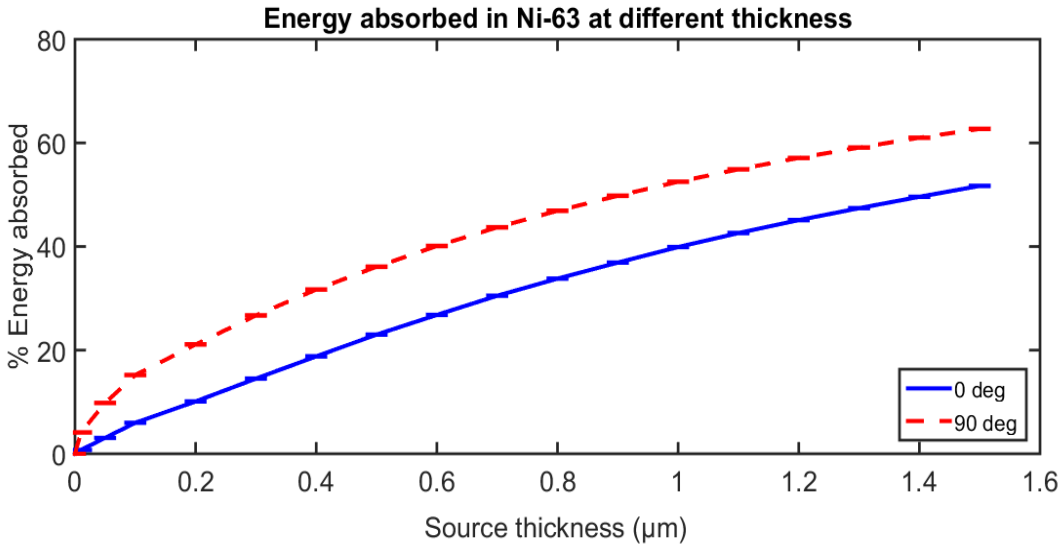

Figure 3-17: Energy absorbed within the source (Ni-63) due to self-absorption

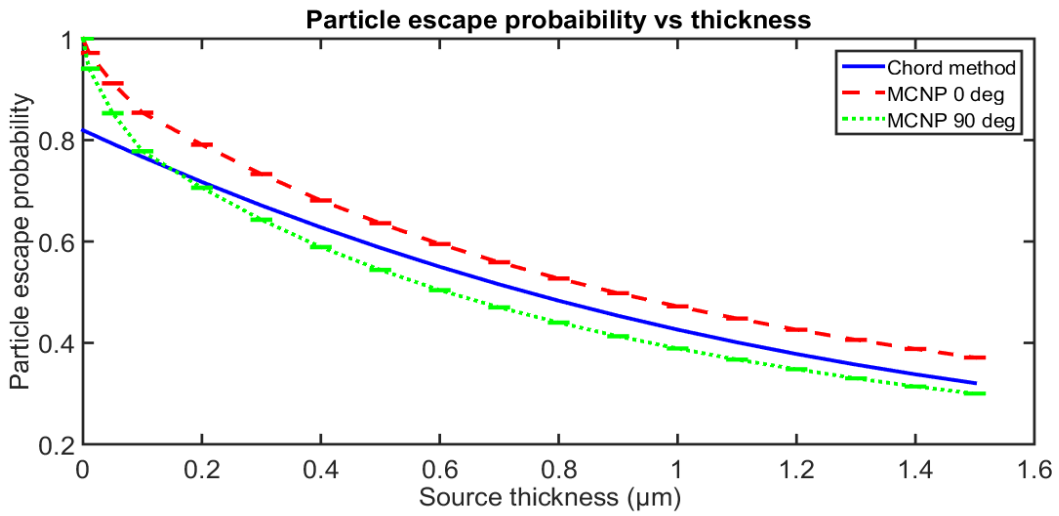

Figure 3-18: Comparisons of particle escape probability for Ni-63 source

were compared with the MCNP results for both 0 degree and 90 degree distributions in Figure 3-18 and Figure 3-19 respectively. Both Figure 3-18 and Figure 3-19 show that the particle and energy escape probability are lower for 90 degree distribution due to more inelastic and elastic scattering as well as higher absorption in the source. It is noted that the particle and energy escape probabilities are approximately 1 for a very thin source as most of the particles can escape. However, the chord model predicted lower particle and energy escape probabilities for a very thin source. Figure 3-18 shows that the particle escape probability predicted by the chord model fell in between the MCNP results of 0 degree and 90 degree distributions. However, the energy escape probability predicted by the chord model was much lower than that of the MCNP results as shown in Figure 3-19. The deviation in results could be caused by ignoring the spectrum modification and the assumption of an infinite slab in the chord model.

Besides the self-absorption effect, there could be other reasons for the deviation between the simulated and experimental results. A semiconductor device model with simplified assumptions such as uniform doping, negligible electric field in p-type and n-type regions, no recombination in the depletion region, full ionization of dopants, and a Boltzmann approximation was used. The quality of the device used in the experiment was not verified by measurements such as dopant concentrations and surface recombination velocity. Some important parameters in the model such as semiconductor junction depth, radioisotope source dimension, and device temperature were assumed, as they were not reported in the experiment. This will need to be further analyzed using other experimental data. It is noted that some experimental results on Ni-63 with silicon are available in the literature [15, 34-36]. However, it is difficult to compare the simulated results with the experimental results as the detail of the semiconductor parameters including the source dimension were not reported. Therefore, measurements of all parameters in the experiment will be useful to validate, improve, and optimize the model.

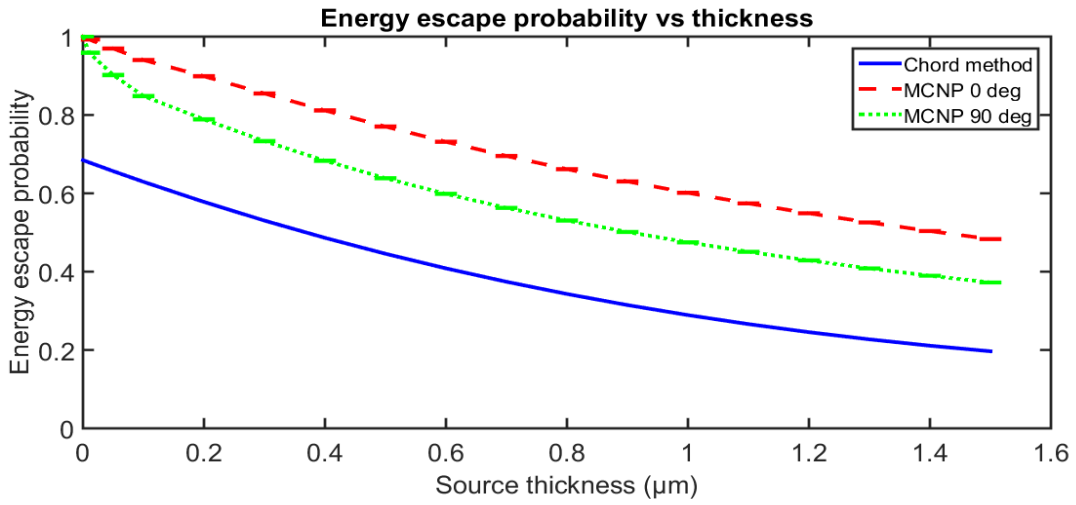

Figure 3-19: Comparisons of energy escape probability for Ni-63 source

3.8 Conclusions

Beta particle penetration depths using MCNP with different types of input energy were estimated for Ni-63 in silicon. The penetration depths from MCNP for inputs of monoenergetic beta particle average energy and monoenergetic beta particle maximum energy were validated by the Katz-Penfold range equation. However, using the actual beta energy spectrum produces significantly different beta particle penetration depths. Factoring in the isotropic angular variation of the beta particle emission reduces the penetration depth and increases the backscattering coefficient up to 0.46. Thus, the key point is when designing a betavoltaic battery a more realistic beta particle transport model needs to be used in order to choose an optimum junction depth for maximum collection of EHPs generated in the semiconductor in order to maximize battery outputs. The exponential distribution of EHP generation from MCNP results were used to solve the drift-diffusion equation of the semiconductor model. The predicted results such as the short circuit current density, the open circuit voltage density, and the leakage current density varied depending on the junction depth of the semiconductor and the angular distribution of beta particles. The power output and device efficiency variations were significant with the junction depth. A shallow junction depth depending on the surface recombination velocity will increase the power output and efficiency. The results were overpredicted when no source self-absorption effect was considered. For isotopic emission of beta particles, a 15% self-absorption effect was observed for an activity of 0.25 mCi with a junction depth of 2 μm. However, the self-absorption effect further increased with higher activity as expected since the source thickness would be greater. Therefore, the energy deposition and penetration depth of beta particles in the semiconductor, the choice of junction

depth, the angular variation in the emission of the beta particles, the backscattering of beta particles, and the self-absorption effect of the source need to be considered carefully in betavoltaic battery design.

3.9 References

[1] Kwon, J. and J.D. ROBERTSON *World's smallest nucleat battery*. American Ceramic Society Bulletin, 2009. **88**, 13-14.

[2] Lal, A. and J. Blanchard, *Daintiest dynamos [nuclear microbatteries]*. Spectrum, IEEE, 2004. **41**(9): p. 36-41.

[3] Wu, K., C. Dai, and H. Guo. *A theoretical study on silicon betavoltaics using Ni-63*. in *Nano/Micro Engineered and Molecular Systems (NEMS), 2011 IEEE International Conference on*. 2011. IEEE.

[4] Prelas, M.A., et al., *A review of nuclear batteries.* Progress in Nuclear Energy, 2014. **75**: p. 117-148.

[5] Prelas, M., et al., *Nuclear Batteries and Radioisotopes*. 2016: Springer International Publishing.

[6] Alam, T.R. and M.A. Pierson, *Principles of Betavoltaic Battery Design.* Jounal of Energy and Power Sources, 2016. **3**(1): p. 11-41.

[7] Ulmen, B., et al., *Development of diode junction nuclear battery using 63 Ni.* Journal of radioanalytical and nuclear chemistry, 2009. **282**(2): p. 601-604.

[8] Thomas, C., S. Portnoff, and M. Spencer, *High efficiency 4H-SiC betavoltaic power sources using tritium radioisotopes.* Applied Physics Letters, 2016. **108**(1): p. 013505.

[9] Alam, T.R. and M.A. Pierson, *Development of a realistic model for optimizing betavoltaic battery design*, in *Transactions of American Nuclear Society 2015 Winter Meeting*. 2015: Washington, DC. p. 518-521.

[10] Goorley, T., *Initial MCNP6 Release Overview.* Nuclear Technology, 2012. **180**: p. 298-315.

[11] Guoping, Z., Z. Jianliang, and K. Guotu, *A Simple theoretical model for 63 Ni betavoltaic battery.* Applied Radiation and Isotopes, 2013. **82**: p. 119-125.

[12] Zaitsev, S., et al., *Comparison of the efficiency of 63Ni beta-radiation detectors made from silicon and wide-gap semiconductors.* Journal of Surface Investigation. X-ray, Synchrotron and Neutron Techniques, 2014. **8**(5): p. 843-845.

[13] Gui, G., et al., *Prediction of 4H–SiC betavoltaic microbattery characteristics based on practical Ni-63 sources.* Applied Radiation and Isotopes, 2016. **107**: p. 272-277.

[14] Polikarpov, M. and E.B. Yakimov, *Characterization of Si convertors of beta-radiation in the scanning electron microscope.* Solid State Phenomena, 2015. **242**: p. 312.

[15] Yakimov, E.B., *Prediction of betavoltaic battery output parameters based on SEM measurements and Monte Carlo simulation.* Applied Radiation and Isotopes, 2016. **112**: p. 98-102.

[16] Evans, R.D., *The Atomic Nucleus* 1955, Malabar, Florida: Krieger Publishing Company.

[17] Zerby, C. and F. Keller, *Electron transport theory, calculations, and experiments.* Nuclear Science and Engineering, 1967. **27**(2): p. 190-218.

[18] Team, X.-M.C., *MCNP - A General N-Particle Transport Code, Version 5*. 2005.

[19] Pelowitz, D.B., *MCNP6 Users Manual - Code Version 6.1*. 2013.

[20] Hughes, H.G., *Recent Developments in Low-Energy Electron/Photon Transport for MCNP6*. 2012: Nara, Japan.

[21] Hughes, H.G., *Quick-Start Guide to Low-Energy Photon/Electron Transport in MCNP6*. 2013.

[22] Hughes, H.G. *Treating Electron Transport in MCNP*. in *Proceedings of the training course on the use of MCNP in Radiation Protection and Dosimetry*. May 13-16, 1996. Bologna, Italy.

[23] Krane, K.S., *Introductory Nuclear Physics*. 1987: Wiley.

[24] Cross, W., H. Ing, and N. Freedman, *A short atlas of beta-ray spectra.* Physics in Medicine and Biology, 1983. **28**(11): p. 1251.

[25] ICRP, *Nuclear decay data for dosimetric calculation.* ICRP Publication 107, 2008. **Ann. ICRP 38(3)**.

[26] Guo, H. and A. Lal. *Nanopower betavoltaic microbatteries*. in *TRANSDUCERS, Solid-State Sensors, Actuators and Microsystems, 12th International Conference on, 2003*. 2003. IEEE.

[27] Zhao, Z., et al. *Effect of three-dimensional cylindrical hole array on energy conversion efficiency of radioisotope battery*. in *Nano/Micro Engineered and Molecular Systems (NEMS), 2011 IEEE International Conference on*. 2011. IEEE.

[28] Oh, K., et al., *Theoretical maximum efficiency for a linearly graded alphavoltaic nuclear battery.* Nuclear technology, 2012. **179**(2): p. 243-249.

[29] Katz, L. and A. Penfold, *Range-energy relations for electrons and the determination of beta-ray end-point energies by absorption.* Reviews of Modern Physics, 1952. **24**(1): p. 28.

[30] Turner, J.E., *Atoms, Radiation, and Radiation Protection*. 2008: Wiley.

[31] Theirrattanakul, S. and M. Prelas, *A Methodology for Efficiency Optimization of Betavoltaic Cell Design using an Isotropic Planar Source having an Energy Dependent Beta Particle Distribution.* Applied Radiation and Isotopes, 2017.

[32] Li, H., et al., *Simulations about self-absorption of tritium in titanium tritide and the energy deposition in a silicon Schottky barrier diode.* Applied Radiation and Isotopes, 2012. **70**(11): p. 2559-2563.

[33] Otto, M., et al., *Extremely low surface recombination velocities in black silicon passivated by atomic layer deposition.* Applied Physics Letters, 2012. **100**(19): p. 191603.

[34] Liu, Y., et al., *Investigation on a radiation tolerant betavoltaic battery based on Schottky barrier diode.* Applied radiation and isotopes, 2012. **70**(3): p. 438-441.

[35] Gao, H., et al., *Demonstration, radiation tolerance and design on a betavoltaic micropower*. Energy, 2013.

[36] Krasnov, A., et al., *Optimization of Energy Conversion Efficiency Betavoltaic Element Based on Silicon.* Journal of nano-and electronic physics, 2015. **7**(4): p. 4004-1.

CHAPTER 4: A MONTE CARLO RADIOISOTOPE SOURCE MODEL AND OPTIMIZATION FOR BETAVOLTAIC BATTERIES

4.1 Abstract

A Monte Carlo source model using PENELOPE was developed to investigate different tritiated metals in order to design a better radioisotope source for betavoltaic batteries. The source model takes into account the self-absorption of beta particles in the source which is a major factor for an efficient source design. The average beta energy, beta flux, source power output, and source efficiency were estimated for various source thicknesses. The simulated results for titanium tritide with 0 degree and 90 degree angular distributions of beta particles were validated with experimental results. The importance of the backscattering effect due to isotropic particle emission was analyzed. The results showed that the normalized average beta energy increases with the source thickness and it reaches a peak energy depending on the density and the specific activity of the source. The beta flux and power output also increase with increasing source thickness. However, the incremental increase in beta flux and power output becomes minimal for higher thicknesses, as the source efficiency decreases significantly at higher thicknesses due to the self-absorption effect. Thus, a saturation threshold is reached. A low density source material such as beryllium tritide provided a higher power output with a higher efficiency. A maximum power output of about 4 mW/cm^3 was obtained for beryllium tritide with SiC. A form factor approach was used to estimate the optimum source thickness. The optimum source thickness was found near the thickness where the peak beta particle average energy occurs.

Keywords: self-absorption, beta flux, source optimization, betavoltaic batteries

4.2 Introduction

A betavoltaic battery harnesses the beta particle emitting radioisotope energy into electrical energy using semiconductors [1-3]. The radioisotope source is the most expensive part of the battery. It is important to analyze the source and optimize it for an efficient battery design. In this work, tritium is the radioisotope source and a wide band gap SiC semiconductor is considered. Tritium is a pure beta emitter with a low average beta energy of 5.68 keV. A low beta particle energy radioisotope will minimize the radiation damage in semiconductors. The half-life of 12.3 years for tritium will provide a long service life for the battery. However, tritium is naturally in a gaseous state (i.e., T_2), and it can create a radiation hazard from leaks (a persistent problem for hydrogen and its isotopes). A solid source is preferred in betavoltaic battery design [4]. Thus, many researchers consider tritiated metals as a better alternative [5-7]. Titanium tritide, scandium tritide, magnesium tritide, lithium tritide and beryllium tritide are investigated in this work. A radioisotope source needs design improvements in order to maximize its power output and efficiency. A higher source thickness increases the battery power output. However, the self-absorption of beta particles in the source increases with the thickness of the source [8-11]. Therefore, the source thickness needs to be optimized to achieve better efficiency in the design. A Monte Carlo particle transport code PENELOPE was used in this work that comprehensively considers the relevant physics for particle transport [12]. A source model using PENELOPE was developed to study the variations in average beta particle energy, beta flux, maximum power output, and source efficiency for different tritiated metals with various source thicknesses.

Different beta particle angular distributions of 0 degrees and 90 degrees were considered for titanium tritide. The simulated results for titanium tritide were validated with experimentally measured results [7] and the backscattering effect was analyzed. The results were compared for different tritiated metals to investigate the impacts of density and specific activity of the source. The source thickness was optimized using a form factor approach in order to design a configuration of multiple alternate layers of source and semiconductors for the purpose of increasing the battery power output.

4.3 Monte Carlo source model

Beta flux is a measure of the surface activity of a radioisotope source. It is an estimate of the rate of beta particles emitted from the source surface. Beta flux estimates inherently take into account the self-absorption of beta particles inside the source. Thomas et al [7] measured the beta flux for a titanium tritide source using an air ionization chamber technique as illustrated in Figure 4-1. Two electrodes were separated with a 0.4 µm thick titanium tritide radioisotope source placed on one electrode. To measure the beta flux, an external voltage was applied to the electrodes

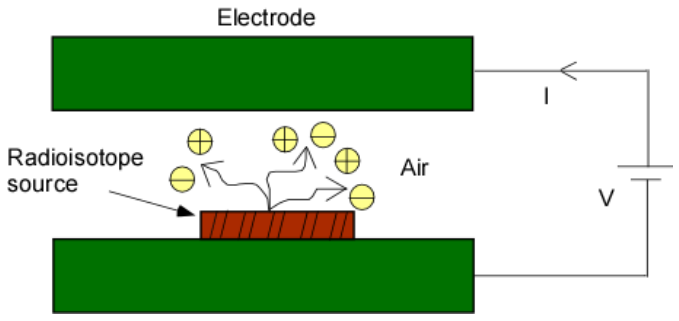

Figure 4-1: Air ionization chamber for beta flux measurement

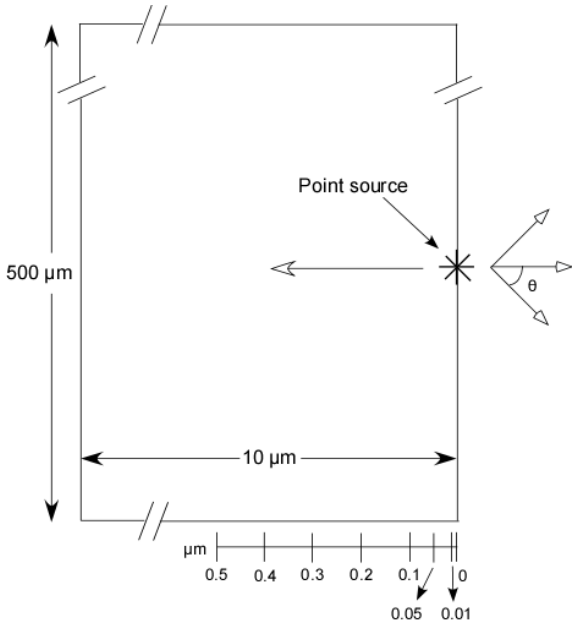

Figure 4-2: Monte Carlo source model

and the beta current was measured. The applied voltage was increased until the beta current reached a saturation of 7.82 nA/cm^2. The saturated beta current provided an estimate for the beta input power of 732 nW/cm^2. The beta flux was then calculated using an average kinetic energy for the tritium beta particles.

In order to estimate the beta particle flux of a radioisotope source, a Monte Carlo source model was developed as depicted in Figure 4-2. Two angular distributions, 0 degree and 90 degree, were considered for the beta particles emission. 0 degree refers to the beta particles emitting perpendicular to the source surface and 90 degree refers to the half isotropic emission (2π steradians) of beta particles in the direction of the semiconductor. Some of the beta particles that are emitted to the opposite direction of interest can backscatter, which is also studied in this work. This model can be applied to any beta emitting radioisotope source using its properties. A three

dimensional volumetric source was used in the model and a point source was moved along the depth direction from its surface back into the source. The distance between two consecutive point sources was used to determine the average effect of the two point sources from the layer in between them. The cumulative effect of each layer was considered for the total thickness of the radioisotope source. The transmission probability and the average energy of beta particles emitted from different layers were then estimated using the PENELOPE Monte Carlo electron transport code.

4.4 Titanium tritide

A titanium tritide radioisotope source with 0 degree and 90 degree angular distributions was simulated for different thicknesses of the source. The resulting beta particle energy spectrum leaving the source surface, the beta particle average energy leaving the source surface and the

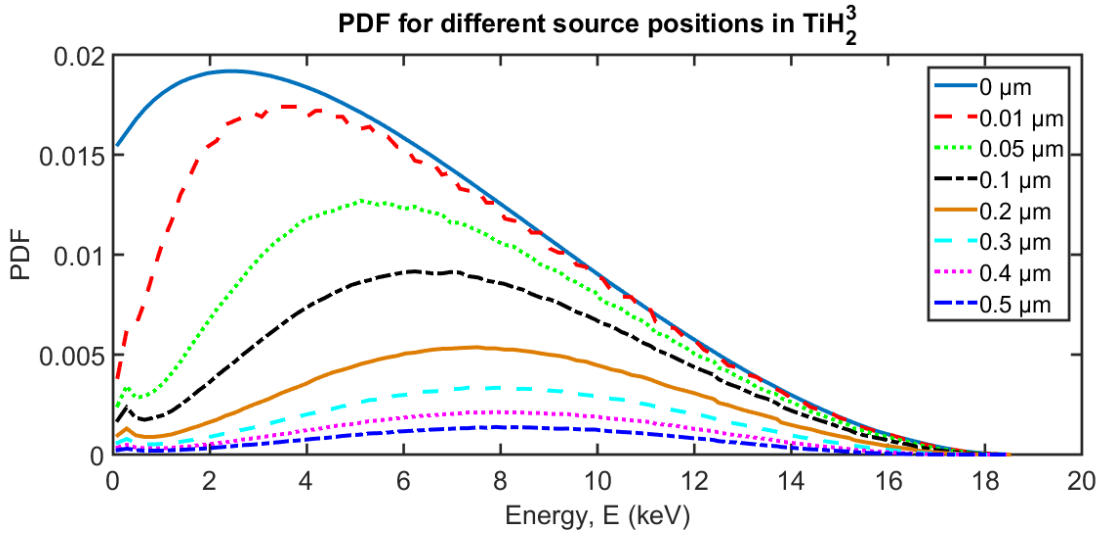

Figure 4-3: Beta particle energy spectrum changes with titanium tritide increasing source thickness

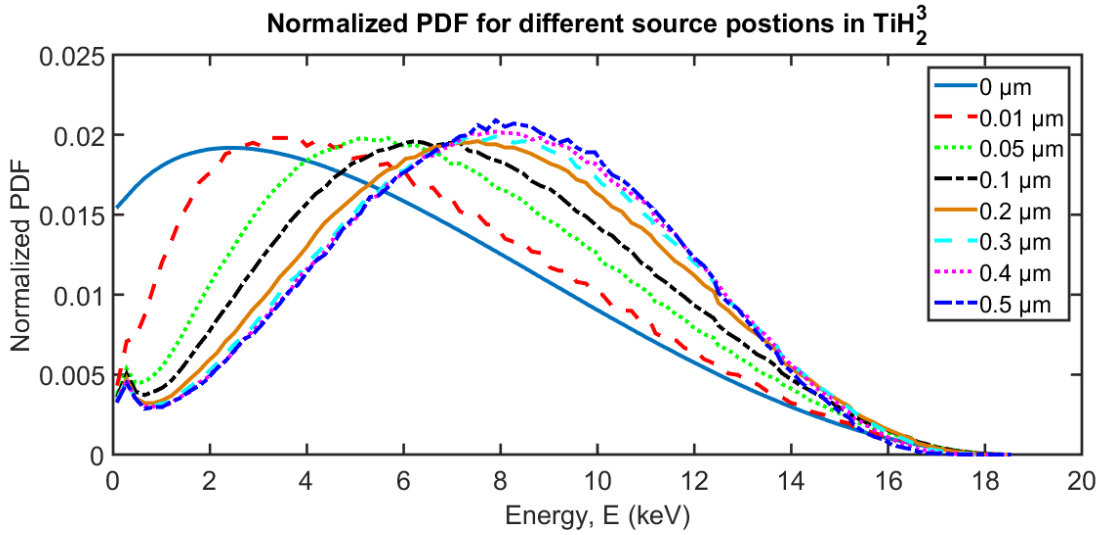

Figure 4-4: Normalized beta energy spectrum for the point source in different thickness

associated beta fluxes were estimated for the simulation results. Figure 4-3 shows that the Fermi distribution [13] of an ideal beta energy spectrum [14] changes with the thickness of the source [8, 9] for 0 degree. The comparison of the beta energy spectrums leaving the source surface for various source thicknesses indicates that fewer particles come out of the surface and the peak of the spectrum shifts toward higher beta energy with increased source thickness resulting in a hardened energy spectrum with a smaller magnitude. This phenomenon is more obvious when the beta spectra are normalized and compared to the same scale as shown in Figure 4-4 for 0 degree. The normalized average beta energy for titanium tritide using 0 degree and 90 degree angular distributions with various source thicknesses are shown in Figure 4-5. The comparison shows that the average beta energy increases with the source thickness and it reaches a peak energy. A deviation in the average beta energy for source thicknesses of about 0.05 μm and higher is observed for 0 degree and 90 degree distributions. Peak energies of 8.04 keV and 7.68 keV were estimated

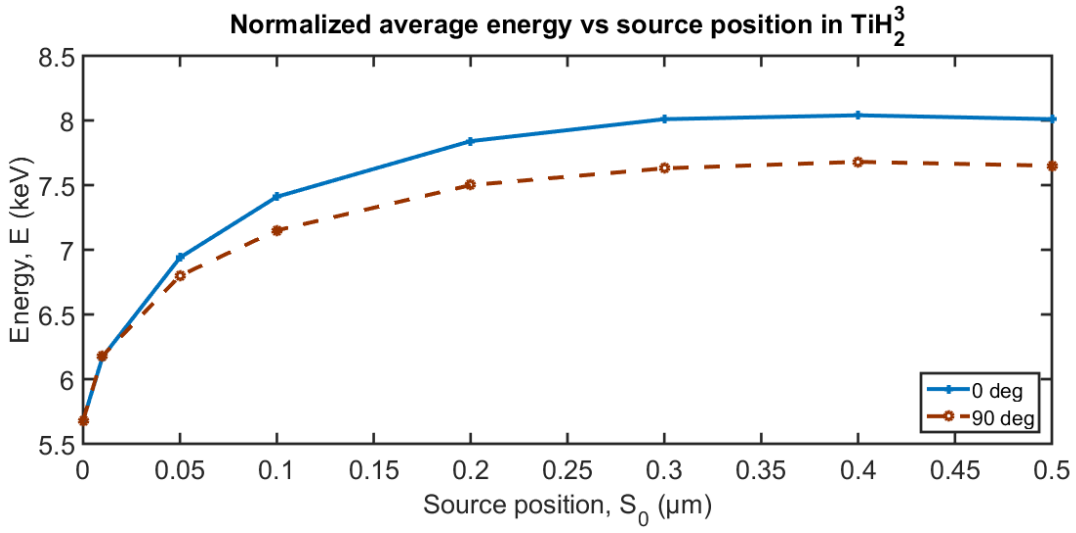

Figure 4-5: Normalized average beta energy changes with source thickness in titanium tritide

for a 0.4 μm thick source with 0 degree and 90 degree distributions, respectively, whereas the average beta particle energy of tritium for an ideal Fermi beta spectrum [13] is about 5.68 keV. The increase in average beta energy can be explained by the fact that low energy beta particles are absorbed inside the source for larger thicknesses while the high energy beta particles can still escape from the source when the source thickness is increased. As a result, the average beta particle energy emitted from the source increases with the source thickness and the beta energy spectrum is modified with the energy peak shifting towards higher energy.

Beta fluxes were estimated for various titanium tritide source thickness using the source model above. An interesting phenomenon was observed in the simulation results for this source model. It is customary in the research community to consider a symmetric condition for the particle transport and to model the particles that are moving in the direction of semiconductor. Only forward moving particles are considered in order to reduce the computation time. However, a

variation in results was observed when backscattering effects were considered for the beta particles moving in the opposite direction. This backscattering effect becomes significant for the 90 degree particle emission distribution. The elastic and inelastic collisions of the particles occurring inside of the source increase for the 90 degree distribution. As a result, the backscattered particle contribution is especially significant for a 90 degree distribution. The inclusion of backscattering effects in the simulation model increases the resulting beta flux leaving the surface for both 0 degree and 90 degree distributions as shown in Figure 4-6.

Beta fluxes were estimated from the probability of transmitted particles exiting the source, the specific activity and the average beta energy of the radioisotope source for various thicknesses. Figure 4-6 shows that the beta flux increases with the source thickness. However, it begins to saturate at higher thicknesses. This indicates that the rate of change of increase in the beta flux, or surface activity, decreases with an increase in source thickness. This effect is

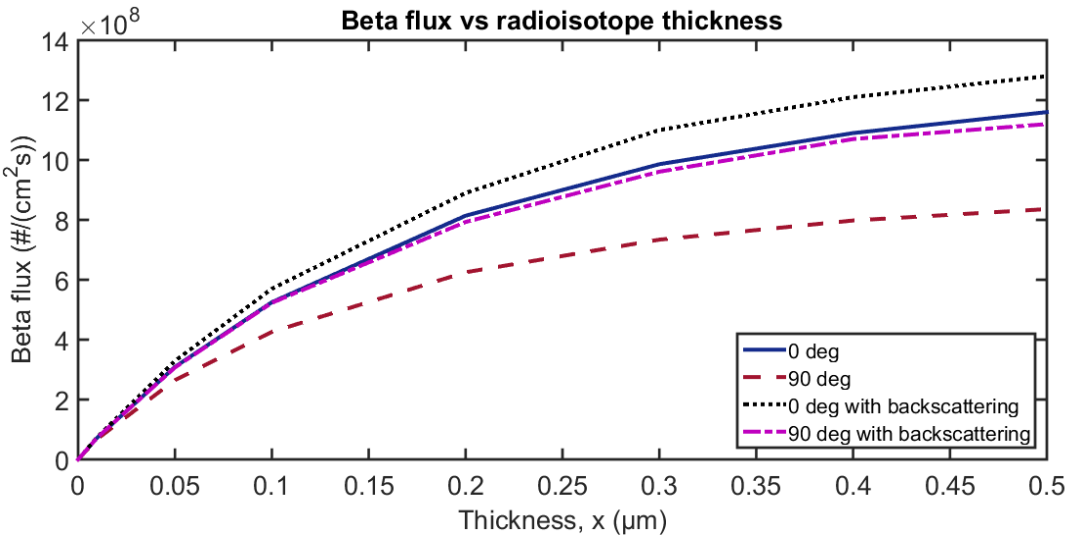

Figure 4-6: Beta flux for titanium tritide at various thicknesses

explained by self-absorption of the beta particles within the radioisotope source. The self-absorption effect is where lower energy beta particles emitted from deeper interior regions of the source material are absorbed before they can escape the source surface. This increase in self-absorption with increased source thickness reduces the differential beta flux increase. The beta particles that are emitted from the radioactive atoms in the deeper interior regions need to travel a longer distance before exiting the surface. Thus, the beta particles can collide with more atoms and the probability of particle transmission decreases. Furthermore, with more collisions the beta particles slow down and can be absorbed in the material. Therefore, a lower percentage of the beta particles produced in the source can come out of the source surface due to higher scattering and energy loss in the source as the thickness increases. This effect is reflected in the calculation of the beta flux. The measured beta input power of 732.9 nW/cm^2 from an actual titanium tritide source was converted into beta flux in order for comparison to the calculated beta flux from the simulation. The resulting weighted average beta particle energy leaving the source material is a parameter used in this conversion. This conversion factor is different for the 0 degree and 90 degree distributions. The differences in the calculated beta flux for the 0 degree and 90 degree distributions stems from higher scattering and atomic collisions in the case of the 90 degree distribution. Table 4.1 shows a comparison of the theoretically estimated and experimentally measured equivalent beta flux for 0.4 μm titanium tritide. Table 4.1 also shows that the backscattering effect is not trivial for a 90 degree distribution and should be included. The simulation results tend to underestimate the beta flux if the backscattering effect for a 90 degree distribution is not considered. The simulated beta flux of 1.07×10^9 ($cm^{-2}s^{-1}$) for a 90 degree distribution with the inclusion of backscattering effect would be a more realistic estimate and it fell in-between the experimentally determined beta fluxes of 1.04×10^9 ($cm^{-2}s^{-1}$) and 1.12×10^9

($cm^{-2}s^{-1}$), which showed a good agreement with the experimental results. Further analyses were carried out including the backscattering effect for the 90 degree distribution (4π steradians). This is a model which is closer to the behavior of the experimental system.

Table 4.1: Beta flux for titanium tritide with 0.4 μm thickness

Beta flux outputs ($cm^{-2}s^{-1}$)	**0 degree**	**90 degree**
Simulated beta flux (without backscattering)	$1.09 \pm 0.0006 \times 10^9$	$0.8 \pm 0.0005 \times 10^9$
Simulated beta flux (with backscattering)	$1.21 \pm 0.0006 \times 10^9$	$1.07 \pm 0.0006 \times 10^9$
Calculated beta flux from experimental measured input of 732.9 nW/cm^2	1.04×10^9	1.12×10^9

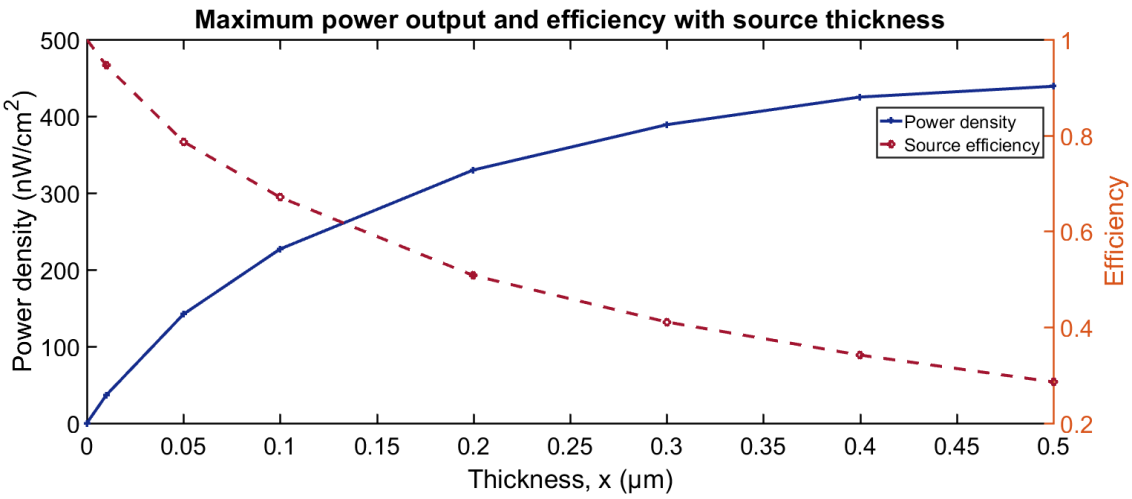

Figure 4-7: Source efficiency and maximum possible power output for titanium tritide with a SiC transducer placed on both sides

The simulated maximum power output and source efficiency for titanium tritide at various thicknesses are shown in Figure 4-7. Source efficiency was calculated from the ratio of the number of particles that come out of the source surface to the maximum number of beta particles emitted from the tritium atoms in the source. The maximum possible power output is found by

estimating the maximum source power and assuming that it is being converted by an ideal SiC semiconductor transducer with a 100% device efficiency and by assuming that there is a transducer placed on both sides of the source. This sandwich configuration of a SiC semiconductor transducers on both sides of the titanium tritide source focuses on the maximizing source efficiency. The source efficiency decreases with increased source thickness due to the self-absorption effect. As a result, the differential increase in the power output is reduced for larger source thicknesses.

Table 4.2: Power output of a 0.4 μm thick titanium tritide source with SiC transducers placed on both sides

Power output (nW/cm^2)	90 degree
Theoretical maximum	425 ± 0.003
Experimentally measured	315.5

Table 4.2 shows a comparison of theoretical maximum power output using 90 degree distribution with the experimentally measured power output for a 0.4 μm thick titanium tritide source with SiC [7]. The experimental power output was calculated from the short circuit current density of 75.47 nA/cm^2 and the open circuit voltage of 2.09 V, then multiplied by a factor of two to consider the effect of two SiC placed on both sides of the source. As the losses in the SiC semiconductor devices were not considered in the theoretical estimates of power output, the estimates predicted a higher power output for the source than was measured. Considering the fact that the device losses were not taken into account in the theoretical estimate of source power output, the power output of 425 nW/cm^2 is in good agreement with the experimentally measured power output of 315.5 nW/cm^2 for a 0.4 μm titanium tritide source with SiC. A source efficiency of 34.2% was estimated for 0.4 μm thickness of titanium tritide source.

4.5 Comparison of different tritiated metals

Different tritiated metals such as titanium tritide, scandium tritide, magnesium tritide, lithium tritide, and beryllium tritide were investigated using the PENELOPE Monte Carlo source model in order to determine which source material would produce the highest beta flux and source efficiency. These metals have different densities and valence electrons. Thus, the tritiation of these metals yield different specific activities as shown in Table 4.3 [5, 10]. The specific activity per unit volume is different from the specific activity per unit mass. The specific activity per unit mass for low density material is higher than that of high density material. However, the specific activity per unit volume is low for the low density material compared to the high density material. The focus of this work is to study the source thickness for the same surface area for different tritiated metals to increase the surface activity.

Table 4.3: Properties of different metal tritides

Tritiated metals	**Density (g/cm^3)**	**Specific activity per unit mass (Ci/g)**	**Specific activity per unit volume (Ci/cm^3)**
Titanium tritide (TiH_2)	3.91	1077.63	4213.53
Scandium tritide (ScH)	3	605.39	1816.17
Magnesium tritide (MgH_2)	1.45	1914.59	2776.16
Lithium tritide (LiH)	0.82	2916.68	2391.68
Beryllium tritide (BeH_2)	0.65	3860.8	2509.52

It was shown above in the case of titanium tritide that the estimates for beta flux and power output for a 90 degree distribution with the backscattering effect matched well with the experimental results. Thus, the comparisons of results for different tritiated metals were presented only for a 90 degree distribution that included the backscattering effect, i.e. a fully isotropic source.

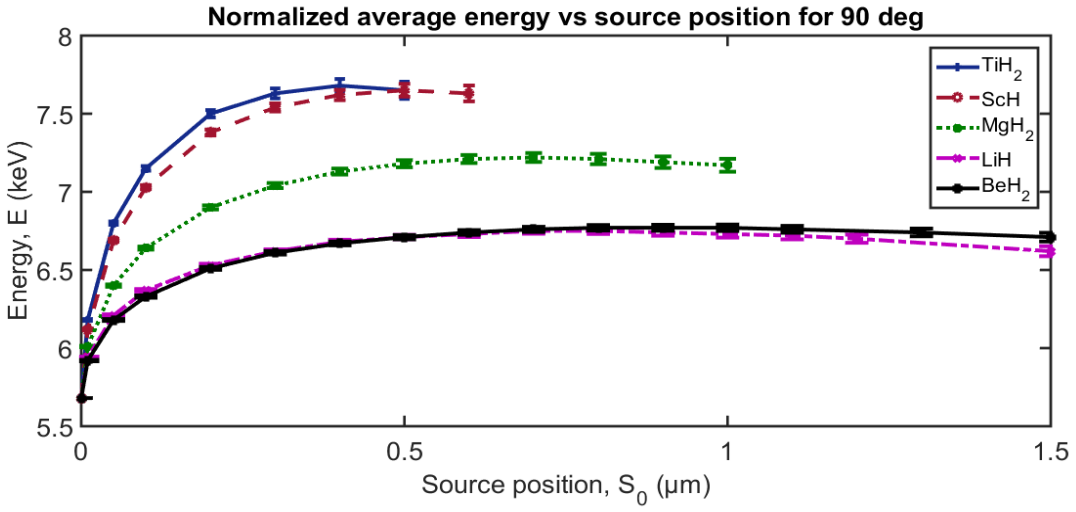

Figure 4-8: Comparison of beta average energy for different metal tritides with increasing source thickness

A comparison of the normalized beta particle average energy increase with source thickness for different tritiated metals is shown in Figure 4-8.

Table 4.4: Peak average beta energy for different metal tritides

Tritiated metals	Source thickness (μm)	Peak energy (keV)
Titanium tritide	0.4	7.68 ± 0.048
Scandium tritide	0.5	7.65 ± 0.041
Magnesium tritide	0.7	7.22 ± 0.029
Lithium tritide	0.7	6.75 ± 0.018
Beryllium tritide	0.8	6.77 ± 0.018

Table 4.4 shows that the peak average energy is higher for high density tritiated metals and it was observed at a lower source thickness. The source thickness for beryllium tritide was twice than that of titanium tritide to obtain the peak energy.

A comparison of beta flux with various source thicknesses for different tritiated metals is shown in Figure 4-9. The beta fluxes are all approximately on the order of billions per square centimeter per second for all the tritiated metals. Except for scandium tritide, beta fluxes for all other tritiated metals are of a similar magnitude for a source thickness below 0.5 µm. A maximum beta flux of 2.73×10^9 ($cm^{-2}s^{-1}$) was obtained for 3 µm thickness of beryllium tritide. Beryllium tritide has the lowest density compared to the other tritiated metals considered in this work. Although low density materials have low specific activities per unit volume compared to the high density materials, low density materials have the advantage of low self-absorption in the source. In the case of low density tritiated metal, beta particles that are emitted from the deeper tritium atoms encounter fewer atomic collisions and the probability of transport to exit the surface is higher. Thus, a greater source thickness can be employed to increase the beta flux which will in turn increase the battery output.

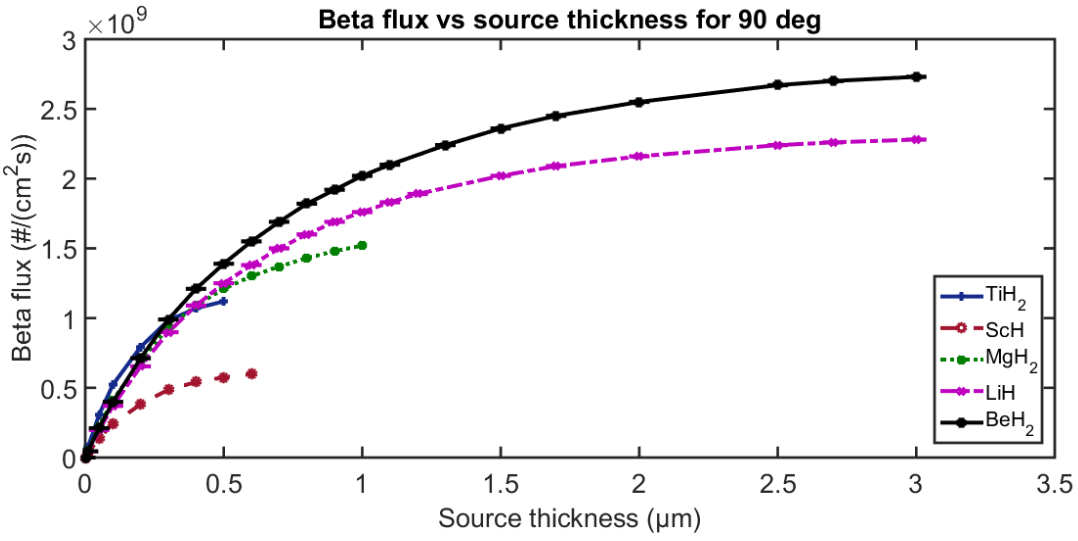

Figure 4-9: Comparison of beta flux for different metal tritides with increasing source thickness

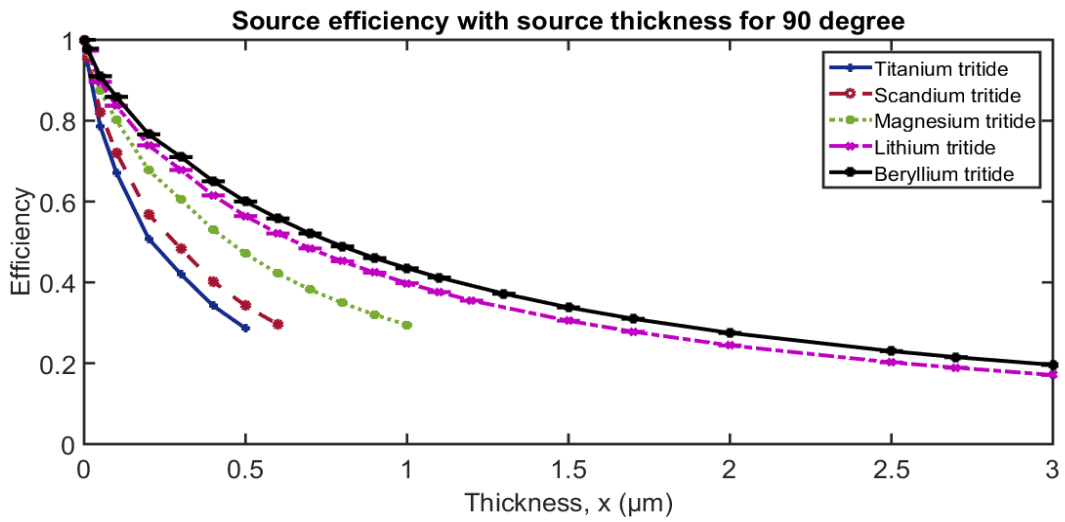

Figure 4-10: Comparison of source efficiency for different metal tritides at various source thicknesses and assuming that ideal SiC transducers are placed on both sides of the source

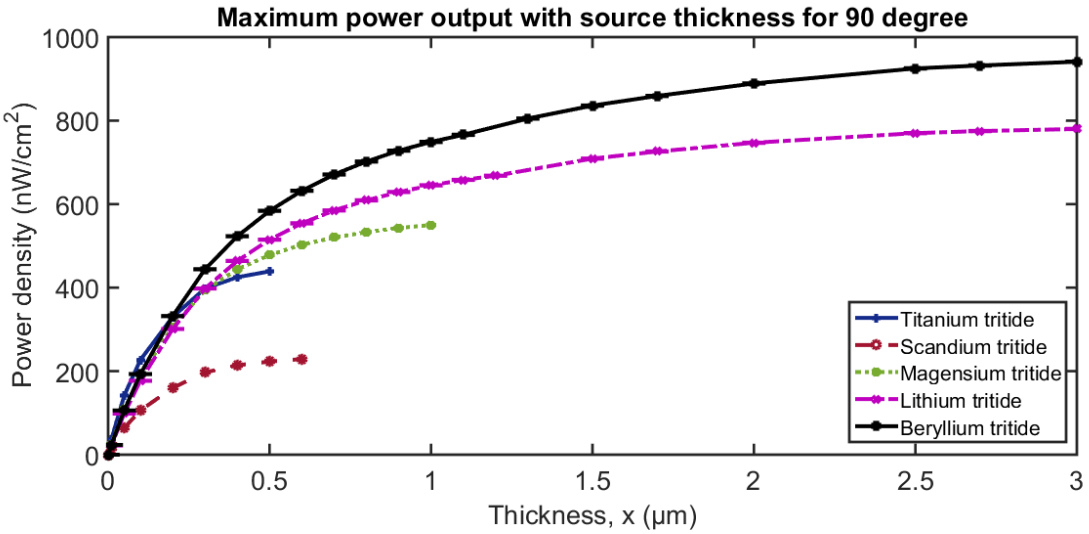

Figure 4-11: Comparison of maximum possible power output for different metal tritides at various source thicknesses and assuming that ideal SiC transducers are placed on both sides of the source

The maximum possible power outputs for the various tritiated metals are calculated for SiC semiconductor transducers placed on both sides of the source and making the assumption that there are no device losses. Power outputs were derived from the estimated beta fluxes from the radioisotope sources. The efficiencies for different tritiated metals and the maximum possible power outputs are compared in Figure 4-10 and Figure 4-11 respectively. It shows that the highest power output and efficiency were achieved with beryllium tritide. A 3 µm thick beryllium tritide source provides a power density of 941 nW/cm^2 with a source efficiency of about 20%. However, Figure 4-10 and Figure 4-11 signify that there is an optimum source thickness for each metal tritide in order to maximize the battery output efficiency.

4.6 Source optimization

The power output of a betavoltaic battery can be increased by increasing the source thickness up to a point where it begins to saturate. However, there is a trade-off between maximum

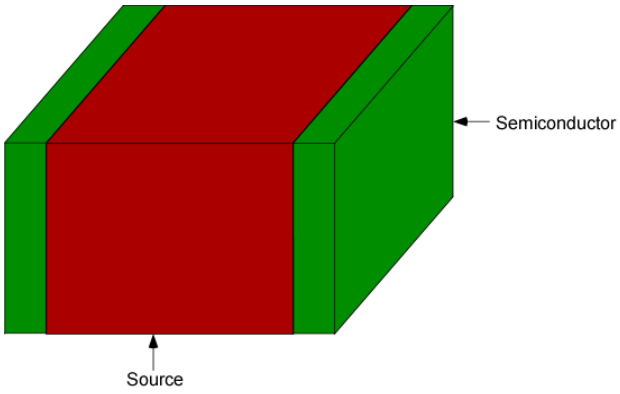

Figure 4-12: Ideal battery configuration where the source is sandwiched by the semiconductors in a cubic volume

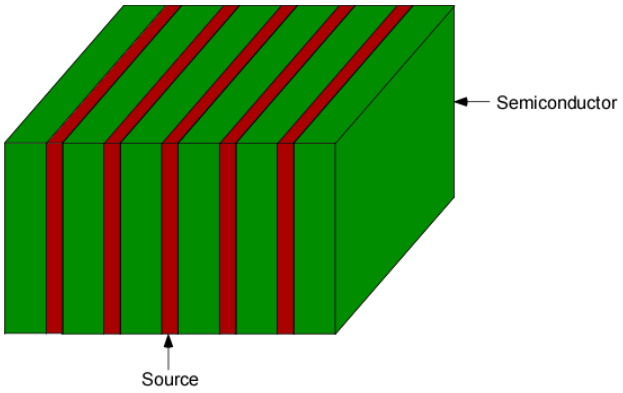

Figure 4-13: Practical battery configuration for source optimization with layers of source and semiconductor in a cubic volume

possible power output and source efficiency. The increase in maximum possible power output comes at the expense of reducing the source efficiency. A radioisotope source is very costly compared to semiconductor material. For example, the price of tritium is $30,000/gm and this is very high compared to the price of SiC which is $0.036/gm [15, 16]. Therefore, an optimization of the source thickness is very important in betavoltaic battery design. A form factor approach was used in this work to optimize the maximum possible power output and source thickness for different tritiated metals. A form factor is defined for a volumetric source that takes into account the self-absorption effect. An ideal radioisotope volumetric source without the self-absorption effect would provide the maximum power output for its volume. To harness this power two SiC semiconductors can be placed on both sides of the volumetric source. The maximum beta energy of tritium is 18.59 keV, which is a very low energy. A very low thickness of SiC is required to absorb all the energy of a tritium source. The penetration depth of tritium beta particles in SiC is about 1 µm [17]. For a given volume of an ideal radioisotope source, only a 2 µm thickness for the SiC semiconductor material placed on each side of the source will be needed for harnessing its

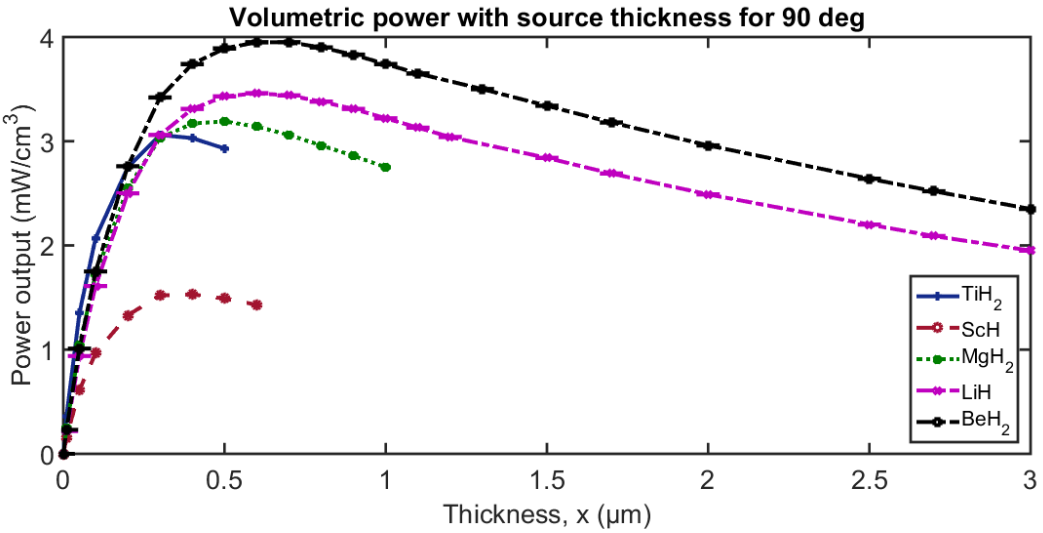

Figure 4-14: Optimum power output and source thickness for different metal tritides using form factor approach

power. This typical setup of a betavoltaic battery is illustrated in Figure 4-12. However, in reality, this ideal configuration will be a very inefficient design due to the beta particle self-absorption in the source. To make the design more efficient, it requires an intermediate placement of SiC semiconductor material inside the volume of the source. This configuration as illustrated in Figure 4-13 becomes an alternating periodic layered structure of the radioisotope source and the semiconductor material. This design is more practical and reduces the self-absorption effect significantly, which in turn increases the battery efficiency. However, in this design, the total volume of the radioisotope source is lower than its total volume in the ideal configuration. This volumetric ratio given in equation (1) is defined as the form factor for the radioisotope source.

$$form\ factor = \frac{volume\ of\ radioisotope\ source - n\ layers\ of\ semiconductor\ volume}{volume\ of\ the\ radioisotope\ source - 2\ layers\ of\ semiconductor\ volume} \quad (1)$$

Form factors, maximum possible power outputs, and source efficiencies were computed for different source thicknesses of each of the tritiated metals. A comparison of the power outputs for the alternating layered structure of the source and the semiconductor is shown in Figure 4-14. A peak was observed at different source thicknesses for each tritiated metal. For all tritiated metals, the maximum possible power output was obtained below a 1 μm source thickness. Table 4.5 shows the optimum source thickness, maximum possible power output for a one cubic centimeter battery including the source and semiconductor layers, and the form factor for each metal tritide. A maximum possible power output of approximately 4 mW/cm^3 was obtained for beryllium tritide with an optimum thickness of 0.6 μm and a form factor of 0.15. The total number of source layers decreases with the higher source thickness. The total source thickness is about 37% of the battery thickness for both lithium tritide and beryllium tritide. However, since the specific activity per unit volume for beryllium tritide is higher than that of lithium tritide, a higher power output is obtained with beryllium tritide. It is interesting to note that the optimum source thickness of each tritiated metal for the alternating layered design occurs at a thickness near the peak average beta particle energy. Therefore, the normalized average beta energy analysis can provide an approximate estimate for the source thickness optimization.

Table 4.5: Results comparison of optimum thickness, maximum possible power output, and form factor for various tritide metal sources

Tritiated metals	Optimum source thickness (μm)	Maximum power output (mW/cm^3)	Form factor	Number of source layers	Total source thickness (cm)
Titanium tritide	0.3	3.06 ± 0.0023	0.0703	7691	0.23075
Scandium tritide	0.4	1.53 ± 0.0011	0.0817	7142	0.28569
Magnesium tritide	0.5	3.19 ± 0.0011	0.1108	6666	0.3333
Lithium tritide	0.6	3.46 ± 0.0019	0.1396	6249	0.37496
Beryllium tritide	0.6	3.95 ± 0.0021	0.1519	6249	0.37496

4.7 Conclusions

It is very important to optimize the source thickness to increase the power output and the efficiency of a betavoltaic cell. A Monte Carlo transport code with isotropic emission of beta particles using the full beta energy spectrum was used to obtain theoretical results. In this work, a Monte Carlo analysis of the source model was developed to analyze the radioisotope beta particle self-absorption effect. This model is applied to different tritiated metals to estimate the rate of change in the average beta particle energy, beta flux, maximum possible power output, and source efficiency for various source thicknesses. The results demonstrated the importance of considering a fully isotropic emission of beta particles from the radioisotope atoms in the source material. The emitted beta particle energy spectrum for tritium varies with the source material thickness. The normalized average beta energy increases with the source thickness, as the low energy beta particles are absorbed in the source while the higher energy beta particles can still exit the surface. It reaches a peak value for a thickness depending on the density and the specific activity of the

source. For a beryllium tritide source with a low density of 0.65 g/cm^3, a peak average beta particle energy of 6.77 keV was obtained for a 0.8 µm source thickness. On the other hand, for a titanium tritide source with a higher density of 3.91 g/cm^3, a peak average beta particle energy of 7.68 keV was obtained at a lower thickness of 0.4 µm. There is a trade-off that low density material reduces the self-absorption effect but it holds less tritium atoms due to lower specific activity per unit volume. However, low density materials can still increase the maximum possible power output due to much lower self-absorption. The beta particle flux and the maximum possible power output increases with increased source thickness. However, the differential increase in the beta flux and the maximum possible power output becomes lower for a higher source thickness and the source efficiency drops due to an increase in the beta particle self-absorption. A low density source is better as it minimizes the self-absorption effect and will also often have a higher specific activity in the case of tritiated metals. A thicker source can be used for a low density source material in order to increase the beta flux, maximum possible power output, and source efficiency. A form factor approach was employed to efficiently design a battery with multiple alternating layers of the source and the semiconductor. The optimum thickness of the source was found to be near the thickness where the peak average beta particle energy was observed. Beryllium tritide provided the highest source power output of about 4 mW/cm^3 for an optimum thickness of 0.6 µm.

4.8 References

[1] Olsen, L.C., *Review of betavoltaic energy conversion.* 1993.

[2] Prelas, M.A., et al., *A review of nuclear batteries.* Progress in Nuclear Energy, 2014. **75**: p. 117-148.

[3] Prelas, M., et al., *Nuclear Batteries and Radioisotopes*. 2016: Springer International Publishing.

[4] Adams, T.E., *A study of palladium thin-films for radioisotope storage in betavoltaic power sources designs*. 2011, Purdue University.

[5] Kherani, N. and W. Shmayda, *Electron flux at the surface of titanium tritide films.* Fusion Science and Technology, 1992. **21**(2P2): p. 334-339.

[6] Liu, B., et al., *Power-scaling performance of a three-dimensional tritium betavoltaic diode.* Applied Physics Letters, 2009. **95**(23): p. 233112-233112-3.

[7] Thomas, C., S. Portnoff, and M. Spencer, *High efficiency 4H-SiC betavoltaic power sources using tritium radioisotopes.* Applied Physics Letters, 2016. **108**(1): p. 013505.

[8] Li, H., et al., *Simulations about self-absorption of tritium in titanium tritide and the energy deposition in a silicon Schottky barrier diode.* Applied Radiation and Isotopes, 2012. **70**(11): p. 2559-2563.

[9] Gui, G., et al., *Prediction of 4H–SiC betavoltaic microbattery characteristics based on practical Ni-63 sources.* Applied Radiation and Isotopes, 2016. **107**: p. 272-277.

[10] Bower, K.E., et al., *Polymers, Phosphors, and Voltaics for Radioisotope Microbatteries*. 2002: CRC Press.

[11] Alam, T.R. and M.A. Pierson, *Principles of Betavoltaic Battery Design.* Jounal of Energy and Power Sources, 2016. **3**(1): p. 11-41.

[12] Salvat, F. *PENELOPE-2014: A code system for Monte Carlo simulation of electron and photon transport*. in *Workshp, Barcelona*. 2015. Spain

[13] Krane, K.S., *Introductory Nuclear Physics*. 1987: Wiley.

[14] Cross, W., H. Ing, and N. Freedman, *A short atlas of beta-ray spectra.* Physics in Medicine and Biology, 1983. **28**(11): p. 1251.

[15] Willms, S. *Tritium supply considerations*. in *Fusion Development Paths Workshop*. 2003.

[16] http://web.mit.edu/course/3/3.11/www/modules/props.pdf

[17] Theirrattanakul, S. and M. Prelas, *A Methodology for Efficiency Optimization of Betavoltaic Cell Design using an Isotropic Planar Source having an Energy Dependent Beta Particle Distribution*. Applied Radiation and Isotopes, 2017.

CHAPTER 5: A COMPARISON OF NARROW AND WIDE BAND GAP BASED BETAVOLTAIC BATTERIES

5.1 Abstract

A Monte Carlo electron transport code PENELOPE was used to analyze beta particle energy deposition in semiconductors for titanium tritide and beryllium tritide. The source thickness was incorporated in the model in order to take into account the self-absorption of beta particles in the source material. Furthermore, an isotropic source was modeled with the full beta energy spectrum of tritium to make the beta particle transport method as realistic as possible. The simulated betavoltaic battery results for a 0.4 μm thick titanium tritide source with silicon carbide semiconductor material using a drift-diffusion semiconductor model agreed well the experimental results. The simulated betavoltaic battery results obtained for an optimized 2.5 μm thick beryllium tritide source with silicon carbide semiconductor material was about two times higher than the power for a 0.4 μm thick titanium tritide source with silicon carbide. A comparison of betavoltaic batteries for beryllium tritide with silicon and silicon carbide semiconductor materials showed that about a two times higher short circuit current density was obtained for silicon. However, the power output density was about ten times higher for silicon carbide. A depletion layer analysis showed that the combination of high p-type and low n-type dopant concentrations increases the depletion layer width. The width of the depletion region for a p-type dopant concentration of 1×10^{19} /cm^3 and an n-type dopant concentration of 5×10^{14} /cm^3 is about 1.4 μm and 2.5 μm in silicon and silicon carbide respectively. The estimated beta particle penetration depth using PENELOPE

showed that the penetration depth is about 1.48±0.015 μm and 1.03±0.015 μm in silicon and silicon carbide respectively. This suggests that the proper choice of dopant concentrations will achieve greater energy deposition in the depletion region. The results also indicate that a shallow junction depth and passivated surface will increase the power output for betavoltaic batteries.

Keywords: Design principles of betavoltaic batteries, self-absorption, betavoltaic battery model

5.2 Introduction

A betavoltaic battery is a radioisotope battery that is a method of direct conversion using semiconductors to convert the kinetic energy of beta particles into electrical energy [1-3]. It has applications mainly in MEMS and remote sensors due to its high energy density and long service life but relatively low power output [4, 5]. Many researchers have focused on tritium for betavoltaic batteries [6-8]. The maximum beta particle energy emitted during tritium decay is 18.59 keV, which minimizes the displacements from Non Ionizing Energy Loss (NIEL) or radiation damage in semiconductors [2]. However, tritium is a gas and the leakage of tritium in the gas phase can create a radiation hazard. Therefore, a tritiated metal in a solid state is a preferred radioisotope choice for tritium instead of its gaseous state [9]. A low density, low Z metal tritide has the advantage that it can reduce the self-absorption effect of the beta particles emitted within the source. As a result, a higher thickness source material can be used to increase the surface activity, which will in turn increase the power output of the battery. Titanium tritide with a density of 3.91 g/cm^3 [9] was used as a radioisotope source by Thomas et al. [6] for an experimental

betavoltaic battery. The surface activity was measured to be about 30.2 mCi/cm^2 for a 0.4 μm thick titanium tritide source, which is about the maximum possible thickness due to the saturation of the emitted beta flux resulting from self-absorption. On the other hand, a much higher surface activity of 72 mCi/cm^2 was estimated for a 2.5 μm thick beryllium tritide source, due to its low density and low Z, of 0.65 g/cm^3 [10]. The simulated and experimentally measured results for titanium tritide with silicon carbide were compared using the semiconductor drift-diffusion model.

A Monte Carlo beta particle (electron) transport model was deployed using PENELOPE [11] to estimate the energy deposition in the semiconductor. The source thickness was modeled in order to take into account the self-absorption of beta particles in the source [7, 12]. The self-absorption effect of beta particles is a major factor in betavoltaic battery design that modifies the theoretical beta energy spectrum of the source [12]. This effect also reduces the total number of electron hole pairs (EHPs) generated in the semiconductor. Furthermore, a full beta energy spectrum for tritium with isotropic beta particle emission was considered in the model. The incorporation of all these design factors will make the model more realistic.

Many researchers have designed betavoltaic batteries using narrow and wide band gap semiconductors [6, 13, 14]. In this work, simulated results for beryllium tritide with silicon and silicon carbide were compared. The design principles for betavoltaic batteries are discussed with respect to energy deposition and penetration depth analyses for beryllium tritide source material in silicon and silicon carbide. Semiconductor device parameters such as dopant concentrations, depletion layers, junction depth, and surface recombination velocities are analyzed.

5.3 Monte Carlo Model using PENELOPE

The beta particle penetration depths in silicon and silicon carbide were estimated for a tritium point source using PENELOPE. The penetration depths were estimated based on a 99% energy deposition along the thickness direction in the semiconductors. Different beta particle input energies such as monoenergetic average beta energy, monoenergetic maximum beta energy and full beta energy spectrum with 360 degree spherical distribution of beta particles i.e. full isotropic beta particle emission were used in PENELOPE. The penetration depths were also estimated by the Everhart and Hoff equation [15] for both monoenergetic average beta energy and monoenergetic maximum beta energy. The Everhart and Hoff equation is an empirical range equation for low Z materials given by equation (1)

$$R(E) = 4E^{1.75}, (5 \leq E \leq 25\ keV) \qquad (1)$$

where *R(E)* is the range density in μg/cm^2 and *E* is the beta particle energy in keV. *R(E)* is then divided by the density of silicon or silicon carbide to estimate the penetration depths. Equation (1) does not consider the isotropic emission of beta particles. This equation is valid for tritium as it has an average beta particle energy of 5.68 keV and a maximum beta particle energy of 18.59 keV. Table 5.1 shows the comparison of the penetration depth analysis of tritium beta particles in silicon and silicon carbide for different beta input energies.

Table 5.1: Comparison of penetration depths analyses

Input type	Penetration depth by PENELOPE		Penetration depth by Everhart-Hoff	
	Si (µm)	SiC (µm)	Si (µm)	SiC (µm)
Monoenergetic average beta energy (5.68 keV)	0.44±0.015	0.32±0.015	0.36	0.26
Monoenergetic maximum beta energy (18.59 keV)	3.32±0.015	2.44±0.015	2.86	2.07
Isotropic full beta energy spectrum (0-18.59 keV)	1.48±0.015	1.03±0.015		

Penetration depths are dependent on the density of the material. The densities of silicon and silicon carbide are 2.33 g/cm^3 and 3.21 g/cm^3. Table 5.1 shows that the penetration depth for tritium beta particles in silicon carbide is lower than silicon due to its higher density. A slight deviation in penetration depths was observed for PENELOPE and the Everhart-Hoff equation.

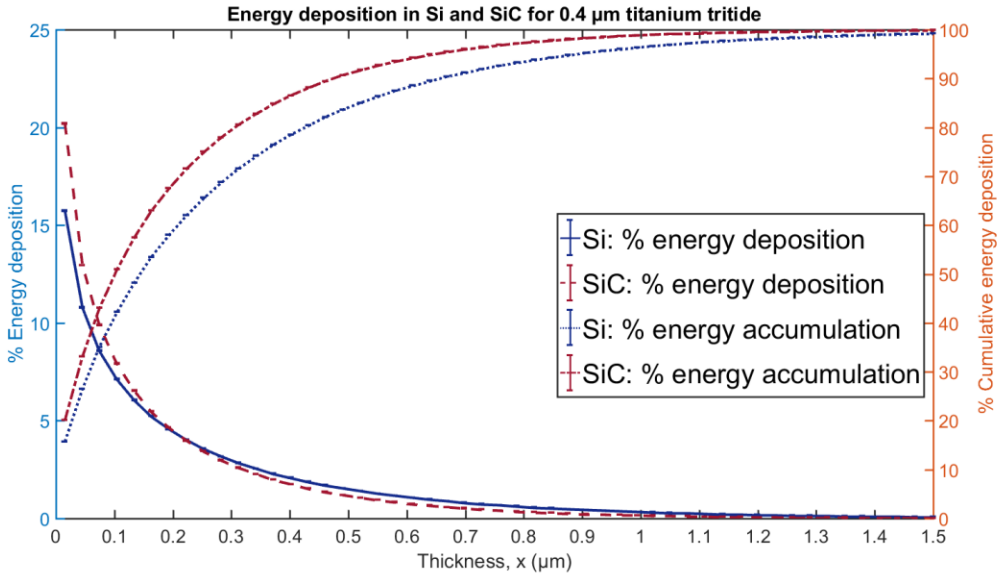

Figure 5-1: A comparison of energy deposition in silicon and silicon carbide for a 0.4 µm thick titanium tritide source

Table 5.1 also shows that penetration depth for the isotopic full beta energy spectrum case is in between the penetration depths of the monoenergetic average beta energy case and the monoenergetic maximum beta energy case. As a result, most of the beta particle energy for tritium will be deposited in silicon and silicon carbide within about 1.5 µm and 1 µm respectively. Besides the penetration depth, it is important to estimate the energy deposition profile in order to design a betavoltaic battery. The comparison of beta particle energy deposition in silicon and silicon carbide are shown in Figure 5-1 for the isotropic full beta energy spectrum of tritium. Figure 5-1 shows that the energy deposition decreases with the semiconductor thickness and most of the beta particle energy is deposited near the surface. This indicates that about 90% of the beta particles' energy for a 0.4 µm titanium tritide source is deposited within about 0.67 µm and 0.49 µm thicknesses in silicon and silicon carbide respectively. The estimate of energy deposition is important for calculating the generation of EHPs in semiconductors. The generation of EHPs has a linear

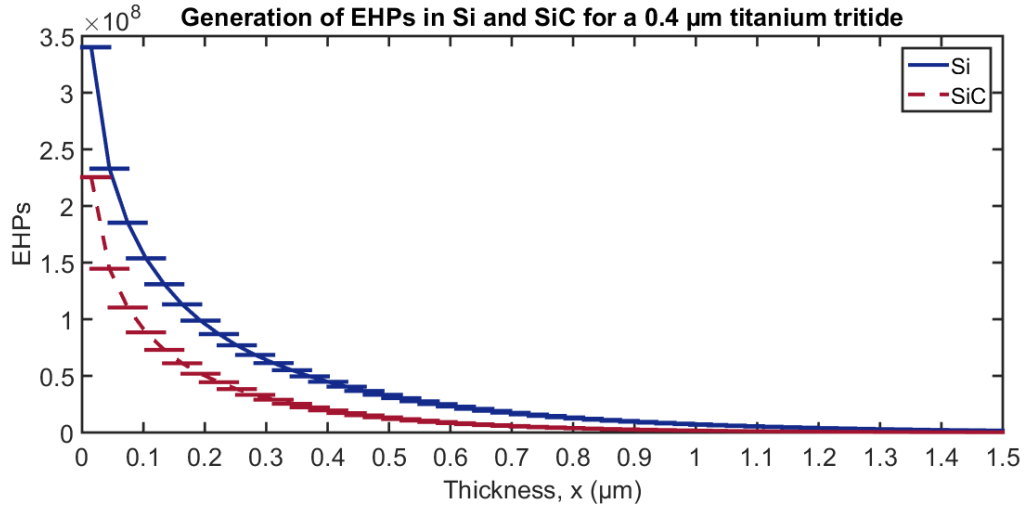

Figure 5-2: A comparison of EHP generation in silicon and silicon carbide for a 0.4 µm thick titanium tritide. The error bars in EHPs come from the Monte Carlo uncertainties in energy deposition estimates

relationship with the estimate of energy deposition depending on the electron hole pair ionization energy of the semiconductor. The electron hole pair ionization energies for silicon and silicon carbide are 3.64 eV and 7.28 eV respectively. This indicates that the generation of EHPs is two times higher in silicon than that of silicon carbide for the same amount of energy deposition. Figure 5-2 shows the comparison of EHPs generated in silicon and silicon carbide for a 0.4 μm thick tritiated titanium source. It indicates a higher generation of EHPs in silicon compared to silicon carbide as predicted.

A semiconductor model is required to estimate the short circuit current and the open circuit voltage from the collection of EHPs in semiconductors.

5.4 Semiconductor Design Analysis for Betavoltaic Batteries

A drift-diffusion semiconductor model was used with some simplified assumptions in order to obtain a closed form solution for the short circuit current and the open circuit voltage. The major assumptions are that the electric field is confined to the depletion region and all the EHPs generated in the depletion region are collected. Therefore, the minority carrier diffusion equations (2) and (3) were solved only for the p-type and n-type regions. The generation of EHPs was assumed to be an exponential function along the thickness direction of the semiconductor.

$$\frac{d^2\Delta n}{dx^2} - \frac{\Delta n}{L_n^2} = -\frac{A_0 a e^{-bx}}{D_n} \tag{2}$$

$$\frac{d^2\Delta p}{dx^2} - \frac{\Delta p}{L_p^2} = -\frac{A_0 a e^{-bx}}{D_p} \tag{3}$$

Two boundary conditions were applied to solve the minority carrier diffusion equation in the p-type and n-type regions. The surface boundary condition considers the surface recombination velocity for the recombination losses at the surface given in equations (4) and (6) for each type region. The depletion edge boundary conditions given in equations (5) and (7) assume no excess minority carriers at the edge of the depletion region since the minority carriers are swept across the depletion region due to the presence of the high electric field.

$$D_n \frac{dn}{dx} = S_n \Delta n \quad (4)$$

$$\Delta n(x_p) = 0 \quad (5)$$

$$-D_p \frac{dp}{dx} = S_p \Delta p \quad (6)$$

$$\Delta p(x_n) = 0 \quad (7)$$

In equations (2) to (7), *n* is the minority carrier concentration in the p-type region, *p* is the minority carrier concentration in the n-type region, *L* is the minority carrier diffusion length, *D* is the diffusion coefficient, A_0 is the surface activity for the beta particle emissions in the direction of the semiconductor surface, *S* is the surface recombination, and *a* and *b* are the coefficients for the EHP generation plot exponential curve fitting from the PENELOPE model. Equations (2) and (3) were solved to obtain the short circuit current and open circuit voltage. The simulated results were compared to the experimental results obtained by Thomas et al. [6] using a 0.4 μm thick titanium tritide source with SiC semiconductor material. Table 5.2 shows the parameters used to estimate the simulation results at 300 K. A surface activity of 30.2 mCi/cm^2 was estimated from the experimentally measured beta particle input power of 732.9 nW/cm^2 for a

0.4 µm titanium tritide source [6]. The p-type and n-type dopant concentrations were $1 \times 10^{19}/cm^3$ and $5 \times 10^{14}/cm^3$ in silicon carbide respectively. The experimentally measured junction depth was 0.2 µm. All these experimentally measured parameters were used in the simulation.

Table 5.2: Parameters used in the model [6, 16, 17]

Minority carrier diffusion length (µm)		**Diffusion coefficient (cm^2/s)**		**Surface activity (mCi/cm^2)**	**Surface recombination velocity (cm/s)**		**Coefficients of the exponential curve fitting (ae^{-bx}) of EHPs**	
L_n	L_p	D_p	D_n	(A_0/S)	S_p	S_n	a (cm^{-3})	b (cm^{-1})
0.3	9.01	3.13	4.05	30.2	10^5	10^5	2.216×10^8	7.497×10^4

Table 5.3 shows the comparison of simulated short circuit current density, open circuit voltage, and leakage current density to the experimental results. The simulated short circuit current density and open circuit voltage for an isotropic source agree well with the experimental results. The theoretical leakage current is very small for wide bandgap semiconductors. The experimental leakage current density was measured at a bias voltage that was not reported. It requires extrapolation to 0 V to compare to the theoretical leakage current density. Furthermore, there could be some localized defects perpendicular to the semiconductor surface as well as some surface defects that increased the leakage current density. However, these defects did not have major impacts in EHP collection in the bulk semiconductor material.

Table 5.3: Simulated and experimental results comparison for a 0.4 µm thick titanium tritide source with SiC

Outputs	**Simulation results (isotropic)**	**Experimental results**
Short circuit current (nA/cm^2)	77.55 ± 0.05	75.47
Open circuit voltage (V)	2.22 ± 0.00002	2.09
Leakage current (pA/cm^2)	4×10^{-33}	6.1

The dopant concentrations in semiconductors are important parameters in order to improve the collection of EHPs [18, 19]. Minority carrier diffusion lengths determine the collection of EHPs in both p-type and n-type regions. Minority carrier diffusion lengths in silicon are given by equations (8) and (9) [20, 21]

$$L_n = \sqrt{\frac{kT}{q}\left[232 + \frac{1180}{1+\left(\frac{N_a}{8\times10^{16}}\right)^{0.9}}\right] \cdot \frac{1}{3.45\times10^{-12}N_a + 9.5\times10^{-32}N_a^2}} \qquad (8)$$

$$L_p = \sqrt{\frac{kT}{q}\left[130 + \frac{370}{1+\left(\frac{N_d}{8\times10^{17}}\right)^{1.25}}\right] \cdot \frac{1}{7.8\times10^{-13}N_d + 1.8\times10^{-31}N_d^2}} \qquad (9)$$

where k is the Boltzmann constant, T is the temperature, q is the electron charge, N_a and N_d are the dopant concentrations in the p-type and n-type regions respectively. Figure 5-3 shows the variation in minority carrier diffusion lengths with respect to the dopant concentrations

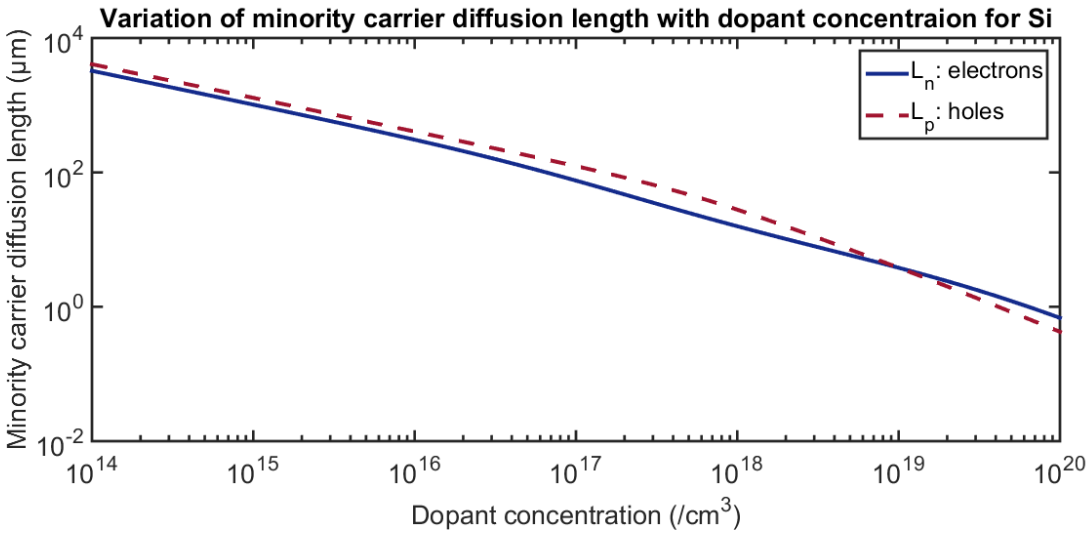

Figure 5-3: Minority carrier diffusion lengths variation with dopant concentration for silicon

in silicon. Minority carrier diffusion lengths decrease with higher dopant concentrations. Minority carrier diffusion lengths decrease due to reduced minority carrier lifetime with higher dopant concentrations. Minority carrier lifetimes are much shorter in wide band gap semiconductors. As a result, minority carrier diffusion lengths in silicon carbide are much lower than that of silicon. For example, the hole diffusion length in silicon carbide at a dopant concertation of 5×10^{14} /cm^3 is about 13 times lower than silicon. Besides, the minority carrier diffusion lengths, the collection of EHPs in the semiconductor device depends on the width of the depletion region. Furthermore, the width of the depletion region is also dependent on the dopant concentrations. Most of the EHPs generated in the depletion region are collected. Therefore, the dopant concentrations in the device need to be designed to increase the width of the depletion region. The width of the depletion region and the built-in potential are given by equations (10) and (11) [22, 23]

$$W = \sqrt{V_D \left(\frac{2\varepsilon_r \varepsilon_0}{q}\right)\left(\frac{N_a + N_d}{N_a N_d}\right)} \qquad (10)$$

$$V_D = \frac{kT}{q}\left(ln \frac{N_a N_d}{n_i^2}\right) \qquad (11)$$

where W is the width of the depletion region, V_D is the built-in potential difference, ε_r and ε_o are the dielectric constants in the regions and vacuum respectively, N_a and N_d are the doping concentrations of p-type and n-type regions and n_i is the intrinsic carrier concentration. Figure 5-4 shows the depletion region width variation with dopant concentrations for both silicon and silicon carbide. It indicates that the depletion layer does not exist for the same amount of accepter and donor dopant concentrations. A combination of high p-type dopant concertation and a low n-type dopant concentration increases the width of the depletion region. Figure 5-4 also shows that a wider depletion region can be obtained for wide band gap semiconductors. The strength of the

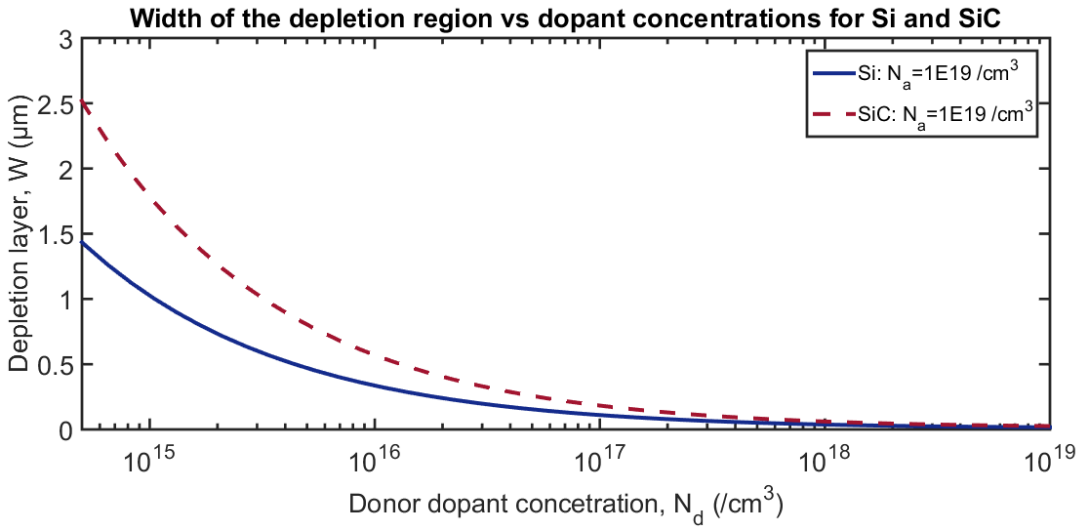

Figure 5-4: Width of the depletion region variation with dopant concentration for silicon and silicon carbide

electric field in the depletion region is indicated by the built-in-potential. The built-in-potential is the limit for the theoretical maximum voltage obtained by the semiconductor. Figure 5-5 shows

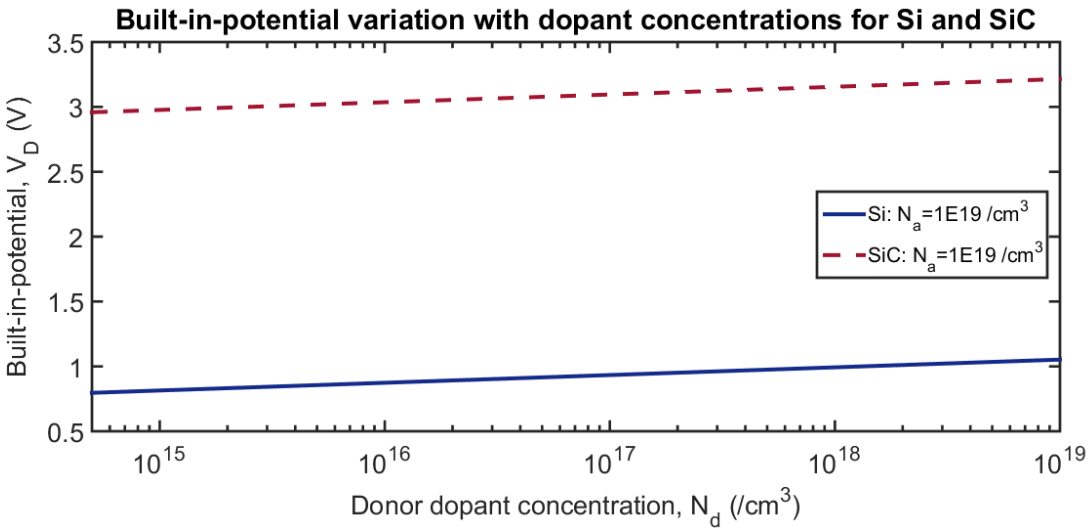

Figure 5-5: Changes in built-in potential with dopant concentrations for silicon and silicon carbide

that the built-in-potential in silicon carbide is about three times higher than that of silicon at a low donor dopant concentration of $5 \times 10^{14}/cm^3$. As a result, it increases the open circuit voltage in silicon carbide.

To compare the short circuit current and the open circuit voltage for silicon and silicon carbide, a beryllium tritide source was considered. Beryllium is a lighter material than titanium. As a result, the self-absorption effect of beta particles in beryllium is less than that of titanium. A higher source thickness of 2.5 μm can be used for beryllium tritide in a single layer betavoltaic battery to increase the surface activity. However, the optimum source thickness of beryllium tritide is about 0.6 μm for multiple layered betavoltaic batteries. In this work, both 0.6 μm and 2.5 μm beryllium tritide source thicknesses were simulated with silicon and silicon carbide. The results were obtained for a p-type dopant concentration of $1 \times 10^{19}/cm^3$, n-type dopant concentration of $5 \times 10^{14}/cm^3$, junction depth of 0.2 μm, and surface recombination velocities of 10^{15} cm/s.

Table 5.4: Results comparison for 0.6 μm and 2.5 μm beryllium tritide with silicon and silicon carbide

Outputs	**Si**		**SiC**	
Source thickness (μm)	0.6	2.5	0.6	2.5
Activity (mCi/cm^{-2})	42	72	42	72
Short circuit current (nA/cm^2)	174.78 ± 0.37	284.53 ± 0.64	84.81 ± 0.13	126.82 ± 0.19
Open circuit voltage (V)	0.09 ± 0.00005	0.1 ± 0.00006	2.22 ± 0.00004	2.23 ± 0.00004
Maximum power (nW/cm^2)	16.03 ± 0.04	29.61 ± 0.07	188.46 ± 0.29	283.13 ± 0.42

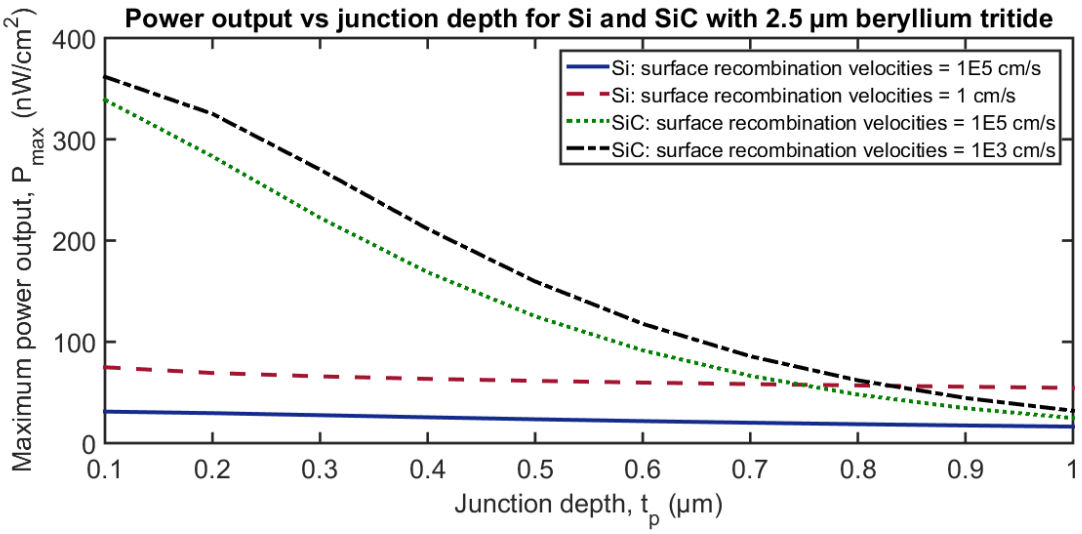

Figure 5-6: Power output variations with junction depths and surface recombination velocities for a 2.5 µm beryllium tritide source with silicon and silicon carbide

Table 5.4 shows that the short circuit current density in silicon is about two times higher than that of silicon carbide for the same amount of activity. This agrees with the fact that the generation of EHPs in silicon is about two times higher than that of silicon carbide for the same amount of energy deposition. On the other hand, the open circuit voltage in silicon carbide is about 20 times higher than that of silicon. As a result, the power output density obtained from silicon carbide is about 10 times higher than that of silicon. The estimated maximum power output in silicon carbide is about 0.28 µW/cm^2 for a 2.5 µm thick beryllium tritide using a single layer betavoltaic battery. This power output density is about two times higher compared to the power output density obtained experimentally using 0.4 µm titanium tritide with silicon carbide.

It is important to analyze the effects of junction depth and surface recombination velocities of the semiconductor in designing a betavoltaic battery. Figure 5-6 shows that an

optimum junction depth for both silicon and silicon carbide is near the surface as energy deposition is higher near the surface. It also shows that a reduction in surface recombination velocity by surface passivation increases the power output.

5.5 Conclusions

A betavoltaic battery model using Monte Carlo method with more realistic approach including the source model was developed. This model provides better prediction of the battery output that includes all the major design factors, which is a significant improvement. In this work, it was shown that a betavoltaic battery with higher surface activity can be designed using beryllium tritide. For a single layer betavoltaic battery design, a 2.5 μm thick beryllium tritide source with silicon carbide can increase the power output about two times higher than a 0.4 μm thick titanium tritide source with silicon carbide. A betavoltaic battery design using a wide band gap semiconductor silicon carbide provides about ten times higher output compared to the narrow band gap semiconductor silicon. However, a betavoltaic battery using silicon generates about two times higher current than silicon carbide. The required application would indicate which semiconductor material would be better. In both cases, the depletion layer width can be designed to be about 1.5 μm, which is about the penetration depth of beta particles for tritium, by using a high dopant concentration in the p-type region and a low dopant concentration in the n-type region. A shallow junction depth increases the power output as most of the beta particle energy for tritium deposit near the surface. Surface passivation is important for increasing the power output as it reduces the surface recombination losses. All of these factors need to be considered for designing a betavoltaic battery.

5.6 References

[1] Olsen, L.C., *Review of betavoltaic energy conversion.* 1993.

[2] Alam, T.R. and M.A. Pierson, *Principles of Betavoltaic Battery Design.* Jounal of Energy and Power Sources, 2016. **3**(1): p. 11-41.

[3] Revankar, S.T. and T.E. Adams, *Advances in betavoltaic power sources.* J. Energy Power Sources, 2014. **1**(6): p. 321-329.

[4] Prelas, M., et al., *Nuclear Batteries and Radioisotopes*. 2016: Springer International Publishing.

[5] Prelas, M.A., et al., *A review of nuclear batteries.* Progress in Nuclear Energy, 2014. **75**: p. 117-148.

[6] Thomas, C., S. Portnoff, and M. Spencer, *High efficiency 4H-SiC betavoltaic power sources using tritium radioisotopes.* Applied Physics Letters, 2016. **108**(1): p. 013505.

[7] Li, H., et al., *Simulations about self-absorption of tritium in titanium tritide and the energy deposition in a silicon Schottky barrier diode.* Applied Radiation and Isotopes, 2012. **70**(11): p. 2559-2563.

[8] Russo, J., et al., *Development of tritiated nitroxide for nuclear battery.* Applied Radiation and Isotopes, 2017. **125**: p. 66-73.

[9] Bower, K.E., et al., *Polymers, Phosphors, and Voltaics for Radioisotope Microbatteries*. 2002: CRC Press.

[10] Kherani, N. and W. Shmayda, *Electron flux at the surface of titanium tritide films.* Fusion Science and Technology, 1992. **21**(2P2): p. 334-339.

[11] Salvat, F. *PENELOPE-2014: A code system for Monte Carlo simulation of electron and photon transport*. in *Workshp, Barcelona*. 2015. Spain.

[12] Gui, G., et al., *Prediction of 4H–SiC betavoltaic microbattery characteristics based on practical Ni-63 sources.* Applied Radiation and Isotopes, 2016. **107**: p. 272-277.

[13] Guo, H. and A. Lal. *Nanopower betavoltaic microbatteries*. in *TRANSDUCERS, Solid-State Sensors, Actuators and Microsystems, 12th International Conference on, 2003*. 2003. IEEE.

[14] Theirrattanakul, S. and M. Prelas, *A Methodology for Efficiency Optimization of Betavoltaic Cell Design using an Isotropic Planar Source having an Energy Dependent Beta Particle Distribution.* Applied Radiation and Isotopes, 2017.

[15] Everhart, T. and P. Hoff, *Determination of kilovolt electron energy dissipation vs penetration distance in solid materials.* Journal of Applied Physics, 1971. **42**(13): p. 5837-5846.

[16] Schaffer, W.J., et al., *Conductivity anisotropy in epitaxial 6H and 4H SiC.* MRS Online Proceedings Library Archive, 1994. **339**.

[17] Galeckas, A., et al. *Evaluation of Auger recombination rate in 4H-SiC*. in *Materials Science Forum*. 1998. Trans Tech Publ.

[18] Tang, X., et al., *Optimization design and analysis of Si-63Ni betavoltaic battery.* Science China Technological Sciences, 2012. **55**(4): p. 990-996.

[19] Tang, X., et al., *Optimization design of GaN betavoltaic microbattery*. Science China Technological Sciences, 2012. **55**(3): p. 659-664.

[20] Swirhun, S., Y.-H. Kwark, and R. Swanson. *Measurement of electron lifetime, electron mobility and band-gap narrowing in heavily doped p-type silicon*. in *Electron Devices Meeting, 1986 International*. 1986. IEEE.

[21] Del Alamo, J., S. Swirhun, and R. Swanson. *Simultaneous measurement of hole lifetime, hole mobility and bandgap narrowing in heavily doped n-type silicon*. in *Electron Devices Meeting, 1985 International*. 1985. IEEE.

[22] Neamen, D., *Semiconductor Physics And Devices*. 2003: McGraw-Hill Education.

[23] Sze, S.M. and K.K. Ng, *Physics of Semiconductor Devices*. 2006: Wiley.

CHAPTER 6: CONCLUSIONS

6.1 Summary

The literature on betavoltaic batteries suggests that a better theoretical model and analysis are required to improve betavoltaic battery design. A detailed end-to-end theoretical model and analyses are missing. This work has focused on filling in the missing parts. It analyzed all of the necessary factors and provided important steps in comprehensively modeling a betavoltaic battery from the source-transducer interface, the material considerations, and the p-n junction design including full system integration. In the development of this comprehensive model for a betavoltaic battery, some fundamental results were developed.

A betavoltaic battery harvests electrical energy from radioactive decay energy. Radioisotopes are the source of energy for this type of battery. Therefore, the study of radioisotopes is very important. In this work, different radioisotopes were explored for betavoltaic batteries. A comparison and detailed discussions were provided for radioisotopes. Not all of the radioisotopes are a pure beta emitter. Radiation damage to the semiconductors is a limiting factor for the selection of radioisotopes. Some radioisotopes emit higher energy gamma, alpha, and beta radiation that is much higher than the radiation damage threshold of the semiconductor. The other limiting factor for the selection of a radioisotope is the half-life. It depends on the battery applications and the desired service life. Ni-63 and H-3 are pure beta emitters with high enough half-lives that are suitable for many applications. Their maximum energies are low enough to minimize the radiation damage to the crystal lattice structure of the semiconductor. Ni-63 and H-3 are the most practical choices of radioisotopes. Both Ni-63 and H-3 are considered in this work.

On the other hand, there are two different types of semiconductors such as narrow and wide band gap semiconductors. Both of them have some advantages and disadvantages in designing betavoltaic batteries. These were discussed in detail and literature results were compared. In this work, silicon, a narrow band gap semiconductor, and silicon carbide, a wide band gap semiconductor, were studied for betavoltaic battery design.

It is important to estimate the energy deposition and the penetration depth of beta particles in semiconductors for the battery design. The traditional design method of the betavoltaic battery uses a monoenergetic average beta particle energy. Some empirical equations provide the penetration depth for monoenergetic average beta particle energy. These equations assume monodirectional emission of beta particles perpendicular to the surface. This direction is referred to as 0 degree emission. Many theoretical models were based on this approach. However, beta particles have a wide range of energy distribution from zero to a maximum energy. This wide distribution of beta particle energy is referred to as a full beta energy spectrum. A Monte Carlo method of electron transport code considers the comprehensive physics of electron transport in materials. It has better accuracy and precision in estimating the penetration depth and energy deposition compared to other empirical equations. A Monte Carlo approach such as MCNP and PENELOPE was used in this work. Besides monoenergetic average beta particle energy and monoenergetic maximum beta particle energy, the full beta energy spectrum was modeled using a Monte Carlo method. A significant difference was observed in energy deposition and penetration depth for these different approaches. These effects were analyzed in detail with regard to their impact on the battery design. It was shown that a betavoltaic battery design based on the monoenergetic average beta energy would not be accurate. A full beta energy spectrum is required to provide a more realistic approach to the battery design. A simplified full beta energy spectrum

can be derived for any radioisotopes based on their average and maximum beta particle energy. This type of spectrum is referred to as a generalized full beta energy spectrum. An actual full beta energy spectrum derived from the Fermi distribution including coulomb interactions showed that the full beta energy spectrum is different than the generalized spectrum for some isotopes. Thus, an actual full beta energy spectrum specific to the radioisotope needs to be used in the betavoltaic battery model.

The angular distribution of beta particle emission is an important factor for betavoltaic battery design. In reality, the beta particles are emitted in all angular directions. The empirical equations that consider monoenergetic beta particles energy do not take into account the angular emission of beta particles. As mentioned above, they only provide an estimates for a 0 degree distribution. A 90 degree distribution captures the isotropic forward emission of beta particles. Both 0 degree and 90 degree distributions of beta particles were modeled using a Monte Carlo method. The effects of angular distribution in the modeling were studied and analyzed in detail. The betavoltaic battery outputs for both 0 degree and 90 degree distributions were compared. It was shown that a 90 degree (or forward isotropic) distribution of beta particles emission provides a more realistic approach to the battery design. This approach significantly improved the betavoltaic battery model.

Backscattering is also an important phenomenon of beta particle transport in semiconductors. The backscattering effect reduces the energy deposition in the semiconductor. This effect was not studied in the literature for betavoltaic battery design. A detailed work was presented for the backscattering effect. It showed the importance of backscattering effects in betavoltaic battery design. The backscattering effect with respect to the angular distribution of beta particle emission was analyzed. It shows that the backscattering of beta particles increases with

the higher angular distribution of beta particle emission. As a result, the energy loss increases due to this effect. However, there is a trade-off in battery design for this effect. Beta particles with higher angular emission also travel a long distance in the depletion region of the semiconductor which can increase the collection of electron hole pairs (EHPs) in the semiconductor. The results for backscattering of particles have significant impact on the principles of betavoltaic battery design.

A Monte Carlo radioisotope source model was developed in this work. A source model takes into account the transport and self-absorption of beta particles within the source material. The radioisotope source is one of the most important parts of betavoltaic battery design, and has not been studied in detail in prior work by others. The self-absorption effect of beta particles has a significant impact on the battery design. In this work, these effects were analyzed in order to improve the battery design. It was shown that the number of beta particles emitted within the source and the number of beta particles actually coming out of the source surface is significantly different. The self-absorption of beta particles reduces the number of beta particles coming out of the surface. This effect increases with the source thickness and when the fully isotropic emission of the beta particles is taken into account. A higher source thickness increases the activity of the source and increases the power output of the battery. However, the power output of the battery saturates with higher thickness due to te self-absorption effect. These analyses were conducted in detail in this work. There are other effects from the source model that are also discussed such as the change in the beta energy spectrum and change in beta particle average energy, in other words the energy spectrum becomes hardened. The detailed study of all these effects is significant for improvements in the battery design. In the traditional approach of modeling a betavoltaic battery, the radioisotope source dimension is neglected. Thus, only a point source is considered in prior

models that do not consider the all these effects including self-absorption. In this work, the source dimension was considered to make the modeling approach as realistic as possible. It is a general practice to model betavoltaic batteries with one semiconductor layer and a point source that assumes symmetry. Only beta particles moving in the direction of the semiconductor are usually considered by others in the model. However, it is shown in this work that the beta particles in the source that are emitted away from the semiconductor can still backscatter towards the semiconductor increasing the total number of beta particles travelling in that direction. This has a significant impact on the battery design. Neglecting this effect underestimates the beta flux leaving the source in the model. This effect is not evident when a source model is not considered. Therefore, this detailed analysis of the radioisotope source model is a significant improvement for betavoltaic battery design.

A radioisotope source is the most expensive part of the betavoltaic battery. The increase in source thickness increases the battery output. However, it reduces the source efficiency due to the self-absorption effect. Therefore, the source material needs to be optimized. The Monte Carlo source model was used in this work to optimize different metal tritides for betavoltaic battery design. A form factor approach was used to determine the optimum source thickness. Multiple source and semiconductor layers were studied and compared for different metal tritides. It was shown using the source model that a low density metal tritide increases the power output. This work is significant to design a better metal tritide radioisotope source that will increase battery power output. This study will allow a cost effective source design of the betavoltaic battery.

The principles of betavoltaic battery design for silicon and silicon carbide were investigated. The depletion region is very important in betavoltaic battery design. The EHPs generated in the depletion region have a higher probability of collection to the electrode. The

junction depth in the semiconductor determines the position of the depletion region. The variation in junction depth is analyzed in order to maximize the power output. An optimum junction depth near the surface where most of the beta particle energy is deposited increases the power output. A wider depletion region also increases the collection efficiency of EHPs, which in turn increases the power output of the battery. The width of the depletion region is dependent on the dopant concentrations in the p-type and n-type regions. A higher dopant concentration in the p-type region and a lower dopant concertation in the n-type region increase the width of the depletion region. The dopant concentrations have an impact on the minority carrier diffusion lengths and the leakage current of the semiconductor. All these effects were analyzed to improve the betavoltaic battery design. The surface recombination velocity of the semiconductor was also studied. This indicates that a passivated surface can have a significant effect in increasing the battery output. All these semiconductor parameters were analyzed and optimized, and a detailed discussion was provided for the principles of betavoltaic battery design. This will allow the optimization of the semiconductor design parameters.

Betavoltaic battery designs for silicon and silicon carbide with tritiated metals were investigated. An optimized beryllium tritide source was developed in this design. The energy required to create one EHP in silicon carbide is almost twice than that of silicon. As a result, the generation of EHPs is almost twice in silicon compared to silicon carbide. This effect also increased the short circuit current density in silicon. However, the leakage current is very high in silicon than that of silicon carbide. As a result, the open circuit voltage is very low for silicon. Although the short circuit current density is low for silicon carbide, it provides much higher output density due to its high open circuit voltage. The study with the model developed in this work showed that about ten times higher power output could be obtained for beryllium tritide with

silicon carbide compared to beryllium tritide with silicon. Furthermore, the results indicate that beryllium tritide with silicon carbide can provide power output about two times higher than that of titanium tritide with silicon carbide. The optimization of semiconductor design parameters can further increase the battery output. These results and analyses have major significance for the improvements of betavoltaic battery output and better design.

The betavoltaic battery model developed in this work was validated with different experimental results. The model was validated by the battery outputs for Ni-63 with silicon and titanium tritide with silicon carbide. It was also validated for the beta flux for titanium tritide. All these validations are substantial and imply the validity of the model. However, more experimental data with the measurements of all design parameters including the source thickness are required for betavoltaic batteries. In this work, all the significant aforementioned improvements in the model made the model more realistic to predict the betavoltaic battery output more accurately. Furthermore, the analyses of the design principles of betavoltaic battery provide major improvements in the battery design.

In conclusion, the contributions of this work are significant for the advancement of the field of betavoltaic batteries. All the beta particle transport analyses in this work were conducted using the Monte Carlo method of particle transport, which is a better method compared to the traditional method of designing the batteries using the empirical equations. The detailed analyses of beta particles energy deposition and penetration depth in semiconductors, beta particles angular distribution, backscattering effect, and self-absorption were significant improvements in the modeling and design of betavoltaic batteries. Furthermore, the development of the Monte Carlo radioisotope source model and source optimization, and the detailed analysis of the semiconductor design parameters and optimization have major impacts in the field of betavoltaic batteries.

Finally, all these major factors included in the model enabled the model to predict the experimental results for betavoltaic batteries more accurately.

6.2 Future Work

The methodology developed in this study provides a template for optimization of betavoltaic battery design. This work provides valuable information and observations. However, like any research labor, improvements can be made in the model. It is recommended that as future work the following can be done:

- A three-dimensional textured semiconductor device structure increases the surface area. It can increase the power output by reducing the self-absorption effect of the radioisotope. Different three-dimensional structures can be investigated to increase the power output. For example, a three-dimensional pillar structure on the semiconductor surface allows the source to be coated on the pillars. This will significantly improve the power output density of the battery. This type of structure needs optimization for the pillar dimensions and spacing of the pillars. A detailed analysis of different shapes of three-dimensional structures such as pillars, inverted pyramid, cylinders, and V-channel shapes can be investigated and optimized for higher power output.
- Different radioisotope sources can be investigated using the methodology developed in this work. Different metal tritides were examined in this work. This work can be further expanded for tritiated nitroxide polymeric compound to increase the tritium atoms in the source. The potential improvements can be med for the liquid phase of the source to reduce the self-absorption effect in the source. Besides, the liquid phase of the source has

the advantage of coating the aforementioned textured semiconductor device. All these effects can be studied in details to improve the power output.

- A multilayer structure of betavoltaic batteries can be designed using the methodology developed in this work to maximize the power output from a betavoltaic battery. In this work, the multilayer design of betavoltaic battery was studied for the maximum source power output without considering the semiconductor loss. The multilayer structure design can be explored including the semiconductor loss.
- A gallium nitride based betavoltaic batteries can be modeled. In this work, silicon carbide was modeled as a wide band gap based betavoltaic battery. Like silicon carbide, gallium nitride is also a wide band gap semiconductor. A gallium nitride based betavoltaic battery can be studied and compared to the silicon carbide betavoltaic battery.
- Schottky barrier junction based betavoltaic batteries can be investigated. Many experimental data are available for Schottky-based betavoltaic batteries. This model can be modified to apply to Schottky-based betavoltaic battery, and the results can be compared to the p-n junction based betavoltaic battery.

APPENDIX A: APPENDIX A: SUPPLEMENTARY MATERIALS

A.1 Comparison of MCNP and PENELOPE results

Besides comparison with the simulation and experimental results, it is helpful to compare similar results using different Monte Carlo particle transport codes in order to avoid simulation errors. For example, Figure A-1, Figure A-2, and Figure A-3 show the comparison of MCNP and PENELOPE results for Ni-63 with silicon. The results from MCNP and PENELOPE are in good agreement.

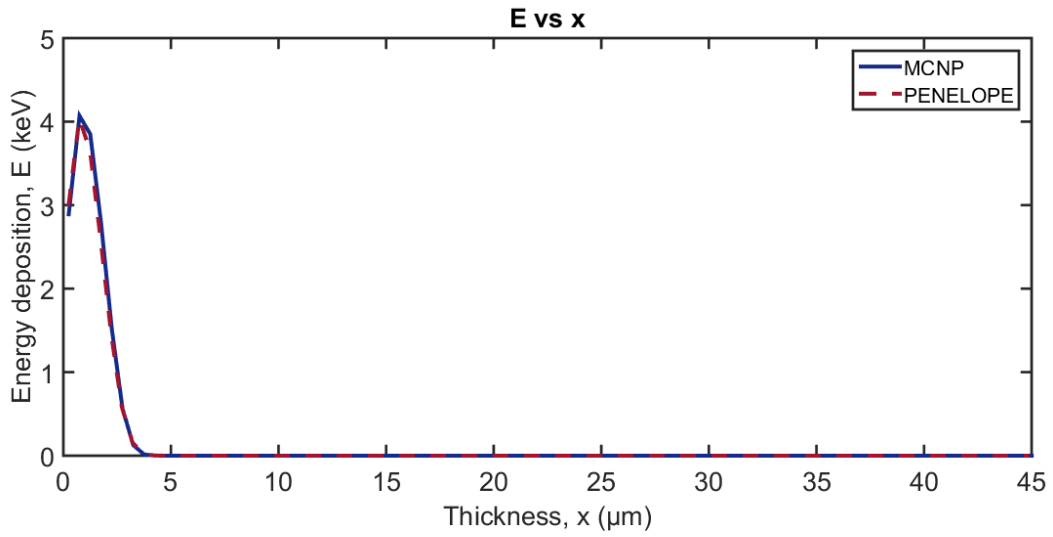

Figure A-1: Energy deposition for monoenergetic average beta particle energy of Ni-63 in silicon (0 degree)

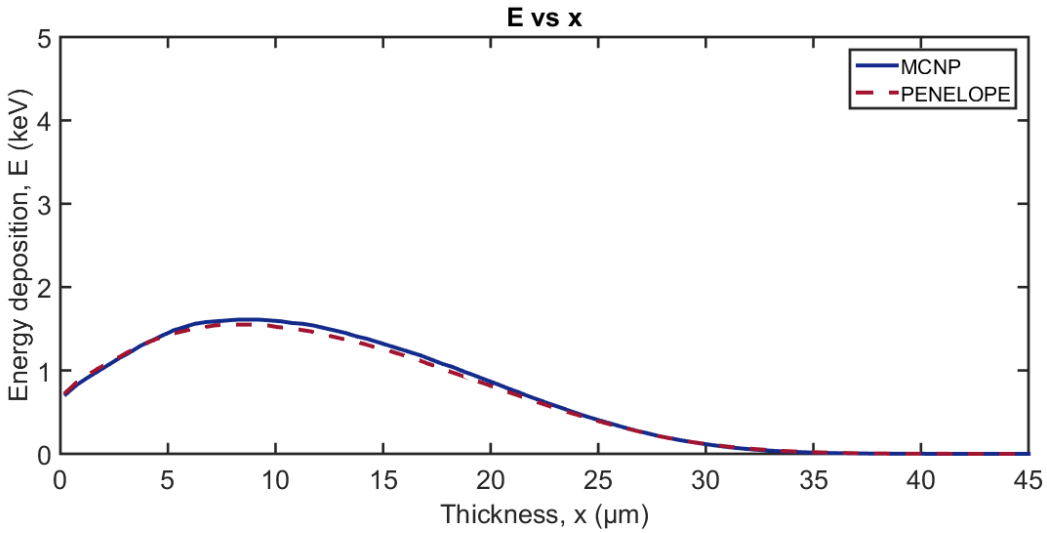

Figure A-2: Energy deposition for monoenergetic maximum beta particle energy of Ni-63 in silicon (0 degree)

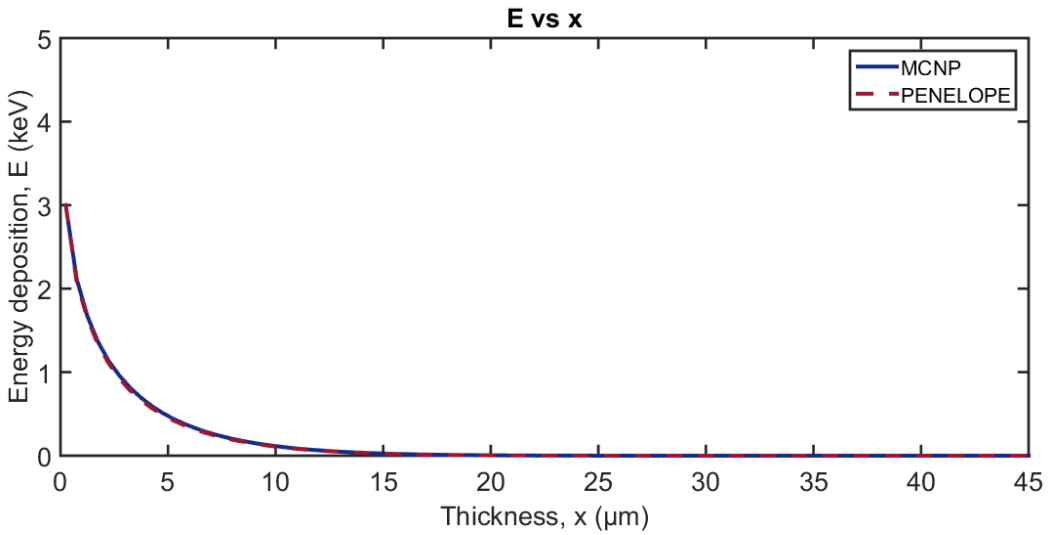

Figure A-3: Energy deposition for full beta energy spectrum of Ni-63 in silicon (0 degree)

A.2 Energy deposition parameters for Monte Carlo simulations

In this work, different radioisotope sources were simulated with different semiconductors to estimate the energy deposition of beta particles using MCNP and PENELOPE. From Monte Carlos simulations, an exponential approximation for beta particle energy deposition in the semiconductor was used as a generation function of EHPs in the semiconductor model. Table A.1 shows the summary of exponential parameters for the simulation of isotropic sources using full beta energy spectrum of Ni-63, titanium tritide, and beryllium tritide with silicon and silicon carbide.

Table A.1: Summary of exponential approximation parameters for EHP generation function (ae^{-bx}) for different radioisotopes with different semiconductors

Radioisotope and semiconductor combination	**a (/cm^3)**	**b (/cm)**
Ni-63 (point source) with silicon	1.284×10^8	7123
0.4 µm thick titanium tritide with silicon carbide	2.216×10^8	7.497×10^4
0.6 µm thick beryllium tritide with silicon	1.884×10^8	4.671×10^4
0.6 µm thick beryllium tritide with silicon carbide	1.685×10^8	7.285×10^4
2.5 µm thick beryllium tritide with silicon	1.997×10^8	5.177×10^4
2.5 µm thick beryllium tritide with silicon carbide	1.432×10^8	7.125×10^4